CWP-489
January 2004

Time-Lapse Monitoring with Multiply Scattered Waves

Carlos Pacheco

— Master's Thesis —
Geophysics

Committee members:
Prof. Reuben T. Collins
Prof. Thomas L. Davis
Prof. Paul Martin
Prof. Roelof K. Snieder
Prof. Terrence K. Young

Center for Wave Phenomena
Colorado School of Mines
Golden, Colorado 80401
(1) 303 273-3557

ABSTRACT

I have developed a technique which uses multiply scattered waves to relate temporal changes in the acoustic velocity to changes in the phase of the multiply scattered waves. This study is an extension of a previous technique called coda wave interferometry where multiply scattered waves are used to detect temporal changes in the scattering medium by measuring the time lag between the unperturbed and perturbed wavefield due to a temporal change in the medium. In this work, the propagation of multiply scattered sound is described using the diffusion approximation, which allows us to relate time-lapse changes of the wavefield to the temporal change of the velocity of the scattering medium. Previous formulations of coda wave interferometry make it possible to assess the average change in the medium, but they do not allow for the spatial localization of this change. I present a new formulation that relates the change in the phase of the scattered wavefield to a localized perturbation in a strongly scattering medium, and test it with synthetic seismograms calculated with finite-differences. The technique is tested numerically for 2D acoustic waves. Using the diffusion approximation for the energy transport in multiple-scattering media, I predict the change in the phase of the scattered wavefield given a localized velocity or slowness perturbation.

TABLE OF CONTENTS

Chapter 1

INTRODUCTION

Many problems in geophysics require the estimation of subsurface parameters from waves that have been scattered by heterogeneities in the earth. The desired result is, in many cases, a map of properties that provides an image of the subsurface structure. However, there are instances when creating a deterministic image in the medium is not the main goal, but rather the main interest is to detect and localize temporal changes in the medium. Examples of such cases include time-lapse monitoring of volcanoes and hydrocarbon reservoir monitoring during enhanced recovery operations. Dynamic reservoir characterization provides for optimal management of a reservoir, which leads to increased production. Time-lapse (4D) seismic aims at inferring changes from the medium from changes in the seismic amplitudes and/or traveltimes from seismic reflection data that has been acquired at two different times. As an example, a 4D dataset on Weyburn Field, Canada, has been used to infer time-lapse changes in the oil reservoir caused by a massive miscible CO_2 flood to enhance oil recovery (Li, 2003; Davis *et al.*, 2003). The main goal of these 4D studies is to extract information about local changes in the reservoir using mainly the amplitude information. However, these methods may be hindered by low signal to noise ratio of the seismic data in certain areas.

This thesis concerns the use of coda waves to monitor temporal changes in scattering media. The term coda refers to the recorded energy after the passage of the primary waves (Herraiz, 1987; Aki & Chouet, 1975). Depending on how strong the scattering is in the medium, these waves are either singly or multiply scattered waves. This gives rise to two different regimes in wave propagation. If the scattering is weak, the waves that are recorded are mostly singly scattered waves. In the single-scattering regime wave propagation can be modeled using the Born approximation (Morse & Feshbach, 1953; Aki & Chouet, 1975). At the other extreme, when scattering is strong, the description of the propagation of waves is achieved using the diffusion approximation (Dainty & Toksoz, 1990). The solution of the diffusion equation determines the redistribution of energy in strongly scattering media (Page *et al.*, 1995b).

There has been a considerable amount of work in the characterization of the medium and the detection of changes in the medium using singly and multiply scattered waves (Aki & Chouet, 1975; Lin & Ishimaru, 1974; Claerbout, 1985; Snieder, 2002; Weitz & Pine, 1993). Imaging techniques, as used in seismic imaging (Claerbout, 1985), crustal imaging (Braile *et al.*, 1995), non-destructive testing (Langenberg *et al.*, 2002) and medical imaging (Jensen, 2002), usually rely on the single-scattering approximation.

Multiply scattered waves have been used to determine the average structure or statistical distribution of scatterers in complex or random media. In this media the size of the heterogeneity is generally smaller than or equal to the wavelength. In biophysics and

medical imaging, diffusing photons are now used to view body function and structure after it was found that photon transport within tissues is dominated by scattering rather than absorption (Yodh & Chance, 1995). Diffuse transmission spectroscopy (Lemieux *et al.*, 1998) has been used to probe the structure of opaque materials such as colloids, foams and sand, using multiply scatttered photons.

Multiply scattered waves have also been used to study the dynamics of complex media and turbulent fluids. Diffuse light spectroscopy (Yodh & Chance, 1995) has been used to measure the spatial variations in the absorption and scattering of large tissue volumes. Weitz & Pine (1993) developed a technique called *Diffusing wave spectroscopy* (DWS) in which multiply scattered light is used to study the dynamics of colloidal suspensions; this technique was adapted later to acoustic waves by Cowan *et al.* (2002). This technique, called diffusing acoustic wave spectroscopy, estimates the average motion of the scatterers from the temporal fluctuations of multiply scattered sound. In this technique, the propagation of multiply scattered sound is described using the diffusion equation, which made it possible to relate the temporal field fluctuations with the dynamics of the multiple scattering medium. Recently, coda waves have been used to study the temperature dependence of the seismic velocity in granite (Snieder *et al.*, 2002) using a technique called *Coda Wave Interferometry* (CWI). In CWI, multiply scattered waves are used to detect temporal changes in a medium by using the scattering medium as an interferometer. For small changes in the medium, estimates of this perturbation can be derived from multiply scattered waves by a cross-correlation in the time domain.

Little attention has been paid to the problem of spatially localizing temporal changes with scattered waves. Instead, most of the studies have focused in the detection of temporal changes in the medium (Weitz & Pine, 1993; Snieder *et al.*, 2002; Cowan *et al.*, 2002). In most of the previous work on detection of temporal changes the assumption has been that the change is homogeneous on the sample space. To spatially localize this temporal or dynamic change, one wants to determine the position, size, shape and magnitude of the perturbation. Jian *et al.* (2003) obtained information about individual scattering events experienced by the diffusing field by computing correlation functions between electric fields measured at different positions. These measurements permits us to obtain information about the locations of individual scattering events experienced by portions of the diffusing field.

I present an approach to quantitatively estimate temporal and spatially variable changes in the medium by taking differential phase or traveltime measurements of the coda waves before and after a small change in the slowness has been introduced in the medium. This work is an extension of earlier work on coda wave interferometry (Snieder *et al.*, 2002), by modifying the theory to account for localized changes in the medium. I solve the forward problem of estimating the phase or traveltime change for the strong scattering or multiple-scattering regime, when the energy transport can be modeled as a diffusion process, and arrive at an expression relating the evolution of the phase change of coda waves with traveltime to spatially variable changes in the background velocity or slowness of the medium. The technique is tested numerically for 2D acoustic waves using synthetic seismograms computed with a finite difference technique in a 2D medium with random velocity fluctuations

which produce strong scattering.

I simulate time-lapse changes by calculating the finite-difference seismograms in this strongly scattering medium before and after the velocity field is perturbed. I then assess the validity of our theory by measuring the traveltime change of the synthetic seismograms and comparing it with the predicted traveltime change calculated using the theory developed in this work. The estimation of the velocity perturbation from the measured traveltime changes constitutes the inverse problem that can be solved to localize the change in the medium. Complete information about the shape, size and location of the perturbation will require a tomographic approach to inversion. This inversion scheme is not addressed in this work; this study is concerned with the modeling of the phase changes given a spatially variable velocity or slowness perturbation.

1.1 Coda Waves

The description of the propagation of acoustic waves through strongly scattering media is a problem of considerable importance to many areas of physics (Sheng, 1995). Coda waves have been used extensively to study energy transport and scattering through the randomly heterogeneous structure of the earth (Sato, 1993). Aki & Chouet (1975) proposed that the coda observed in earthquake seismograms is caused by scattering of waves by the small-scale heterogeneities in the lithosphere that are randomly distributed in space. The characterization of the earth as a random medium is complementary to the classical stratified media characterization. Coda waves have also been used to estimate the attenuation due to multiple scattering (Aki & Chouet, 1975; Wu, 1982; Zeng & Aki, 1991; Scales & Van Wijk, 1999). Different models have been formulated to explain the seismic coda. An extensive review of the different models and applications of coda waves is given by Sato & Fehler (1998).

Using a model with random heterogeneities, Frankel & Clayton (1984) simulated multiply scattered waves with finite-differences. In Chapter 2 I describe how to numerically simulate coda waves using finite-differences. I use as a scattering medium a velocity field with random velocity fluctuations in which the deviations from the mean value constitute the random heterogeneities. Then, I calculate finite-difference seismograms for a medium characterized with homogeneous statistical properties, and analyze the scattering for a range of values of the velocity fluctuations and characteristic length scales. By doing ensemble measurements of the wavefield and the transmitted intensity we estimate the scattering properties of the medium, that include the group velocity, scattering and transport mean free path and the diffusion coefficient. By tuning the scattering properties of the medium (e.g. by changing the magnitude of the standard deviation of the velocities) I change the scattering regime and the way the energy propagates through the random medium.

1.2 Time-lapse Monitoring in the Multiple-scattering Regime

Prior to the work of Aki & Chouet (1975), Wesley (1965) proposed a diffusion-like process to explain the late arriving energy after the primary arrivals in seismic waves. When

the scattering is strong, and the Born approximation is not valid, the transfer of seismic energy is described as a diffusion process (Weaver, 1982). Diffusion of multiply-scattered energy has been used in global seismology (Aki & Chouet, 1975; Margerin *et al.*, 1998), ultrasonics (Page *et al.*, 1995a) and medical imaging (Yodh *et al.*, 1997). I take advantage of the fact that wave transport acquires a diffusive character in a strongly scattering medium to obtain an expression for the mean or average traveltime change of the diffusive wavefield caused by a temporal and localized change in the velocity or slowness field. I find that if the diffusion approximation for the energy transport is valid, I can accurately predict the perturbation in the phase of the coda wavefield given a localized perturbation in the velocities.

Chapter 3 presents the derivation of the theory that allows to account for the temporal variation in the phase of the coda waves given a perturbation in the slowness. I test the theory for 2D acoustic waves using finite-difference simulations of multiple-scattering in a strongly scattering medium for different perturbations in the slowness field. I show two examples of localized velocity perturbations in the scattering medium and compare the mean traveltime change predicted using our technique with the traveltime change measured on the synthetic seismograms using a time-windowed cross-correlation technique. The results show good agreement between the theory and the numerical experiment.

Chapter 2

NUMERICAL SIMULATIONS OF CODA WAVES : FROM SINGLE TO MULTIPLE SCATTERING

2.1 Summary

I investigate wave propagation in two-dimensional random media using numerical simulations to better understand scattering of acoustic waves. Synthetic seismograms produced by the finite difference method are used to study the scattering of acoustic waves in two dimensional media with random spatial fluctuations in seismic velocity. The scatterers are represented by velocity fluctuations. Realizations of random media with Gaussian autocorrelation function are considered, with variations in seismic velocities over a range of length scales smaller than the seismic wavelength. The scale length of the heterogeneities and the magnitude of the velocity fluctuations determine the amount of scattering that a wave undergoes as it travels through the scattering medium. For weak fluctuations in the velocity we observe that most of the energy on the seismograms comes from single-scattering whereas for stronger fluctuations multiple-scattering dominates the seismograms. I study the transition from single to multiple scattering by adjusting the parameters that characterize the velocity fluctuations and estimate the scattering properties of the medium from ensemble measurements of the wavefield using synthetic seismograms calculated with finite differences. Finally, I show that in the diffusion regime wave propagation can be modeled as a random walk process.

2.2 Introduction

I study the transition from single to multiple scattering of acoustic waves in two dimensional random media using a finite difference algorithm. Wave propagation in two-dimensional random media has been studied by numerous authors (Frankel & Clayton, 1984, 1986; Shapiro & Kneib, 1993; Sato, 1993). Frankel & Clayton (1984) and Shapiro & Kneib (1993) performed finite-difference simulations of wave propagation in random media to study the effects of scattering on apparent attenuation and the variation of waveforms and amplitudes across seismic arrays. For a given magnitude of the random velocity fluctuations the scattering regime falls somewhere between the single and multiple scattering regime which are the two end member models which describe the transport of energy in random media (Sato & Fehler, 1998).

In this study we consider a 2D random medium with velocity fluctuations with scale lengths smaller than the seismic wavelength. Such fluctuations can be caused by lithology changes, the grain structure of the rock and the presence of cracks and pore fluids (Herraiz, 1987). The amount of scattering that the waves experience through the medium depends

on the characteristics of the velocity fluctuations of the medium (Lin & Ishimaru, 1974). In general, the larger the magnitude of the velocity fluctuations with respect to the background velocity, the more severe the scattering. Thus, by changing the magnitude of the velocity fluctuations we go from the single-scattering regime (when the scattering is weak), to the multiple-scattering regime (when the scattering is strong).

By changing the spatial distribution of the random velocity fluctuations, the calculated synthetic seismograms are used to estimate the group and transport velocity v_g (velocity of the signal envelope), scattering mean free path l and transport mean free path l^* and the diffusion coefficient D of the media. Using several realizations of wave propagation in random media we estimate these properties of scattering media from average measures of the wavefield and of the coherent and total intensities. I show that for weak velocity fluctuations, wave propagation in the 2D random media can be modeled using the single-scattering approximation. As I increase the magnitude of the velocity fluctuations, the energy transport is better described by a diffusion process. In general, I find that the wavefields behave diffusively after the waves have propagated through the scattering medium for distances r on the order of several transport mean free paths ($r > 4l^*$), which agrees with results obtained by van Albada & van Tiggelen (1991), Kuga (1993), Lemieux *et al.* (1998) and Page *et al.* (1995b).

Finally, when wave transport can be described as a diffusion process we show that waves propagating on a multiply scattering medium can be thought of as the superposition of waves with trajectories that can be described as a random walk from source to receiver. Each step length on this random walk is approximately equal to the transport mean free path l^*, and the latter can be obtained with knowledge of the diffusion coefficient and the transport velocity of the medium.

2.3 Two Models of Coda waves

Depending on the random distribution of the velocity fluctuations, we can consider two different extreme models for the origin of coda waves. When the particle density is tenuous and/or the scattering is weak, we can use the single-scattering approximation (Herraiz, 1987) to describe the transport of wave energy through the medium. In this model, the coda can be considered as a superposition of wavelets scattered from different heterogeneities which act as secondary sources. Each wavelet is due to a single scatterer in the absence of other scatterers (Aki & Chouet, 1975). In the single-scattering regime the scattering is a weak process, and we can use the Born approximation to describe the wave propagation process. We find the second model at the other extreme for a dense distribution of stronger scatterers, when the diffusion model has been used to describe the energy transport (Wesley, 1965; Aki & Chouet, 1975; Page *et al.*, 1995b; Schriemer *et al.*, 1997).

The transition from the ballistic to diffusive propagation is not fully understood and various approaches have been used to study the energy transfer in this crossover (Paasschens, 1997; Lemieux *et al.*, 1998; Zhang & Sheng, 1999). More accurate expressions for the probability density of intensity as a function of position have been proposed based on the *Boltzman equation*, also known as the *Radiative transfer equation* (Paasschens, 1997).

2.3.1 Single-Scattering Model

Aki (1969) first showed that the coda waves of local earthquakes can be treated as singly scattered waves. This model assumes that the scattering is weak and therefore multiple-scattering can be neglected. Single scattering invokes the Born approximation, which assumes that the energy lost from the direct wave during the scattering process is small for propagation distances smaller or approximately equal to the transport mean free path(Aki & Chouet, 1975). If intrinsic attenuation is neglected, the dominant energy loss mechanism in this model is geometrical spreading.

The application of the single scattering formulation for the study of coda waves is based on assumptions that the medium is not strongly heterogeneous and that the transport mean free path is greater than or equal to the travel distance between the source and the receiver (Gao, 1983). Because of these oversimplifications the law of energy conservation is violated. According to this model, the waves have traveled outward from the source, been scattered once, and then propagated back to the receiver.

In the single-scattering approximation, both the energy loss and the dispersion associated with the interaction of waves with the scatterers is small (Gao, 1985). As a result, the primary waves show little, if any, distortion as they travel through the medium. In this model the ballistic or direct pulse carries most of the energy as it propagates through the medium with no scattering (Cowan *et al.*, 1998).

In the single scattering model, scattering is a linear process and therefore we can calculate the scattered wavefield from the incident wavefield using the Green's function method. Following Bleistein *et al.* (2001) we can represent the true wave speed as being the sum of a background wave speed profile plus a perturbation, also called the *scatterer.* Following this logic, we may consider the true wavefield u as being of the background field plus a perturbation, also called the *scattered field.* It is proper then, to think of u as being made up of an incident field u_I which would be present in the absence of the scatterer or velocity fluctuation α, plus u_S, which represents the departure from u_I due to the presence of the perturbation α. For a harmonic wave of angular frequency ω propagating in one-dimensional medium the total wavefield $u(x, x_s, \omega)$ at receiver x due to a source at x_s is

$$u(x, x_s, \omega) = u_I(x, x_s, \omega) + u_S(x, x_s, \omega), \tag{2.1}$$

which is known as the wavefield perturbation expression (Bleistein *et al.*, 2001). An advantage of this decomposition is that the Helmholtz equation, which is the forward wave modeling operator in the frequency domain, may be written as the sum of two Helmholtz equations. If we solve the Helmholtz equation using Green's function method we obtain the integral expression relating the observations of the scattering field at receiver x_g, $u_S(x_g, x_s, \omega)$ to the interior values of that unknown field and the perturbation $\alpha(x)$ which represent the scatterers:

$$u_S(x_g, x_s, \omega) = \omega^2 \int \frac{\alpha(x)}{c^2(x)} \left[u_I(x, x_s, \omega) + u_S(x, x_s, \omega)\right] g(x, x_g, \omega) dx, \tag{2.2}$$

where $c(x)$ is the background wave speed and $g(x, x_g, \omega)$ is the Green's function for the 1D

Helmholtz operator. Eq. 2.2 is nonlinear because the expression for the scattered field u_S contains a term that depends on the product of the unknown scattered u_S and the velocity perturbation $\alpha(x)$. For acoustic wave propagation (constant mass density) $\alpha(x)$ becomes the scattering coefficient. In the Born approximation we assume that $\alpha(x)$ (scattering is weak) and therefore the product of u_S and $\alpha(x)$ is much smaller than the product of the incident wave u_I and $\alpha(x)$. Here, "linearization" means removing the product $u_S \times \alpha(x)$ from the right hand side of Eq. 2.2. The scattered field in this approximation becomes accurate to linear order in $\alpha(x)$, yielding

$$u_S(x_g, x_s, \omega) = \omega^2 \int \frac{\alpha(x)}{c^2(x)} u_I(x, x_s, \omega) g(x, x_g, \omega) dx. \tag{2.3}$$

The linearization performed here is often called the *Born approximation.* The same derivation is valid for higher dimensions with the only difference being on the Green's function which describes the propagation of the incident pulse in the constant wave speed profile.

2.3.2 Multiple-Scattering Model

When the scattering is strong, i.e. the product $u_S \times \alpha(x)$ is of comparable size to the incident wavefield u_I, the Born approximation is no longer valid and therefore the scattered wavefield can not be calculated using Eq. 2.3. The medium is characterized as a constant background wave speed profile with added perturbations that represent the scatterers, but in this case the fluctuations α are large when compared to the background wave speed c. In this regime, the scattered wavefield does not depend linearly on the scattering coefficient α as the wave emanated from the source interacts with multiple scatterers on its trajectory from source to receiver and its energy becomes redistributed in multiple directions. This process gives rise to the multiply scattered waves that make up the coda. In this regime, the multiple wave pulses measured at the receiver at different times are the result of the superposition of waves with different trajectories on the multiple scattering medium.

Given an energy impulse detected at time t at the receiver, it is extremely difficult to determine which specific trajectory from the source to the receiver gave rise to such event. The problem is, however, simplified if instead of considering one specific trajectory we consider the average wavefield obtained after summing the contributions from different trajectories. Therefore, when scattering is strong and waves follow infinitely many trajectories, wave propagation can be considered as a random walk process. It is when we make such a connection that the problem becomes simplified because, as we will see later, a random walk process can be described as a diffusion process.

In the multiple scattering regime the seismic energy transfer is thus considered to be a diffusion process and the total energy in the system is conserved (Page *et al.*, 1995b). As the number of scatterings become large, the direction of the emerging waves become randomized and the multiple-scattering process tends to redistribute the energy in all directions (Margerin & Campillo, 2000). Many investigators have determined the propagation distance at which the diffusion approximation becomes valid (Page *et al.*, 1995b; Paasschens,

1997; Cowan *et al.*, 2002). For example, diffusing wave spectroscopy experiments (Cowan *et al.*, 2002) have indicated that the energy transport becomes diffusive for propagation distances longer than a few mean free paths ($r > 4l$). Therefore, for scattered waves to be in the diffusion regime the transport mean free path l^* must be small when compared to the propagation distance.

Compared to the single scattering regime, the incident pulse in multiple scattering is greatly attenuated due to scattering. Besides attenuation, the wavefield propagated in the strongly scattering media is also strongly affected by dispersion. This dispersion is related to the scattering attenuation by the Kramers-Kronig relation. The dispersion is caused by the high heterogeneity of the medium, where waves of different frequencies travel at different speeds (Elmore & Heald, 1969; Stein & Wysession, 2003). Dispersion strongly affects the frequency content and velocity of the incident wave (which is commonly referred in the literature as the ballistic wave) and this will be demonstrated in later sections with synthetic seismograms calculated with the finite differences method.

2.3.3 Multiple Scattering as a Random Walk Process

To better understand the dynamics of wave transport in a multiple scattering medium, the propagation of sound through the material can be modeled using the diffusion approximation. In this section we show how diffusive motion comes out of a simple model of a random walk. This provides us with the advantage of a simple physical picture where the diffusively scattered wavefield is represented as the sum of partial waves traveling along various diffuse paths (Skipetrov & Maynard, 2003). Each one of these diffuse paths is usually thought of as a random walk from source to receiver with a characteristic step length equal to the transport mean free path l^*.

Let us assume that the seismic energy transport can be described with random walks. This is a good approximation for a strongly heterogeneous medium where multiply scattered waves are produced. Let's consider first a random walk in one dimension and that the particle takes discrete steps of length h for every increment of time τ. We define the random variable X_t as the position of a random walk particle at a given time t. We can define the probability P_{ij} that a particle with an initial position at i will end up at j. One way of defining the transition probability is as follows:

$$P(X_{t+\tau} - X_t = h) = P(X_{t+\tau} - X_t = -h) = \frac{1}{2}. \tag{2.4}$$

which simply means that the variable X (the subscript stands for the time) has an equal probability of increasing or decreasing by h at each time step. This process is both homogeneous (since the transition probability is only dependent on the distance between the initial and final points) and isotropic (the transition probability is independent of the direction of movement). To get to position x the walker must be at position $x - h$ or position $x + h$ at the previous step. In either case, the probability that it moves to position x is 0.5. Hence,

the following difference equation holds

$$P(X_{t+\tau} = x) = \frac{1}{2}\left[P(X_t = x + h) + P(X_t = x - h)\right]. \tag{2.5}$$

If we subtract $P(X_t = x)$ to Eq. 2.5 and divide the result by τ, and consider P to be a function of both position x and time t, the above equation becomes

$$\frac{P(x, t+\tau) - P(x,t)}{\tau} = \frac{h^2}{2\tau}\frac{P(x+h,t) - 2P(x,t) + P(x-h,t)}{h^2}, \tag{2.6}$$

where $P(x,t)$ is the probability of the particle being at x at time t (it is important to note that these are still discrete variables). In the limit $h \to 0, \tau \to 0$, $\frac{P(x,t+\tau)-P(x,t)}{\tau}$ becomes $\frac{\partial P(x,t)}{\partial t}$ (now, of course, x and t are continuous) and $\frac{P(x+h,t)-2P(x,t)+P(x-h,t)}{h^2}$ becomes $\frac{\partial^2 P(x,t)}{\partial x^2}$. Hence, in this limit, we get the following equation for the one-dimensional random walk

$$\frac{\partial P(x,t)}{\partial t} = D\frac{\partial^2 P(x,t)}{\partial x^2}, \tag{2.7}$$

where $D = h^2/2\tau$. Eq. 2.7 is, of course, the diffusion equation which should not come as too much of a surprise as diffusion is the result of the random movement of molecules. For an unbounded 1D homogeneous medium, the solution of the diffusion equation with the initial condition $P_0(x,0) = \delta(x)$ is given by the Gaussian

$$P_0(x,t) = \frac{1}{2\sqrt{\pi D t}}\exp\left(-\frac{x^2}{4Dt}\right), t > 0. \tag{2.8}$$

In terms of random walk, this initial condition means that the particle starts at the origin. If we generalize this to $m-$dimensions, Eq. 2.6 is replaced by

$$\frac{P(\mathbf{x}, t+\tau) - P(\mathbf{x},t)}{\tau} = \sum_{i=1}^{m}\frac{h^2}{2\tau m}\frac{P(x_i - h, t) - 2P(x_i,t) + P(x_i + h, t)}{h^2} \tag{2.9}$$

(the subscripts refer to the components of $\mathbf{x}$) whose continuum limit is

$$\frac{\partial P(x,t)}{\partial t} = D\Delta P(x,t), \tag{2.10}$$

where D is now $h^2/2\tau m$ and Δ is the m-dimensional Laplacian. The solution to this equation for $m = 2$ and assuming isotropic scattering with the initial condition $P(\mathbf{x}, 0) = \delta(\mathbf{x})$ is given by

$$P_0(\mathbf{x}, t) = \frac{1}{(4\pi D t)}\exp\left(-\frac{r^2}{4Dt}\right) \tag{2.11}$$

where $r = |\mathbf{x}|$ is the distance to the source. $P_0(\mathbf{x}, t)$ then stands for the probability of a particle on a random walk of visiting location $\mathbf{x}$ at time t. This describes the distribution of a Brownian particle, given the information that it started at the origin at time $t = 0$.

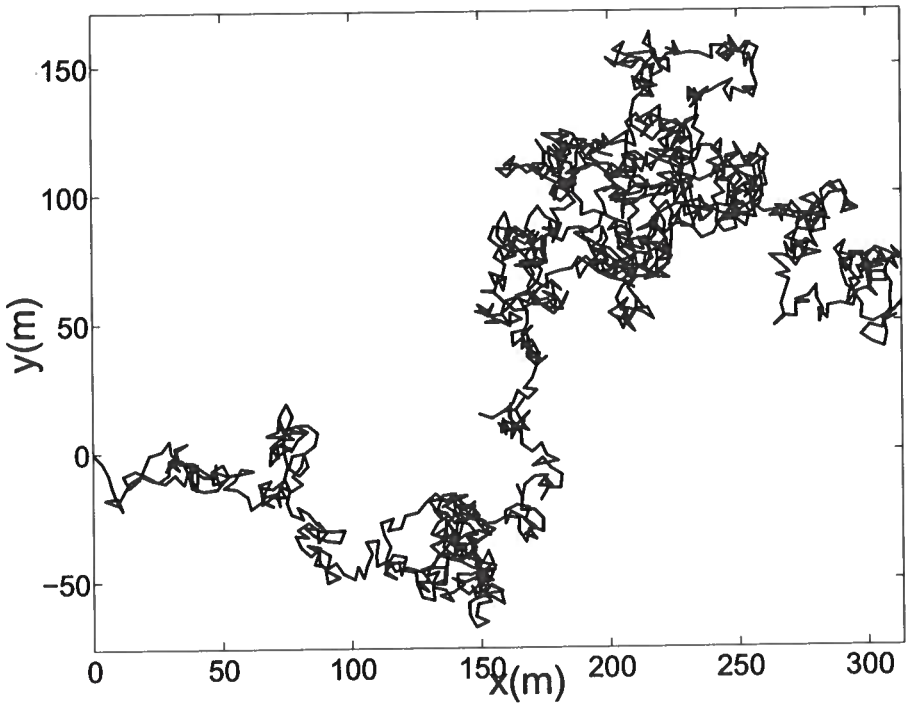

Figure 2.1. The trail of a Brownian particle in the plane, from a computer simulation.

The distribution varies with time and its main characteristic is that the width broadens according to a $\sqrt{t}$ law. More precisely, the mean square displacement

$$\langle r^2 \rangle = \int r^2 P_0(\mathbf{r}, t) d^2\mathbf{r} = 4Dt, \tag{2.12}$$

is proportional to t. In other words, the distribution varies with time according to a $\sqrt{t}$ law. Figure 2.3.3 shows a single realization of random walk in the plane.

The scattering of waves is responsible for the attenuation in the medium. The simplest model of wave transport in a disordered medium is a random walk. A wave with energy velocity v_e travels for a typical distance, the transport mean free path l^*, before being scattered by a heterogeneity from its straight line path. In the wave transport picture, $P_0(\mathbf{x}, t)$ represents the fraction of energy at location $\mathbf{x}$ and time t given a wave energy impulse at time $t = 0$ at the origin. The definition of the diffusion coefficient D in 2D is $D = v_e l^*/2$ (Weaver, 1982; A. & Weaver, 1995) where v_e is the energy velocity and l^* is the transport mean free path. It is important to remember that $P_0(\mathbf{r})$ describes the space and time evolution of diffusive intensity in the media. In multiple scattering this diffusive energy corresponds to the ensemble averaged or mean intensity $\langle I \rangle$. In Section 2.6.3 we show how to estimate the diffusion coefficient D from the mean intensity of multiple realizations of wave propagation in 2-dimensional media.

2.4 Scattering Model for Acoustic Waves in 2D

Chernov (1960) and Karal & Keller (1964) used random velocity models to analyze the Earth's small scale heterogeneities. These models are examples of the use of stochastic theory in seismology. There are numerous possible parameterizations for two-dimensional homogeneous random media. In this work we restrict ourselves to media with a Gaussian probability distribution of the velocity fluctuations. Velocity fluctuations about the mean velocity are exactly the same as the velocity perturbation $\alpha(x)$ added to the constant background wave speed profile in the previous section. This model is one with continuous random fluctuations with a Gaussian autocorrelation function, and is useful to model multiple-scattering in the diffusion regime (Frankel & Clayton, 1984) when the magnitude of the velocity fluctuations is large. Single scattering can be achieved, however, by making the magnitude of the velocity fluctuations small. Following Frankel & Clayton (1984), I model the 2D velocity field as a constant velocity background with added random velocity fluctuations. The total velocity field is decomposed as

$$v(\mathbf{r}) = v_0 + v_r(\mathbf{r}), \tag{2.13}$$

where v_0 is the constant background velocity and v_r describes the random velocity fluctuations. We characterize our medium statistically with the following assumptions: the random process is statistically homogeneous, and the extent of the medium is much greater than the correlation distance a (Lin & Ishimaru, 1974). The spatial correlation function $N(r)$, which expresses the correlation of the fluctuations between two points within the

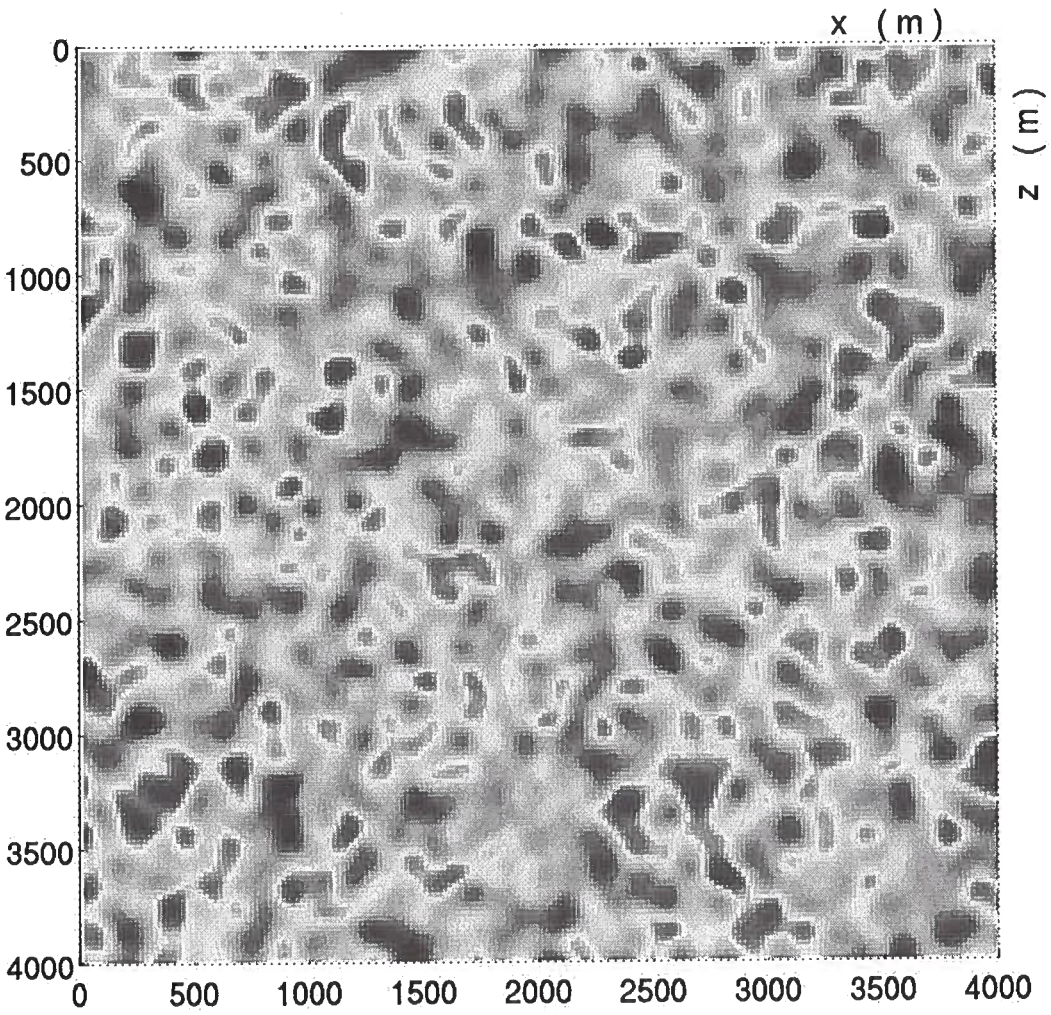

Figure 2.2. Realization of a 2D random velocity model with a Gaussian autocorrelation function. The correlation distance a is 100 m.

heterogeneous region, is assumed to be Gaussian, i.e.

$$N(r) = < v_r(\mathbf{r}')v_r(\mathbf{r}'+\mathbf{r}) > = {\sigma_v}^2 \exp\left[\frac{-r^2}{a^2}\right], \tag{2.14}$$

where σ_v is the standard deviation of the velocity, and a is the correlation distance. Note that the autocorrelation function $N(r)$ is isotropic as it only depends on the distance r. The correlation distance a is essentially proportional to the average size of the scatterers (Frankel & Clayton, 1986). It is useful to define a dimensionless parameter that describes the variation of the velocity in the random medium, as the relative variation of the velocity with respect to the mean value determines the imprints of the velocity fluctuations on the scattering strength. Hence, we define the normalized standard deviation of the velocity as

$$\sigma = \sigma_v / v_0. \tag{2.15}$$

In general, the amount of scattering depends in a nonlinear way on the following factors: the magnitude of the relative velocity fluctuations σ, the correlation distance a, and the frequency spectrum of the source wavelet. In general, the scattering increases with the magnitude of the velocity fluctuations, i.e., the bigger σ the stronger the scattering. The correlation distance a also affects the strength of the scattering in a nonlinear way. In the next section we show variations of scattering parameters for different values of σ and a.

The two-dimensional random velocity fluctuation field v_r was constructed by specifying a random velocity value for each point in the grid with a random number generator. The random velocity field is Fourier transformed to the wave-number space and then filtered to achieve the desired spectrum (Frankel & Clayton, 1986). Finally, we transform back to the space domain and after normalizing to obtain the desired standard deviation, the velocity fluctuations v_r are added to the homogeneous velocity field v_0. The random component v_r has a Gaussian probability distribution. Figure 2.1 shows a realization of such a velocity model with a Gaussian autocorrelation function for a=100m.

The amplitude and phase of wavefields fluctuate in random media (Shapiro & Kneib, 1993). However, as we mentioned on previous sections, we concentrate on this study on the behavior of average quantities such as the wavefield and the intensities. Averaged wavefields are characterized by scattering attenuation, dispersion and anisotropy (Ishimaru, 1978). In this model, there are no preferential orientations in the shape of the velocity fluctuations and therefore scattering is approximately isotropic. The values of the correlation distance a and the standard deviation of the velocity σ can be set to produce the desired scattering strength. Usually, a is made to be smaller than the seismic wavelength and σ is made big enough to produce multiple scattering. For a given variance in the velocity, random media with different correlation distances (i.e., scatterer sizes) produce different amounts of scattering attenuation at different frequencies (Herraiz, 1987). For scatterers with a size comparable to the wavelength, the effects of dispersion and resonant scattering are stronger (Page & Sheng, n.d.). When ka (k being the wavenumber) is comparable to unity or greater, the effect of the scatterer shape is important, and the waveform becomes highly distorted after a few scattering events.

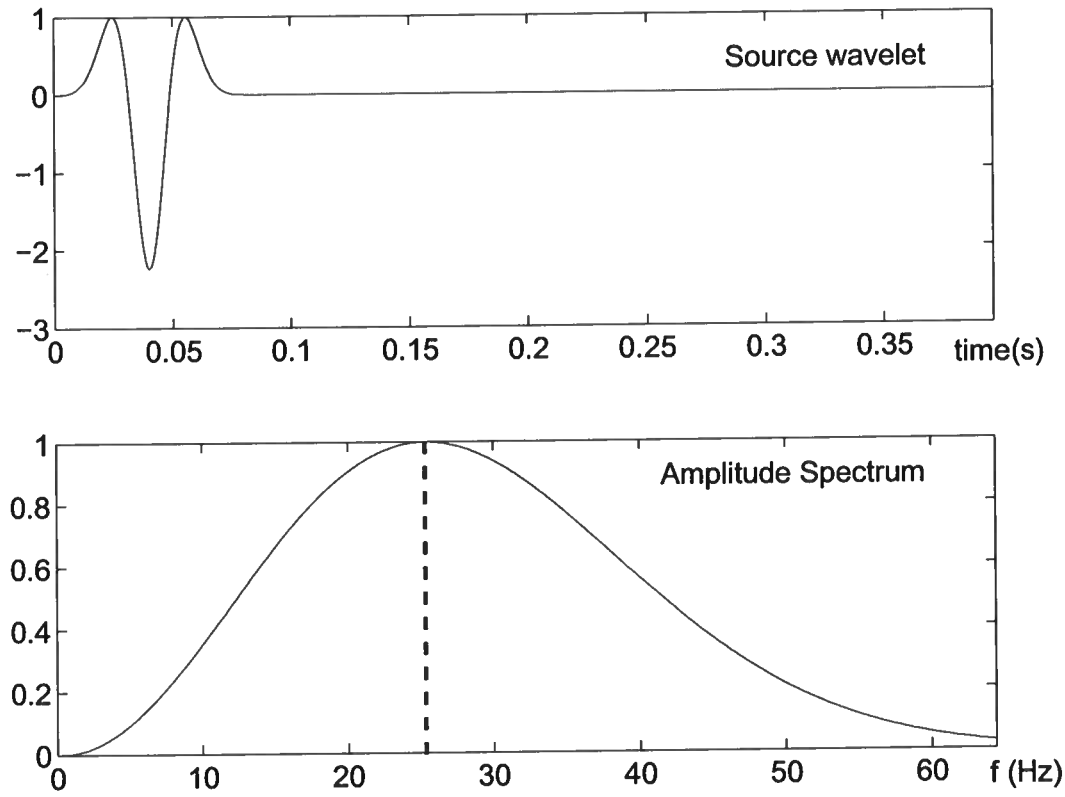

Figure 2.3. Source wavelet (top) and amplitude spectrum of the source (bottom). The dashed line indicates the dominant frequency of 25 Hz.

2.5 Finite-Difference Modeling of Coda Waves

The finite-difference method used in this work solves the acoustic wave equation for a heterogeneous medium on a two-dimensional grid. The reader is referred to Alford & Kelly (1974) and Kelly *et al.* (1976) for a more detailed description of the method. The finite-difference technique retains all singly and multiply scattered waves, and also accounts for transmission losses due to scattering (Frankel & Clayton, 1984).

In this study, we assume that the mass density is constant and that the velocity fluctuations are the only cause for the scattering of waves. The two-dimensional acoustic wave equation describing the pressure (P) where the velocity v is a function of x and z and the mass density is constant is given by

$$\frac{\partial^2 P}{\partial t^2} = v^2(x,z)\left[\frac{\partial^2 P}{\partial x^2} + \frac{\partial^2 P}{\partial z^2}\right]. \tag{2.16}$$

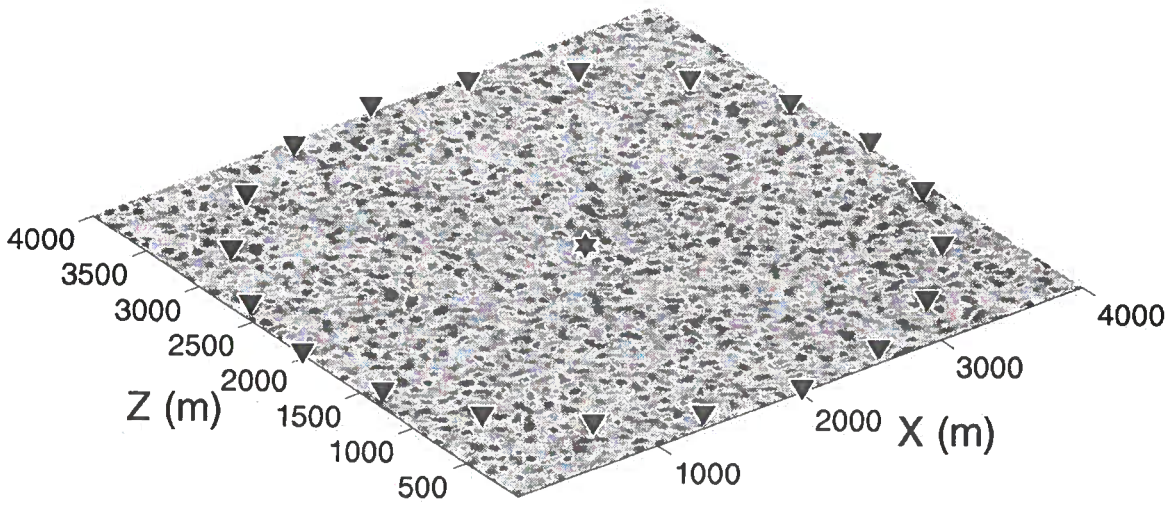

Figure 2.4. Typical configuration for the study of scattering of waves in random media. The star is the source and the triangles are the receivers around the source.

The solution for this equation contains all the multiple reflections and diffractions. These equations are solved numerically by replacing the partial derivatives by their finite-difference approximations for a discrete time step dt and grid spacing dx. The MATLAB finite-difference algorithm used in this study utilizes fourth-order approximations to the spatial derivatives, which are superior in accuracy to the second-order schemes more commonly used in finite difference modeling of seismic waves (Alford & Kelly, 1974).

The synthetic seismograms were created by transmitting a band-limited pulse through the two-dimensional grid. The grid size is 1000 by 1000 points, with a grid spacing dx of $20m$. I generated velocity fields with a mean velocity v_0=6000 m/s and added random velocity fluctuations with Gaussian probability distribution. I used a source time function that was the second derivative of a Gaussian (Ricker wavelet). In general, the pulse width can be varied to represent different source durations and frequency spectrum (Kelly *et al.*, 1976). For simplicity, I kept the source wavelet constant for all of our experiments. The employed source pulse has a duration of about 0.040 s and its dominant frequency is around 25 Hz. Figure 2.3 shows both the source wavelet (top) and the frequency spectrum of the source wavelet (bottom). The choice of the grid spacing dx was based to ensure both that our dominant wavelength is much bigger than the grid size ($\lambda_{dom} >> dx$), and to ensure stability and minimize grid dispersion artifacts in the finite-difference calculations (Alford & Kelly, 1974). We calculated the seismograms up to 3.5 s, which is the time at which the reflections from the boundaries of our model appear.

Several velocity models were created with different statistical properties in order to

study the effect on the scattering and to monitor the transition from the single-scattering to the multiple-scattering regime. The statistical properties to adjust on the continuous random velocity model are the correlation length a and the normalized standard deviation of the velocity σ. Our specific interest is in velocity fluctuations on a scale length smaller than the wavelength. For a mean velocity of $6000m/s$ and a dominant frequency of $25Hz$, the dominant wavelength is approximately 240 m.

We calculate the synthetic seismograms for a range of values of a and σ. First, to study the effect of the magnitude of the velocity fluctuations on the scattering, we kept the correlation distance fixed, a=40m, and calculate the synthetic seismograms for σ=[0.01,0.02,0.03,0.05,0.07,0.10,0.15,0.20,0.25]. Second, for a high value of the magnitude of the velocity fluctuations (σ=0.25) we calculated the seismograms for a=[40,100,140,200] m.

Figure 2.4 depicts the typical receiver configuration used for the ensemble measurements of scattering properties in later sections. The source is centered in the middle of several concentric arrays of receivers located at different distances from the source.

Figure 2.5 show examples of the wavefields recorded at 4000 m for a medium with a constant background velocity and for velocity models with different velocity fluctuation spectra. The correlation length for all models with velocity fluctuations is a=40 m. The standard deviation values for the calculated seismograms are σ=[0.02,0.05,0.10,0.15,0.25]. Note that the ballistic arrival for the models with small velocity fluctuations (σ=0.02,0.05) is coherent in all the detectors and arrives approximately at the same time as the ballistic arrival for the homogeneous velocity field. Also, the transmitted wavelet shows little dispersion (i.e., no broadening of the coherent pulse) when compared to the wavefield in the homogeneous velocity field. For weak fluctuations of the velocity, we expect that the ballistic wave isn't broadened by dispersion and its amplitude to be much larger than the scattered waves. This seems to be case for fluctuations of the velocity smaller of equal than five percent of the mean velocity($\sigma < .05v_0$).

As we increase the magnitude of the velocity fluctuations, the energy loss from the ballistic pulse increases and the contribution of the multiply scattered waves to the total energy of the system increases consequently. Indeed, for larger values of the magnitude of the velocity fluctuations (seismograms with σ=0.10, 0.15 and 0.25 on Figure 2.5) increasing amounts of energy are transferred from the ballistic pulse to the multiply scattered waves. In this case the ballistic arrival is delayed with respect to the ballistic pulse in the homogeneous velocity model and the traveltime of this arrival starts to show random delays. These random delays are associated with phase changes of the wavefield caused by the ballistic waves following paths of different length for different receivers. This slower ballistic arrival shows dispersion (the ballistic wave is the result of the interference of waves traveling at different in the forward direction) because of the increasing attenuation due to scattering. The dispersion is the greatest when σ=0.25. The ballistic arrival has been attenuated severely and shows a smaller amplitude and lower frequency content than the later arriving multiple-scattering events.

Figure 2.5 shows a closer view at some of the seismograms shown in Figure 2.5. Here, five of the seismograms recorded at a 4000 m distance to the source for the random medium

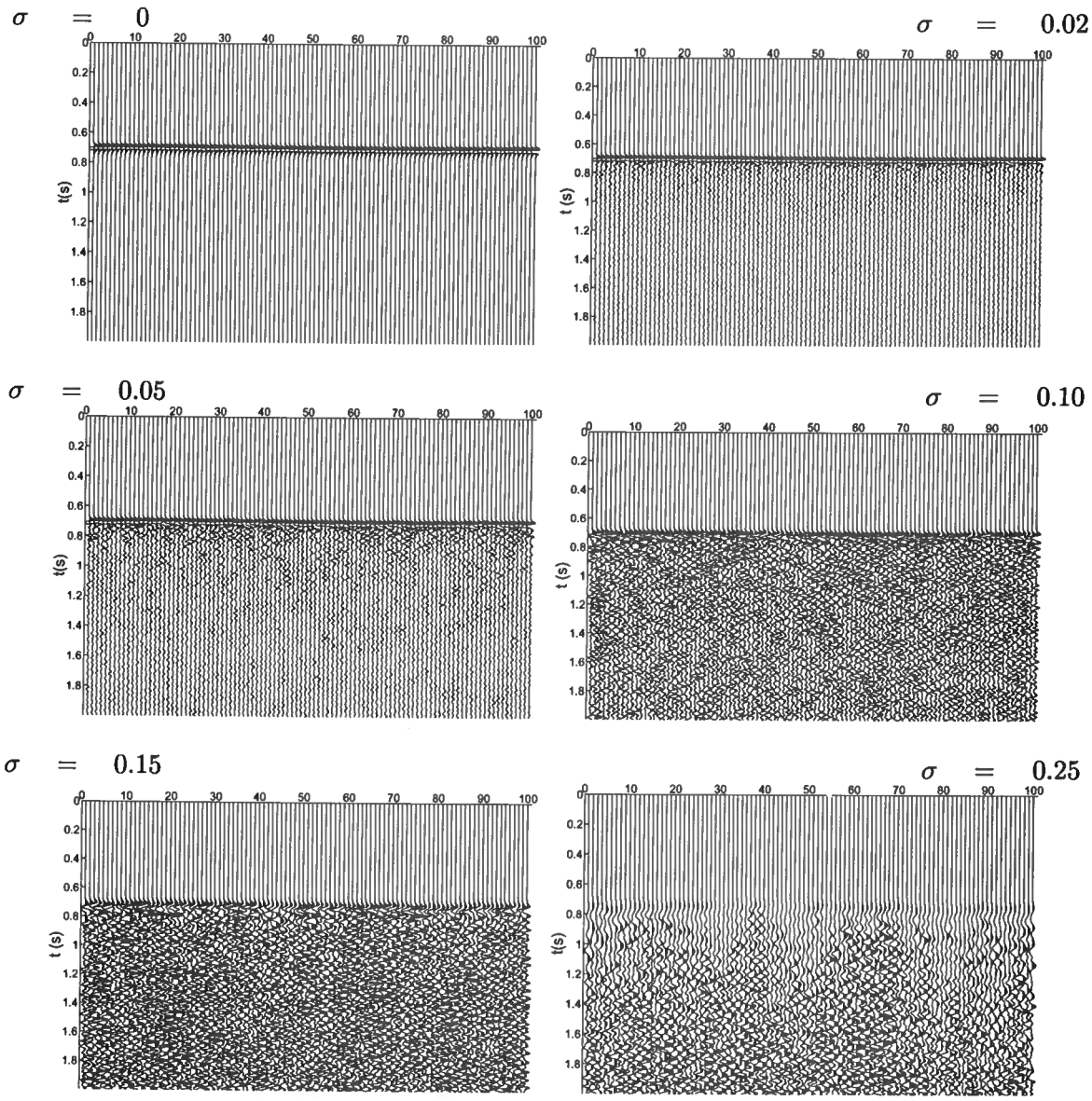

Figure 2.5. Seismograms recorded at 4000 m from the source for: a homogeneous velocity model (top-left) and for random media with continuous random velocity fluctuations with autocorrelation length a=40 m and different standard deviations σ.

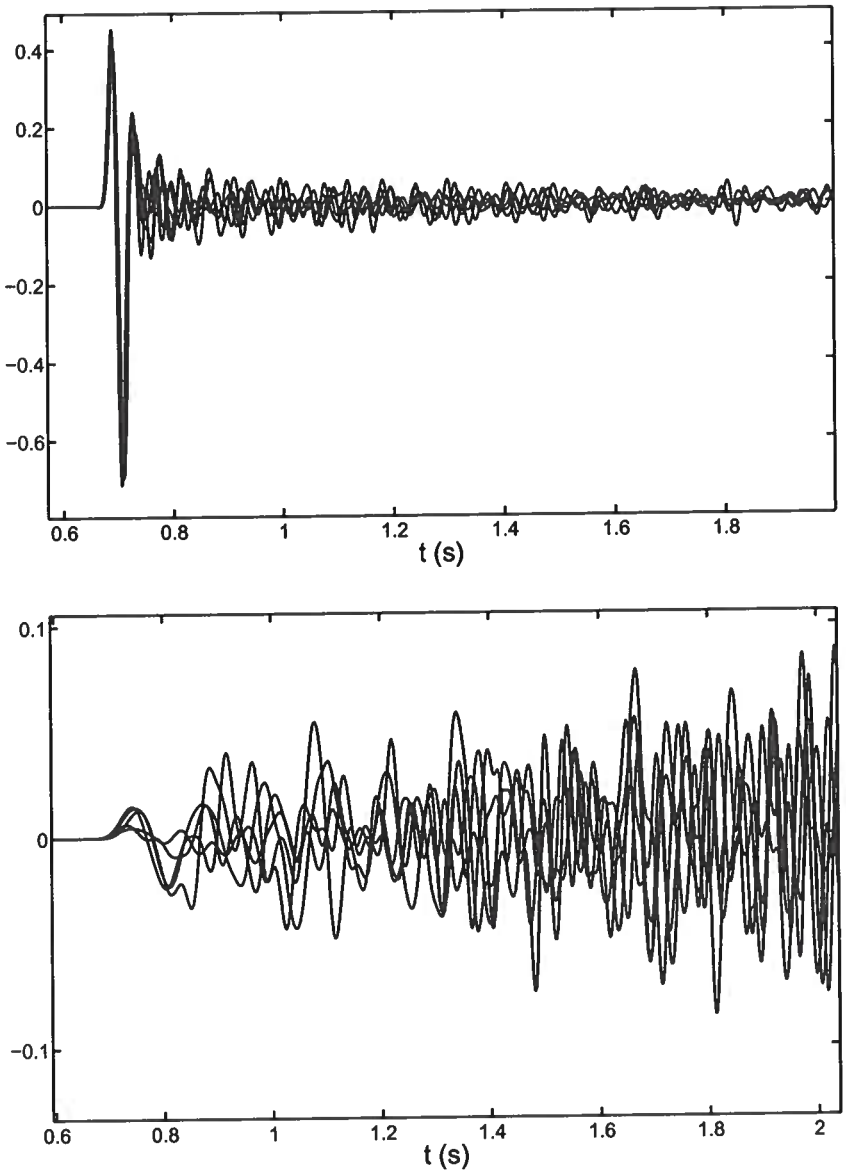

Figure 2.6. (a) Transmitted wavefield for a weak scattering medium ($\sigma = 0.05$). (b) Transmitted wavefield for a strong scattering media ($\sigma = 0.25$). In each case we plot five of the 100 seismograms recorded at a distance to the source of 4000 m.

with σ=0.02 (top); five seismograms for the same receiver locations but for the medium with σ=0.25 are shown at the bottom of Figure 2.5. Note that for the medium with σ=0.02 the scattering is weak and the ballistic pulse is much stronger than the coda. This is not the case for a medium with σ=0.25 where the multiply scattered waves are more energetic than the ballistic wave which has lost most of his energy due to scattering losses. As the waves travel through the random medium, energy is lost from the ballistic wave and is transfered to the multiply-scattered waves via a diffusion-like process. Thus, by increasing the value of σ the scattering regime changes from the single to the multiple-scattering regime. Note that this is a qualitative analysis of the scattering strength in the medium; in the next section we provide more quantitative arguments to measure to which degree the velocity medium acts as a single or as multiple scattering medium.

2.6 Ensemble Measurements of Wave Propagation

When a seismic wave travels through a heterogeneous medium, its amplitude and phase are modified as the wavefront encounters random small-scale velocity deviations from the mean value. If we place a receiver array outside the medium, phase fluctuations are recorded as variations in traveltime of the first arrival from the value expected for a homogeneous velocity structure (Muller *et al.*, 1992). In the same way, amplitudes show large variations across the receiver array. If a mathematical relation between these observed fluctuations and the distribution and magnitude of the medium fluctuations can be established, wave fluctuations can be used to deduce the scattering properties of the medium (Shapiro & Hubral, 1999), such as the scattering mean free path l and the diffusion coefficient D.

If we have access to one seismogram only, it is difficult to estimate the scattering properties due to the fluctuations in the wavefield that propagates though a strongly scattering medium. If, on the other hand, we have an ensemble of seismograms, average measures can be used to estimate the statistical properties of the medium. For a medium with random velocity fluctuations and homogeneous statistical properties, the scattering properties can be obtained from the average wavefield and average intensity.

Coda waves are waves that have longer effective paths than the ballistic wave, and they make up the later portions of the seismograms (Herraiz, 1987). The further the waves travel, the greater the variety of heterogeneities they encounter (Aki & Chouet, 1975). As a consequence of this, for longer paths, the coda waves sample a larger region of the medium and the net effect on the transmitted energy will be an average over the many fluctuations that the wave encountered along its path. Also, the stronger the scattering the more complicated are the paths that the waves follow.

Usually, a straightforward deterministic interpretation of the scattered wavefield propagated through random media is difficult because of the high sensitivity of these waves to the wave paths (Foldy, 1945). This high sensitivity to the wave paths and to small perturbations in the average properties of the medium is what makes coda waves useful to detect small changes in the medium (Weitz & Pine, 1993). To avoid the complexity of the multiple paths, it is useful to resort to a statistical treatment of the heterogeneities in the medium (Chernov, 1960). In this study the problem of the multiple scattering of scalar waves by

a random distribution of scatterers is considered on the basis of ensemble averages of the wavefield and intensity over the randomness of the medium.

Ensemble averaging strictly implies that a set (i.e., an ensemble) of different media is supposed to exist (Shapiro & Hubral, 1999). Each element in the ensemble is called a realization of the random medium. In order to obtain an ensemble average of any wavefield attribute (as e.g. the traveltime fluctuation) this attribute has to be computed for each realization and then averaged over realizations of the random medium (Tourin *et al.*, 2000). The introduction of the concept of "randomness" requires averages to be taken over a statistical ensemble of scatterer configurations.

In this study, ensemble averaging is used as a tool to simplify and to obtain estimates of wave transport parameters as are the energy velocity v_e, the scattering mean free path l and the diffusion coefficient D. Usually, we only have one realization of the random medium. This realization is assumed to be a "typical" one belonging to a random *ergodic* medium. Ergodic means that ensemble averaging can be replaced by spatial averaging in a single realization. In our study we perform the averaging over different receiver locations around the source for our random media.

2.6.1 Average wavefield: Group and Energy Velocities

When scattering is strong, it is difficult to define a unique energy transport velocity v_e since the energy flux is distributed in all directions due to multiple scattering. As the waves propagate through the medium, they are scattered by the random heterogeneities and the ballistic pulse is attenuated and broadened with distance. The ballistic pulse corresponds to the coherent energy transmitted in the forward direction as the pulse propagates through the random medium. This is the velocity which characterizes the transport of energy in a multiple scattering medium.

The coherent pulse can be obtained after averaging the wavefield over many realizations of the random media. With our finite-difference seismograms, we average over different receiver locations in the circular array for a single realization of the random medium. Since the medium is statistically homogeneous, by averaging over different source receiver pair we are indeed averaging over different realizations of randomness. We analyze the coherent wavefield for models with different random velocity fluctuations. This ensemble averaged wavefield describes the ballistic contribution, since the scattered field cancels out in the limit as a result of configurational averaging (Zhang & Sheng, 1999).

The attenuation due to scattering introduces dispersion and as a result waves of different frequencies travel at different speeds. This type of dispersion arises because waves of different frequencies see the medium in different ways. For our medium with a small correlation length a, waves of higher frequencies are scattered more severely than lower frequency waves, and as a result the higher frequencies waves are slowed down in comparison to the lower frequency waves. This type of dispersion is called normal (Stein & Wysession, 2003), because waves of higher frequencies travel slower than waves of lower frequencies. Thus, when the medium is dispersive (as is our case) waves of different frequencies have different *phase velocities.*

For a medium with strong scattering, the *group velocity* differs from the phase velocities at which individual harmonic waves travel (Page & Schriemer, 1997; Cowan *et al.*, 1998). The group velocity v_g for a given frequency band around a central frequency follows from the dispersion relation (Elmore & Heald, 1969; Stein & Wysession, 2003)

$$v_g(\omega) = \frac{d\omega}{dk}, \tag{2.17}$$

where ω is the angular frequency and k is the wavenumber. The group velocity is generally the velocity with which the coherent or ballistic pulse travels through the medium. The ballistic or coherent pulse corresponds to the coherent energy first arriving at the detectors. In a pulsed experiment, this ballistic signal carries important information about the medium, including the behavior of the phase and group velocities, as well as the scattering mean free path l. When scattering is not too strong, the waves behave diffusively and the energy velocity v_e, which corresponds to the average local velocity of energy transport in the diffusion process (Schriemer *et al.*, 1997), is approximately equal to the group velocity v_g.

Dispersion causes the ballistic or coherent pulse to travel with the group velocity. In Figures 2.7 and 2.8 we show the ballistic pulses extracted from the calculated average seismograms for media with different magnitude of the velocity fluctuations σ. The autocorrelation distance is a= 40 m. We also show the frequency spectra for each ballistic wave so that we can appreciate the effects of attenuation and dispersion. The ballistic wave for different propagation distances is superposed in the same plot, the smaller the amplitude the larger the propagation distance. Note that in the homogeneous velocity case (top-left panel on Figure 2.7) the ballistic pulse does not show any change with distance except attenuation caused by geometrical spreading. The corresponding frequency spectra (top-right panel) shows that the frequency content is the same for all propagation distances. The same holds for the medium with σ=0.05 (bottom of Figure 2.7) where the scattering is weak and only a small amount of dispersion occurs at large propagation distances where the peak of the frequency spectra is slightly shifted to the lower frequencies.

In Figure 2.8 we show the ballistic pulses and frequency spectra for random media with σ=0.15 (top) and σ=0.25 (bottom) respectively. In this case the dispersion is strong and the ballistic pulse is broadened significantly as it propagates through the random media. The frequency spectra are also strongly modified, the ballistic pulse showing a much smaller frequency content than in the homogeneous case. Note that the peak of the frequency distribution is shifted to the lower frequencies when compared to the dominant frequency in the homogeneous case (indicated by the vertical lines in the frequency spectrum plots).

In this study we assume that the scattering is not very strong; in this case, the energy transport velocity and the group velocity are approximately the same. We will concentrate in the group velocity v_g which is the velocity with which the coherent energy pulse travels through the scattering media. This velocity can be obtained by measuring the traveltime of the ballistic pulse as we change the source-receiver separation. When scattering is very strong, there is no ballistic pulse and the group velocity loses its meaning. When this happens, the scattered energy is strong, and the peak of the envelope of the total intensity is shifted in time, giving the slower energy velocity v_e. Thus, the energy and group velocity

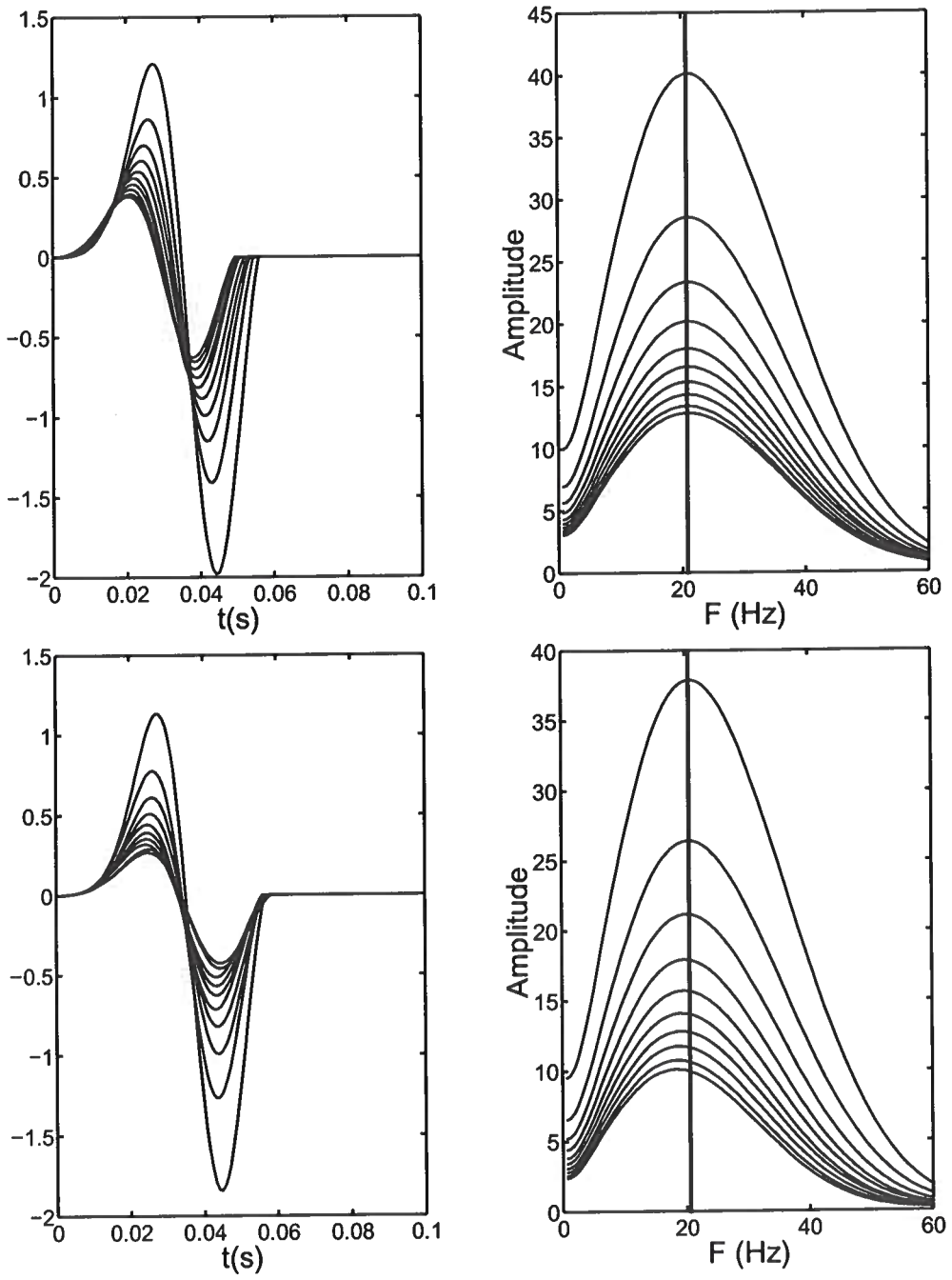

Figure 2.7. Ballistic wave (left) and frequency spectrum (right) for a medium with constant velocity (top) and for a medium with random velocity fluctuations with σ=0.05 (bottom). Different curves correspond to different source-receiver distances.

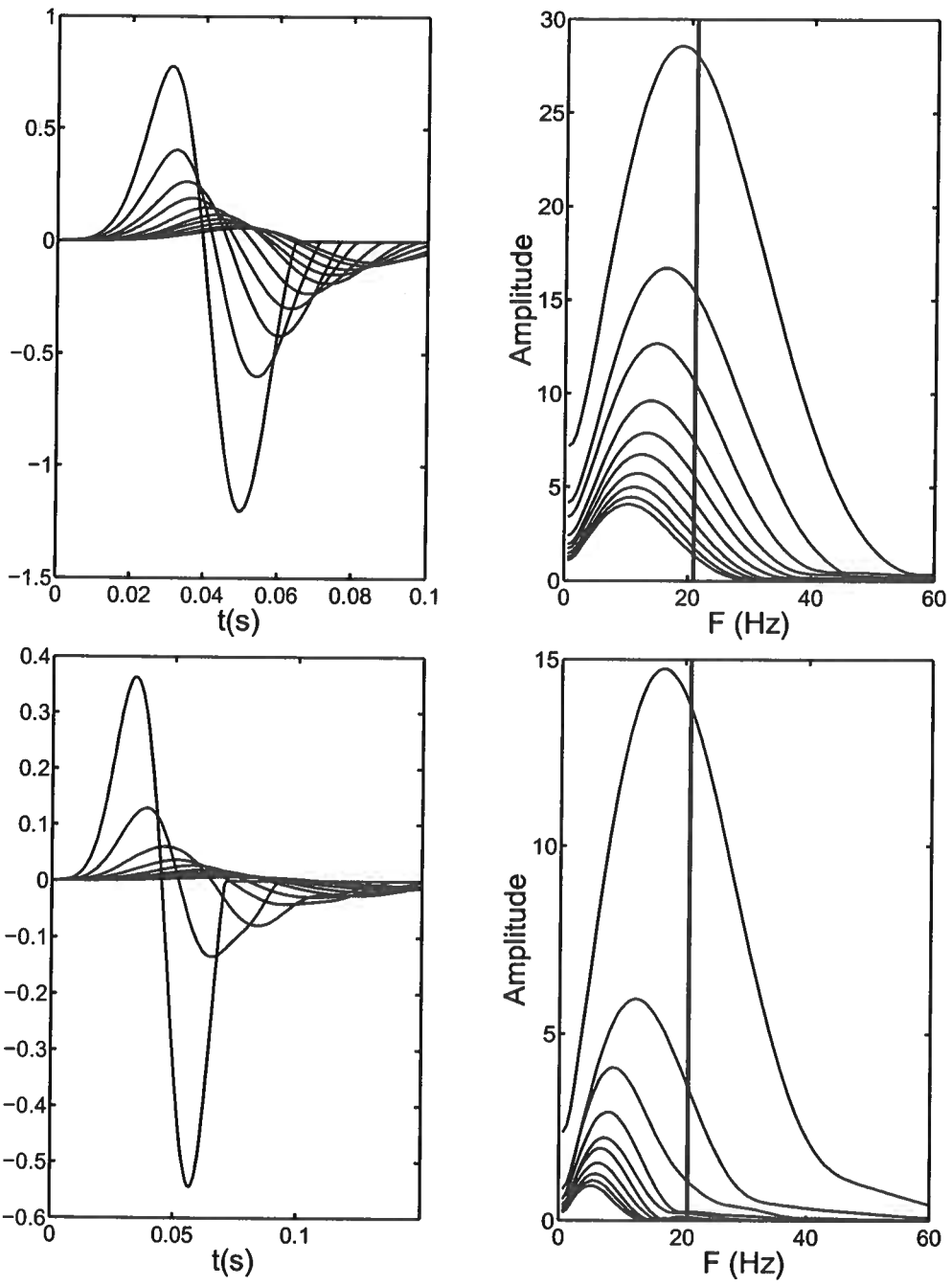

Figure 2.8. Ballistic wave (left) and frequency spectrum (right) for a medium with random velocity fluctuations with σ=0.15 (top) and σ=025 (bottom). Different curves correspond to different source-receiver distances.

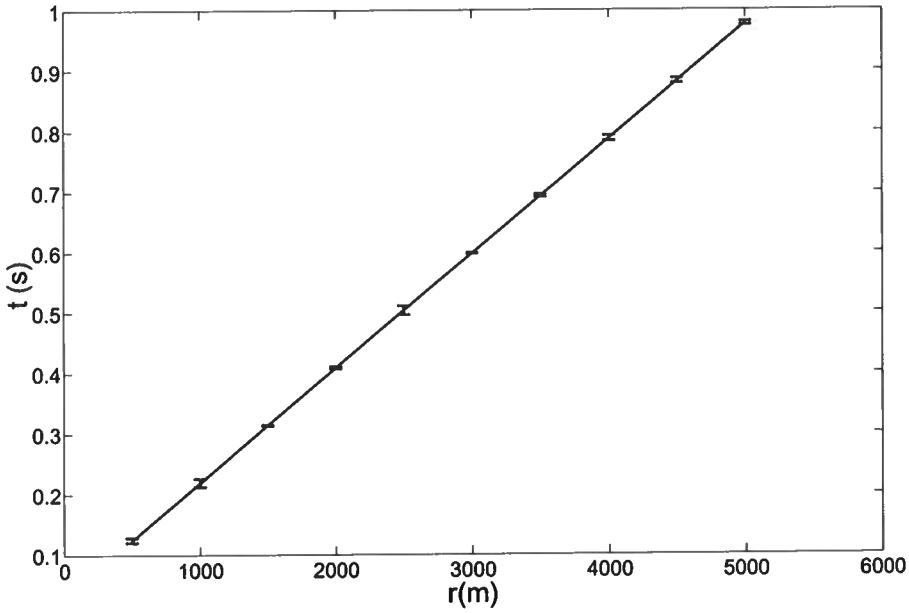

Figure 2.9. Arrival times of the maximum of the coherent energy as a function of offset r for a model with Gaussian probability distribution velocity fluctuations; the measured value of the group velocity is v_{group}=(5280 $\pm$ 25) m/s when a=40 m and σ_v=1500 m/s. The error bars are also shown but the error in the estimation is very small.

are approximately the same except when scattering is strong and the propagation distance is much larger than the transport mean free path ($r >> l^*$).

We estimate the group velocity by measuring the speed with which the coherent or ballistic pulse propagates through the scattering medium. The coherent energy is calculated for each source-receiver distance by squaring the coherent or ballistic wavefield, and the coherent envelopes are calculated using the Hilbert transform. The peaks of these envelopes are automatically picked and the times taken to be the arrival times of the ballistic pulse. This gives an arrival time for each pulse, the set of which is fitted with a straight line as a function of source-receiver distance to arrive at the group velocity.

Figure 2.9 shows the arrival times of the maximum coherent energy for each source-receiver separation and the regression through the arrival times. For a model with correlation distance a=40 m and standard deviation of the velocity fluctuations σ=0.25 m/s, the measured group velocity is v_e=5280 $\pm$ 25 m/s. We repeat the same procedure for the synthetics calculated for different random velocity fluctuation models and the results are given in Table 2.1.

In a medium with large random velocity fluctuations the group velocity decreases due to two main reasons: first, the mean or average slowness $\bar{s}$ is larger than the inverse of the mean velocity, creating an effective velocity $1/s_0$ which is smaller than the mean velocity v_0; second, waves propagating on a multiple scattering medium have longer effective paths due

Table 2.1. Group (v_g) and effective velocities ($1/s_0$) for a medium with random fluctuations with Gaussian probability distribution. $v_0 = 6000m/s$ is the background or mean velocity; a is the correlation length and σ=σ_v/v_0 is standard deviation of the velocity fluctuations.

a (m)	σ	v_g (m/s)	$1/s_0$ (m/s)
40	0.01	5995 ± 3	5999
40	0.02	5992 ± 3	5997
40	0.03	5988 ± 3	5994
40	0.05	5973 ± 3	5985
40	0.07	5945 ± 3	5970
40	0.10	5900 ± 4	5940
40	0.15	5753 ± 7	5867
40	0.20	5551 ± 16	5769
40	0.25	5280 ± 25	5647
100	0.15	5750 ± 29	5867
100	0.25	4050 ± 500	5647
140	0.25	4203 ± 300	5647
200	0.25	4454 ± 400	5647

to the multiple bounces of the wave with the scatterers. In addition, the ballistic wave is the result of the contribution of waves from different paths scattered in the forward direction and interfering constructively to create the broadened ballistic pulse. As a result, in the multiple scattering medium characterized with continuous random velocity fluctuations, the coherent or ballistic pulse is broadened and propagates with a velocity that is slower than the mean velocity v_0.

Let us consider first the effective velocity obtained by taking the inverse of the mean slowness. The traveltime of the ballistic wave can be calculated by integrating the slowness multiplied by distance along the trajectory from the source to the receiver. A larger value of the mean slowness s_0 implies a larger traveltime. Therefore, in a medium with continuous random fluctuations in the velocity, waves propagate in the average with an effective velocity which is equal to the inverse of the mean slowness s_0. To see why the effective velocity $1/s_0$ is smaller than the mean velocity v_0, let us consider again our velocity field with fluctuations with Gaussian autocorrelation function defined on Eq. 2.14. The slowness field $s(\mathbf{r})$ is obtained after taking the inverse of the velocity field $v(\mathbf{r})$. Thus,

$$s(\mathbf{r}) = \frac{1}{v(\mathbf{r})} = \frac{1}{v_0\left[1 + \frac{v_r(\mathbf{r})}{v_0}\right]}, \tag{2.18}$$

where v_0 is the mean velocity and $v_r(\mathbf{r})$ is the random component of the velocities. This random component has zero mean and standard deviation σ_v. Since $v_r(\mathbf{r})/v_0$ is smaller

than one, we can expand the right hand of Eq. 2.18 in a geometric series about $v_r(\mathbf{r})/v_0$, i.e.

$$s(\mathbf{r}) = \frac{1}{v_0}\left[1 - \frac{v_r(\mathbf{r})}{v_0} + \frac{v_r^2(\mathbf{r})}{v_0^2} + ...\right], \tag{2.19}$$

where we have truncated the series after the third term. If we calculate the ensemble average over all possible values of $s(\mathbf{r})$ we obtain the ensemble averaged or mean slowness s_0

$$< s(\mathbf{r}) >= s_0 =< \frac{1}{v_0} > - \frac{1}{v_0^2} < v_r(\mathbf{r}) > + \frac{< v_r^2(\mathbf{r}) >}{v_0^3} + ... \tag{2.20}$$

Since $v_r(\mathbf{r})$ has zero mean and recognizing that $< v_r^2(\mathbf{r}) >$ is the variance of the random velocity fluctuations we obtain:

$$s_0 \approx \frac{1}{v_0} + \frac{{\sigma_v}^2}{v_0^3} = \frac{1}{v_0}\left[1 + \frac{{\sigma_v}^2}{v_0^2}\right] = \frac{1}{v_0}(1 + \sigma^2). \tag{2.21}$$

Since σ^2 is positive we have thus that the mean slowness is greater than the inverse of the mean velocity v_0. Consequently, the "effective" velocity obtained after taking the inverse of the mean slowness is smaller than the mean velocity v_0. In the left panel of Figure 2.10 we plot (as the solid line) the value of this effective velocity $1/v_0$ as a function of the relative fluctuations of the velocity fluctuations σ. We can see that as σ increases this effective velocity decreases.

We also measure the velocity of the ballistic pulse on the synthetic seismograms for different values of σ and a. The group velocity obtained by this procedure is significantly smaller than both the mean velocity v_0 and the effective velocity $1/s_0$. In Figure 2.10 we plot the measured the value of the group velocity as a function of σ (left-panel) and a (right-panel). For small values of the correlation length a and the standard deviation σ, the energy velocity does not differ much from the mean or background velocity v_0. For a medium with small correlation length a and small magnitude of the velocity fluctuations σ, the coherent or ballistic arrival does not undergo much attenuation and dispersion due to scattering. As we increase the magnitude of the velocity fluctuations, the scattering grows stronger and the coherent pulse is strongly attenuated and slowed down.

For larger values of the correlation distance a, the scatterer size becomes comparable to the wavelength, and the shape of the heterogeneity affects the scattering properties of the medium. In general, for the range of models in this study, the larger the correlation length a and standard deviation σ, the larger the dispersion and the more difficult it is to measure the velocity of the ballistic pulse, and the larger also the uncertainty of the measure. For very strong scattering the ballistic pulse is extremely attenuated and distorted at large source-receiver separations and thus the velocity of the ballistic pulse becomes an unreliable measure of the energy or transport velocity in the medium (Page & Sheng, n.d.).

The scattering dispersion and attenuation of the ballistic pulse is a good indicator of the scattering regime. When scattering is weak (single scattering regime) the group and transport velocity are equal to the mean velocity of the medium and the ballistic pulse propagates through the medium without much distortion. As we move into the multiple

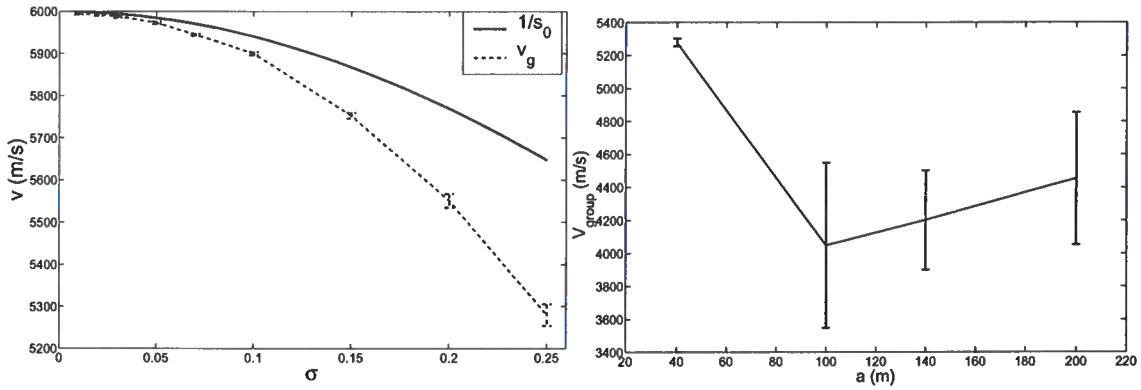

Figure 2.10. Group velocity v_g (measured on the synthetic seismograms) and effective velocity $1/s_0$ (calculated using Eq. 2.21 as a function of σ (left). The correlation distance is a= 40 m. The right panel shows the values of the group velocity for σ=0.25 for different correlation lengths a.

scattering regime, the characteristic velocity of energy transport decreases and the ballistic wave is severely attenuated and broadened.

2.6.2 Coherent Wavefield: Attenuation

The coherent wavefield is mathematically defined as the average field amplitude and denoted by $\langle u(\mathbf{r},t)\rangle$. By the "average" is meant a statistical average over all possible realizations of the scatterers. Physically, the coherent wave corresponds to the remnant of the incident wave. In fact, the many multiple scattering events in the medium add up to the "coherent" wave, which does not seem to be "scattered" at all. It only decays in space and time, and its velocity is changed. The previous section dealt with the change in the velocity. Here we focus on the decay resulting from the scattering process. The decay in space and time, mathematically due to the averaging, can be associated physically with the randomization of the phase.

The scattering mean free path l is associated with the decay of the coherent pulse. It also provides the propagation distance that separates the single and the multiple-scattering regime. In general, for propagation distances much smaller than the scattering mean free path ($ct << l$), the wavefield can be approximated as the result of a single scattering process. On the other hand, for propagation distances much longer than the scattering mean free path ($ct >> l$) the energy transport can be taken as a diffusion process (Paasschens, 1997), where multiple-scattering dominates the signal.

The scattering mean free path l is the parameter that controls the energy transferred from the primary (ballistic) to the scattered waves. This scattering attenuation is not a true loss resulting from dissipation but rather a loss that is the result of the energy that conservatively scatters into other directions (Turner, 1998). Thus, the energy in a beam propagating in a particular direction decays, but the total energy in the system is conserved.

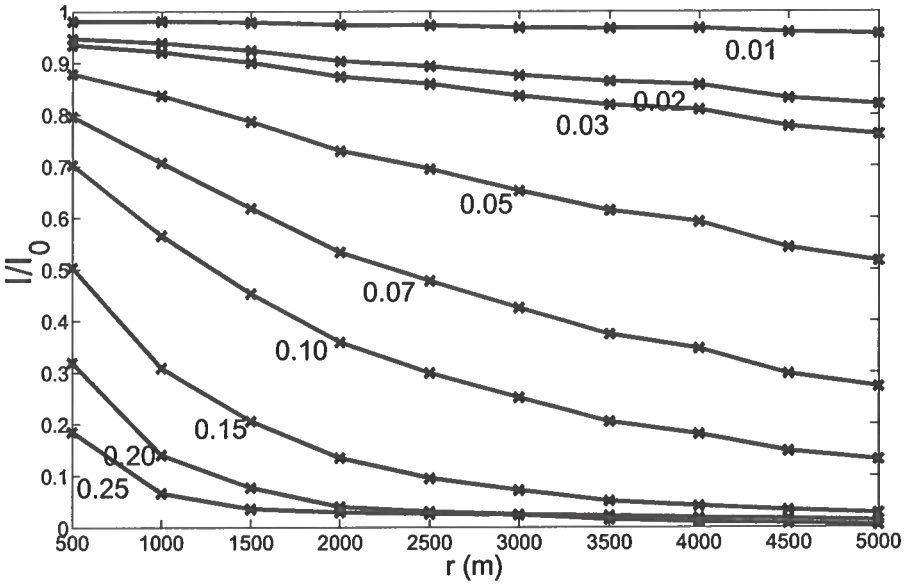

Figure 2.11. Measured intensity ratios I/I_0 versus propagation distance r for different values of the standard deviation of the random fluctuations σ. The numbers under each curve indicate the value of σ. The correlation distance a is 40 m.

The scatterers reduce the mean energy flux of an incident plane wave by $e^{-r/l}$, r being the distance along the propagation direction. When there is neither intrinsic nor scattering attenuation, the transmitted intensity in a 2D homogeneous medium at a distance r from the source is

$$I_0(r) = C\frac{1}{r}, \tag{2.22}$$

where C is an arbitrary constant that denotes the intensity at the source. For a point source in a homogeneous random medium, the decrease of the coherent intensity with distance is an exponential decay modified by geometrical spreading. For two-dimensional wave propagation, the transmitted coherent intensity is given by

$$I(r) = C\frac{e^{-r/l}}{r}. \tag{2.23}$$

The ratio between the transmitted coherent intensity in a homogeneous random medium with background v_0 and the transmitted intensity in an homogeneous medium with velocity v_0 gives the scattering attenuation of the transmitted intensity. This ratio is obtained after dividing Eq. 2.23 with Eq. 2.22

$$\frac{I}{I_0}(r) = e^{-r/l}. \tag{2.24}$$

Thus, in general, scattering causes an exponential decay of the coherent intensity I

Table 2.2. Scattering mean free path l for a medium with random fluctuations with Gaussian probability distribution. $v_0 = 6000m/s$ is the background or mean velocity; a is the correlation length and $\sigma = \sigma_v / v_0$ is the normalized standard deviation of the velocity fluctuations.

$a\ (m)$	σ	$l\ (m)$
40	0.01	61200 ± 7000
40	0.02	21050 ± 792
40	0.03	16034 ± 456
40	0.05	7189 ± 119
40	0.07	3886 ± 86
40	0.10	2609 ± 87
40	0.15	1657 ± 95
40	0.20	1224 ± 97
40	0.25	867 ± 90
100	0.15	1198 ± 70
100	0.25	799 ± 52
140	0.25	948 ± 75
200	0.25	1217 ± 209

with propagation distance r. Let us now consider the limit when $l >> r$, which represents the single scattering regime (Herraiz, 1987). In this case, the argument of the exponential is much smaller than 1 and we can approximate the exponential by the first two terms of its power series

$$e^{-r/l} = 1 - \frac{r}{l}. \tag{2.25}$$

According to Eq. 2.25, when the scattering is weak (single-scattering approximation), the decay of the transmitted intensity is approximately linear. This equation provides a test for single-scattering. We performed this test for our finite-difference synthetic seismograms in order to estimate whether or not the energy transfer can be modeled by means of the single scattering approximation. In Figure 2.11 we plot the measured intensity ratios from the finite-difference simulations for different values of the standard deviation of the velocity fluctuations σ. We can see that when the scattering is weak (σ less than 0.05), a straight line seems to be a good fit for the decaying transmitted intensity.

Now, we measure the scattering mean free path to obtain a measure of the scale lengths by which we can separate the single and the multiple scattering regime. To measure the scattering mean free path we have to correct the transmitted coherent wavefield for geometrical spreading and fit the transmitted coherent intensity with an exponential decay. We followed that procedure with our finite-difference synthetics and obtained a measure of the scattering mean free path l for the same velocity models employed in the previous section.

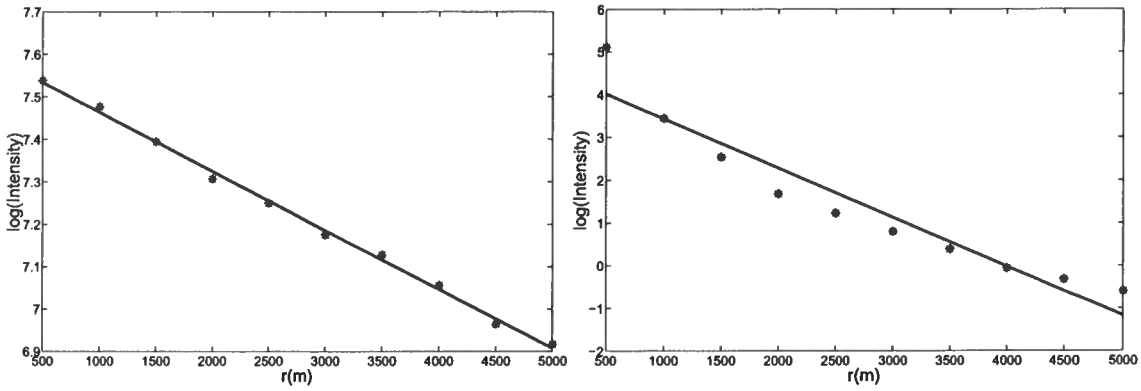

Figure 2.12. Plot of the natural logarithm of the maximum coherent intensity as a function of distance r. The data and the best fit is shown for two continuous random velocity models with different values of the standard deviation of the velocity, σ=0.05 (left) and σ=0.25 (right). The correlation distance is a= 40 m. The asterisks denote the measured maximum amplitudes of the coherent transmitted pulse. The lines indicate the best fitting exponential.

The results are summarized in Table 2.2. In general, the exponential decay describes well the attenuation of the coherent pulse. For a fixed value of a (see left panel of Figure 2.13) the scattering mean free path decreases with increasing σ, which is an indication that the scattering is stronger for bigger values of the velocity fluctuation. Also, the accuracy of the estimation decreases for increasing values of the velocity fluctuations, and for values of σ greater than 0.15 the error in the measurement becomes larger than 6% of the scattering mean free path.

When scattering is strong, the exponential decay no longer describes accurately the attenuation of the ballistic pulse. This is to be expected, because scattering attenuation and dispersion affect severely the transmitted coherent pulse, broadening the wavelet signal and affecting the frequency content of the signal. As the frequency content of the pulse changes due to dispersion, so does the scattering mean free path. Thus, in the presence of dispersion the scattering mean free path becomes frequency dependent. Figure 2.12 shows the peak amplitude of the ballistic pulse and the best fitting exponential for examples of velocity models with weak and strong scattering respectively. Note that for the case of weak scattering we can fit the exponential decay due to scattering. However, when the scattering is strong and multiple scattering is dominant, the exponential decay is no longer a good fit. The reason for this is again the dispersion and resonant scattering that introduce frequency dependence in the scattering mean free path l. We see that the scattering mean free path obtained from the decay of the coherent pulse is no longer a good estimate for propagation distances longer than the scattering mean free path.

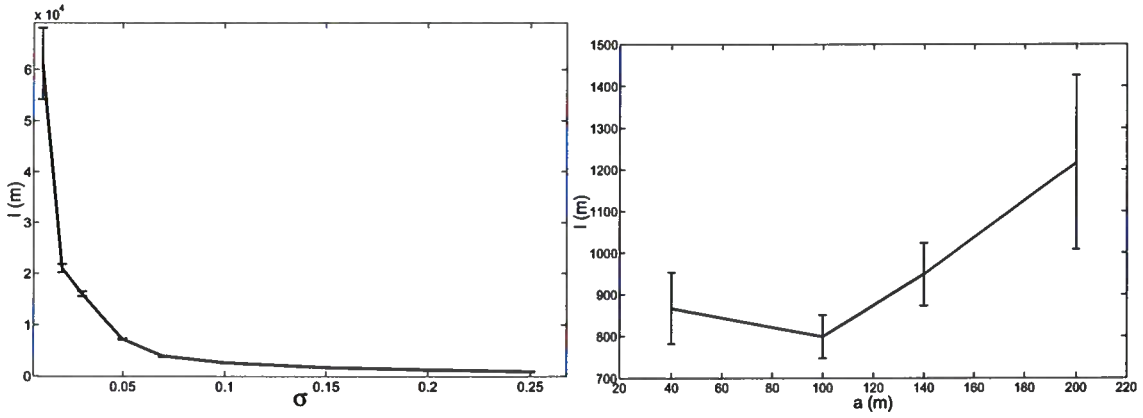

Figure 2.13. Dependence of the mean free path l on σ and a. On the left panel the mean free path is plotted as function of σ for a= 40 m. The right panel shows the values of the mean free path for σ=0.25 for different correlation lengths a

2.6.3 Average intensity: Diffusion constant

In Section 2.2.3 we showed that the evolution of the diffuse intensities can be described by means of the diffusion equation. Therefore, measures of the average intensity which describe the time-dependence of the diffusive intensity can be used to estimate either the transport mean free path l^* or the diffusion constant of the medium D (Page & Sheng, n.d.; Schriemer *et al.*, 1997), using either the radiative transfer equation or the diffusion equation. The transport mean free path is usually larger than the scattering mean free path l and it represents the average distance at which the direction of propagation becomes randomized. The diffusion constant D and the transport mean free path are related by the energy transport velocity in two-dimensional media in the following way:

$$D = \frac{v_e l^*}{2}. \tag{2.26}$$

The diffusion coefficient can be obtained from the incoherent (or diffuse) intensities. The incoherent wavefield consists of waves that have been scattered by the random heterogeneities of the medium. It is usually assumed that the phase of this incoherent wavefield is randomized after the waves have traveled through the medium for a few scattering mean free paths l (Margerin *et al.*, 1998). This incoherent wavefield corresponds to diffuse waves generated by multiple scattering . Each wave in the coda follows a different diffuse path which can be characterized as a random walk as we saw in Section 2.3.3 . Tourin *et al.* (2000) shows that on the average the energy transfer of the incoherent field obeys the diffusion equation. The spatial and temporal evolution of the average intensities $\langle I(r,t)\rangle$ can

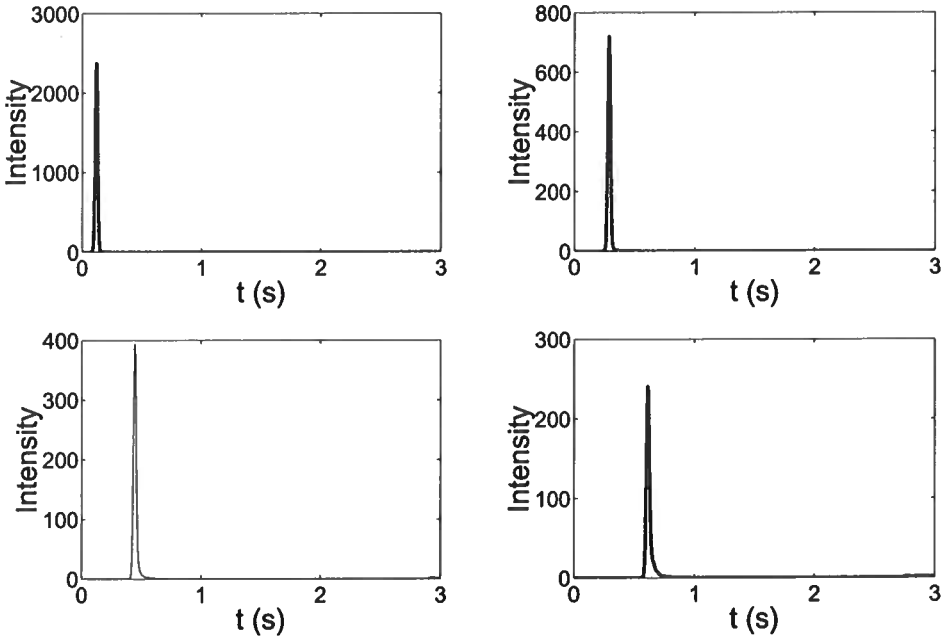

Figure 2.14. Averaged transmitted intensities for receivers at 500, 1500, 2500 and 3500 m from the source for a weakly scattering medium ($\sigma = 0.02$). Almost all energy is contained in the incident pulse.

be described with the solution of the diffusion equation

$$\frac{\partial \langle I(r,t) \rangle}{\partial t} = D\nabla^2 I(r,t), \tag{2.27}$$

with solution given by

$$1\langle I(r,t) \rangle = \frac{1}{4\pi D t} \exp\left[\frac{-r^2}{4Dt}\right], \tag{2.28}$$

where r is the distance to the source and D is the diffusion constant. Eq. 2.28 is valid for media with strong scattering and small intrinsic attenuation. Thus, we see that the average intensity satisfies the same equation as the probability a Brownian particle in an statistically homogeneous medium.

In Figure 2.5 we showed the transmitted wavefield for two different velocity models, one characterized by weak scattering (top) and the other characterized with strong scattering (bottom). In the weak scattering model the ballistic arrival dominates the seismograms, with weaker scattered arrivals coming after the direct wave. In this case we can model the wave propagation as a single-scattering process where the loss of energy of the incoming pulse is minimal. For the strong scattering model, the ballistic arrival is highly attenuated by scattering and the multiple scattering events dominate the signal. In the latter case, it is possible to model this incoherent energy with the diffusion equation. In this section we

obtain an estimate of the diffusion constant D from the averaged transmitted intensities in a medium characterized by multiple scattering.

The time evolution of the averaged intensity of the synthetic seismograms is determined by squaring the envelope of the calculated waveforms for each distance. As we have an ensemble of 100 detectors for each distance, we perform averaging over the 100 receivers located around the source at distance r. Again, we assume that each source-receiver pair samples a different region of the random medium with homogeneous statistical properties. This gives the time evolution of the average intensity for each source-receiver offset. Then, we fit for each source-receiver distance the averaged intensities with the solution of the diffusion equation. As the diffusion coefficient is a constant of the medium we expect the diffusion coefficient to be the same for each source-receiver offset. The estimated diffusion constant is obtained after averaging the values of the diffusion constant estimated for each source-receiver offset.

Figure 2.14 shows the calculated average intensity for a medium with weak scattering ($\sigma = 0.02$). The intensity is shown as a function of time for four different distances: 500, 1500, 2500, and 3500 m respectively. The main contribution to the total intensity comes from the ballistic arrival which shows almost no energy loss except for geometrical spreading. From the last section we learned that the scattering mean free path of this medium is much larger than the propagation distances we use in this experiment. From Section 2.3.1 we know that when this is the case, single-scattering dominates the signal as the energy transfer from the ballistic arrival to the scattered waves is negligible.

In Figure 2.15 we show the total intensity for two models with stronger scattering. Both models share the same correlation length a=40 m, but the standard deviation of the fluctuation differs, σ being 0.15 and 0.25 respectively. For σ=0.25 we are in the diffusion regime ($r > ct$) where the energy transport is described by the diffusion equation and the signal is dominated by multiple scattering. Notice that we obtain a good fit of the intensities with the diffusion curve. The diffusion coefficient estimated is D=(5.80±0.51)×10^5 m^2/s. We show an example of the intermediate regime between the single-scattering and the diffusion regime at the top of Figure 2.15, when σ=0.15. In this case, a crossover between the ballistic and the diffuse transport occurs. The ballistic energy is still strong, but the behavior at long lapse times is well described by the diffusion equation. This departure from the diffusive behavior is usually accounted for with the radiative transfer equation which has in general two terms: one that describes the ballistic propagation, and, other that describes the diffusion behavior at later times (Paasschens, 1997; Margerin *et al.*, 1998). However, for this model we can still fit the later-time portion of the time-intensity profile which shows perfectly diffusive behavior, with an estimated diffusion constant of (3.02±1.80)×10^6 m^2/s. In both cases, the error was determined by measuring the relative deviations from the best fitted curve and calculating the mean square error of these deviations.

2.7 Discussion

The transition of ballistic to diffusive energy transport in random media is studied for 2D random media characterized by the spectrum of its velocity fluctuations. Understanding

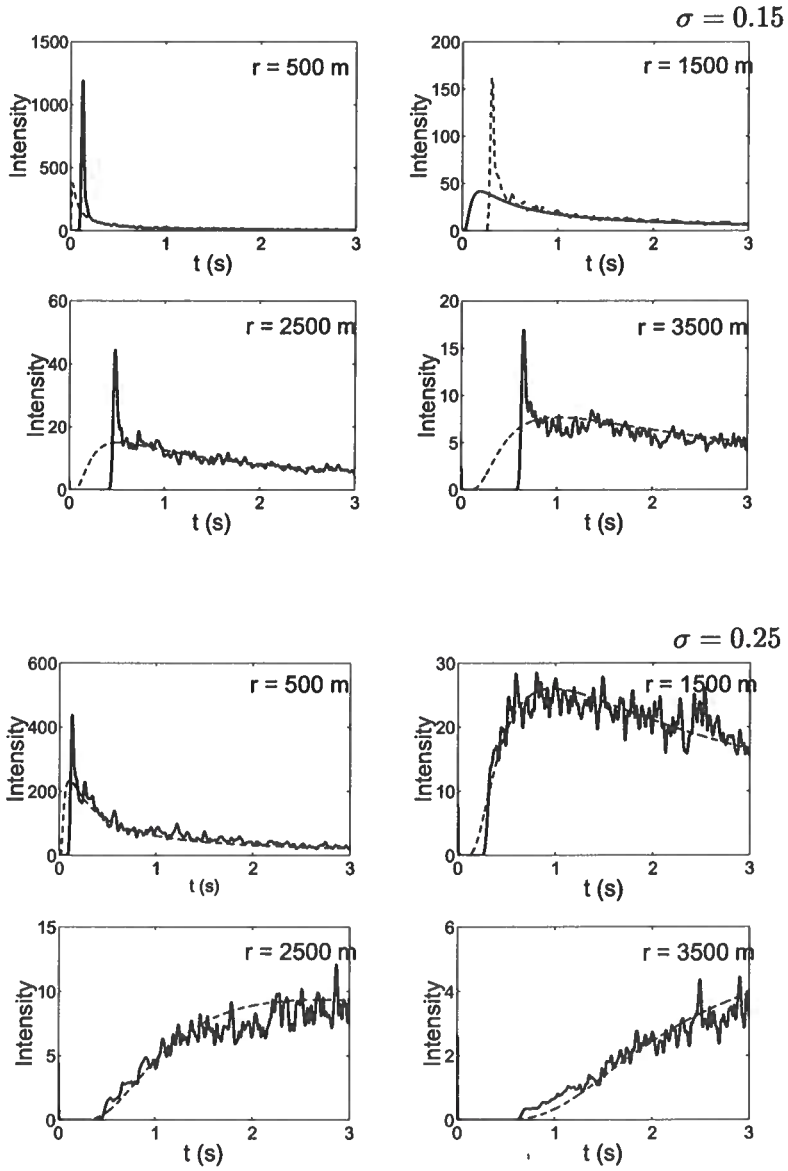

Figure 2.15. Averaged transmitted intensities (solid line) versus the diffusion fit (dashed line) for receivers at 500, 1500, 2500 and 3500 m from the source. Two velocity models with Gaussian probability distribution fluctuations were employed: one with a=40 m and σ=0.15 (top); other with a=40 m and σ=0.25 (bottom). The diffusion values obtained from the least-squares fit are $(3.02\pm1.80)10^6$ m^2/s and $(5.80\pm.51)10^5$ m^2/s respectively.

the transition between the single-scattering and the multiple-scattering behavior is essential for many applications such as medical imaging, ultrasonics and non-destructive testing of highly heterogeneous media. In this study we adopted a phenomenological approach to understand the transition between the ballistic to the diffusive behavior of the energy transport, using synthetic seismograms calculated by finite-differences over media with random variations in its velocity that characterize the scattering.

We studied wave propagation in 2D random media using a model with continuous velocity fluctuations with Gaussian probability distribution. This medium is statistically homogeneous so that the ergodic property of random media can be applied. For large values of the standard deviation of the velocities, the scattering becomes strong and the energy transport can be described as a diffusion process. For larger values of the magnitude of the velocity fluctuations σ multiple scattering dominates over single scattering.

Chapter 3

TIME-LAPSE MONITORING WITH CODA WAVES: MULTIPLE-SCATTERING APPROXIMATION

3.1 Summary

We have developed a technique which uses multiply scattered waves that relates temporal changes in the acoustic velocity to changes in the phase of the multiply scattered waves. This study is an extension of a previous technique called coda wave interferometry where multiply scattered waves are used to detect temporal changes in the scattering medium. In this work the propagation of multiply scattered sound is described using the diffusion approximation, which allows us to relate the temporal fluctuations of the wavefield to the temporal change of the velocity of the scattering medium. Previous formulations of coda wave interferometry make it possible to assess the average change in the medium, but they do not allow for the spatial localization of this change. We present a new formulation that relates the change in the phase of the scattered wavefield to a localized velocity perturbation in a strongly scattering medium, and test it with synthetic seismograms calculated with finite-differences for 2D acoustic waves. Using the diffusion approximation for the energy transport in multiple-scattering media, we can accurately predict the change in the phase of the scattered wavefield given a localized velocity or slowness perturbation.

3.2 Introduction

Most imaging techniques using scattered waves rely on the single scattering approximation. Seismic imaging (Claerbout, 1985) mostly uses primary reflected waves to obtain an image of the subsurface. However, in many physical problems, waves are strongly scattered and the single scattering approximation is not a valid model for the propagation of waves through the medium. In such cases we have to use a model that accounts for the multiple scattering of waves and the associated attenuation. The diffusion model has been used with success to characterize a wide range of wave phenomena in strongly scattering media (Wesley, 1965; Kopnichev, 1977; Shapiro & Kneib, 1993; Page *et al.*, 1995b; Schriemer *et al.*, 1997). In this model, wave energy transport acquires a diffusive character, e.g., wave energy is transported in a process similar to heat diffusion. In medical imaging, for example, diffusing near-infrared light has been used to image localized heterogeneities of tissue (Yodh & Chance, 1995).

In many practical applications the medium changes over time and therefore the image of the medium will change. We then would like to obtain time-lapse measurements in order to monitor temporal changes in the medium. Examples of applications where detecting temporal changes may be useful include the monitoring of volcanoes, oil reservoirs, radioactive

waste disposal sites and fluidized suspensions. In reflection seismology, dynamic reservoir characterization provides optimal management of a reservoir, which leads to increased production. Time-lapse (4D) reflection seismic aims at inferring changes from the medium from changes in the seismic amplitudes and/or traveltimes from seismic reflection data that has been acquired at two different times. As an example, a 4D dataset recorded at Weyburn Field, Canada, has been used to infer time-lapse changes in the oil reservoir caused by a massive miscible CO_2 flood to enhance oil recovery (Li, 2003; Davis *et al.*, 2003). The main goal of these 4D studies is to extract information about local changes in the reservoir using mainly the amplitude information.

When a strongly scattering medium changes, the speckle pattern of multiply scattered waves changes, which reflects the changes that occur in the interference of waves traveling different scattering paths through the sample. Multiply scattered waves are useful in such situations, because they are increasingly sensitive with time to the perturbations in scatterer locations and perturbations in the velocity of the medium. This increased sensitivity is due to the fact that waves bounced more often among scatterers as time increases and as a result, small changes in the medium are amplified through multiple scattering.

More recently, multiply scattered or diffuse waves have been used to study the structure and dynamics of random media with applications to medical imaging and tomography (Weitz & Pine, 1993; Boas *et al.*, 1995; Jensen, 2002; Cowan *et al.*, 2002). Speckle pattern interferometry (Spagnolo *et al.*, 1996) uses the change in the spatial speckle pattern of interfering multiply scattered waves to retrieve the average change in the scatterer locations as a result of changes in the medium. This technique has been used to monitor Brownian motion in colloidal suspensions (Maret & Wolf, 1987), and the passage of ultrasound through a colloidal suspension (Cowan *et al.*, 2002).

In diffusing acoustic wave spectroscopy, the motion of the scatterers in fluidized suspensions is determined from the temporal fluctuations of multiply scattered sound (Cowan *et al.*, 2002) . In this technique the propagation of multiply scattered sound is described using the diffusion approximation. Using this approximation it is possible to relate the autocorrelation function of the temporal field fluctuations to the average motion of the scatterers in the fluidized suspension. In this case, the change in the multiply scattered waves generated by a transient incident wave is used as a diagnostic of the change in the scatterer locations. The same idea is used in coda wave interferometry (Snieder *et al.*, 2002; Snieder, 2002) where change in multiply scattered waves are used to detect minute changes in the medium. With this technique Snieder *et al.* (2002) determined the nonlinear dependence of the seismic velocity in granite on temperature.

However, in none of those approaches has an attempt been made to spatially localize the change in the medium. The inferred change in the scattering medium by both Cowan *et al.* (2002) and Snieder *et al.* (2002) is the average change of the medium. In this study we propose a new technique to spatially localize temporal changes in the medium using the phase of multiply scattered waves. As in diffuse wave spectroscopy this technique relies on the diffusion approximation of the intensity in strongly scattering media. With this formulation we can relate the temporal changes in the traveltime of multiply scattered waves to localized changes in the velocity of the medium. Therefore we can model the mean

traveltime change of waves with traveltime t for a given localized slowness perturbation that has been introduced in the medium at a later time T (T denotes the time scale on which the changes in the medium occur). It is assumed that $T >> t$, i.e., there are no changes in the medium during the propagation of waves (the medium is static during the experiment).

This work is an extension of coda wave interferometry in the sense that it accounts for spatially variable changes in the velocity of the scattering medium. Thus we are able to model the time-lapse fluctuation in the phase of the multiply scattered wavefield for a given localized time-lapse velocity perturbation of the multiple scattering medium. We assess the validity of our theory using finite-difference simulations of multiple scattering of acoustic waves in 2D media.

3.3 Multiple-Scattering Energy Transport

The transport of energy through a strongly scattering medium has attracted considerable attention in numerous fields of physics, such as astrophysics, optics, acoustics, solid state physics and heat conduction. In any of these fields, one can generate a pulse of energy that propagates through the medium with a certain intensity $P(r,t)$. In a two-dimensional medium of infinite extent, and in the long time limit (Paasschens, 1997), the average intensity can be approximated by the solution of the diffusion equation,

$$P(r,t) = \frac{1}{4\pi Dt} \exp\left[\frac{-r^2}{4Dt} - \frac{ct}{l_a}\right], \tag{3.1}$$

where r is the distance to the source and D is the diffusion constant, c is the energy velocity and l_a is the absorption length (attributable to intrinsic attenuation). For the purposes of this work, l_a^{-1}=0 because we ignore intrinsic attenuation. Eq. (3.1) represents the temporal evolution of the mean intensities after the waves have scattered multiple times from small-scale heterogeneities. Tourin and Fink (2000) have shown that the diffusion equation describes the propagation of the average intensity in a multiple scattering medium. In their approach, the average intensity is treated as the probability of traveling a distance r, varying with time, of a particle undergoing a random walk.

Large deviations from the diffusion approximation can be expected at any distance r, for times less than or close to the arrival time of the coherent or ballistic wave ($t \leq r/c$). Therefore, in order to use the diffusion approximation, we must be in the long-time regime where multiple scattering is assured (Paasschens, 1997). When the diffusion approximation is accurate, we can characterize the scattering with two parameters : the diffusion constant D, and the transport or energy velocity c. These two parameters are related to the transport mean free path l^* by

$$D = \frac{v_e l^*}{d}, \tag{3.2}$$

where d is the dimension of the problem (d=2 in 2D media).

When waves behave diffusively, waves propagate through the medium along various random scattering (or diffuse) paths which can be described as single random walks. The diffusion approximation provides a means to calculate the path distribution for a medium

with a given scattering coefficient. Also, the solution to the diffusion equation in homogeneous media given in Eq. 3.1 allows us to calculate the time and spatial evolution of the diffuse intensities in the material.

3.4 Coda Wave Interferometry

In order to localize changes in the scattering medium, we need to derive an expression relating the traveltime change with the localized velocity perturbations in the medium. Snieder(2002) introduced coda wave interferometry whereby multiply scattered waves are used to detect temporal changes in the medium by using the scattering medium as an interferometer.

For a small perturbation in the velocity, estimates of this perturbation can be obtained from multiply scattered waves by a time-windowed cross-correlation of the coda waves recorded before and after the perturbation. The unperturbed wavefield $u_{unp}(t)$ can be written as a summation of waves over all possible paths P (Snieder, 1999)

$$u_{unp}(t) = \sum_P A_P(t), \tag{3.3}$$

where a path P is defined by the sequence of scatterers that a particular multiple scattering wave encounters, and $A_p(t)$ is the corresponding waveform. For diffusive wave propagation the paths P can be described as random walks with a step length equal to the transport mean free path l^*. When we introduce a small perturbation of the velocity, the effect of this perturbation on the geometrical spreading and the scattering strength can be ignored, and the dominant effect on the multiple scattering waveform arises from the change in the traveltime τ_P of the wave that travels along each path

$$u_{per}(t) = \sum_P A_P(t - \tau_P). \tag{3.4}$$

The perturbation in the velocity was introduced after a time T which is much greater than the traveltime t of multiply scattered waves. Therefore, we assume there is no change of the scattering during the propagation of waves. The mean of the traveltime change $< \tau >$ can be extracted from the time windowed cross-correlation of the unperturbed and perturbed wavefield. This average traveltime change $< \tau >$ is defined later in Eq. 3.6. For a small change in the velocity , the velocity change follows from the time of the maximum of the time-shifted cross-correlation function (Snieder *et al.*, 2002),

$$\frac{\delta c}{c} = -\frac{\tau(t,T)}{t}, \tag{3.5}$$

where τ is the time shift of the time-windowed cross-correlation centered at time t with window size T, and c is the propagation velocity in multiple scattering media.

Eq. 3.5 relates the mean traveltime change of scattered waves with traveltime t with the velocity perturbation $\delta c/c$. This equation was used to estimate the change of seismic velocity

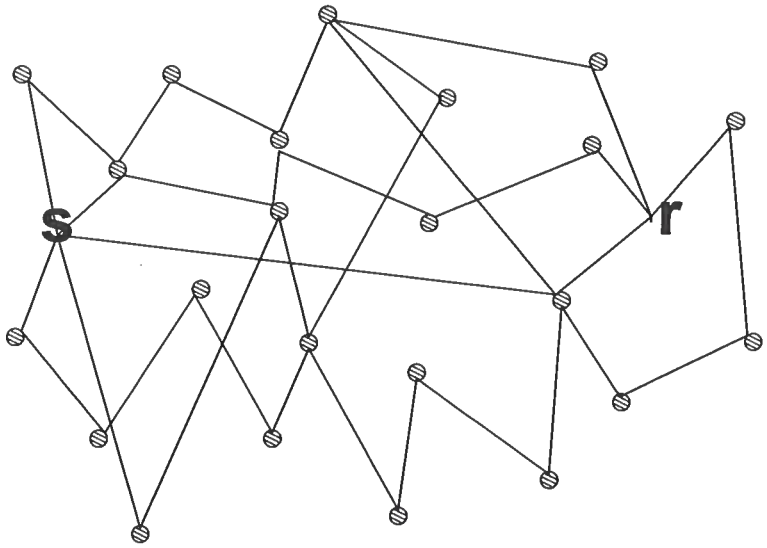

Figure 3.1. Multiple paths from source **s** to receiver **r** in a medium with multiple scatterers.

with temperature of a granite (Snieder *et al.*, 2002). However, the velocity perturbation was assumed to be constant throughout the scattering medium and therefore this expression is not valid for spatially localized changes in the velocity.

3.5 Traveltime Perturbations in the Diffusion Regime

In the strong scattering regime it has been shown that the transport of energy by the scattered waves is well described using the diffusion approximation. In this approximation the total wavefield u can be thought of as the summation over a multitude of possible paths. In the diffusion regime each of these diffuse paths can be characterized as a random walk process with a step length equal to the transport mean free path l^* which is related to the energy velocity v_e and the diffusion coefficient D by Eq. 3.2. Figure 3.5 shows a representation of medium with many scatterers and some of the diffuse paths that waves can follow from the source to the receiver.

Each path from source to receiver has an associated probability which depends on the diffusion of the intensities in a multiple scattering medium. In general the mean traveltime change $< \tau >$ is given by a weighted average of the traveltime change over different paths P, i.e.

$$\langle \tau(t) \rangle = \frac{\sum_P I_P \tau_P}{\sum_P I_P}, \tag{3.6}$$

where I_P is the probability associated with the path P and it can be calculated using the diffusion representation of multiply scattered intensities. A proof of this statement is given by Snieder(2002).

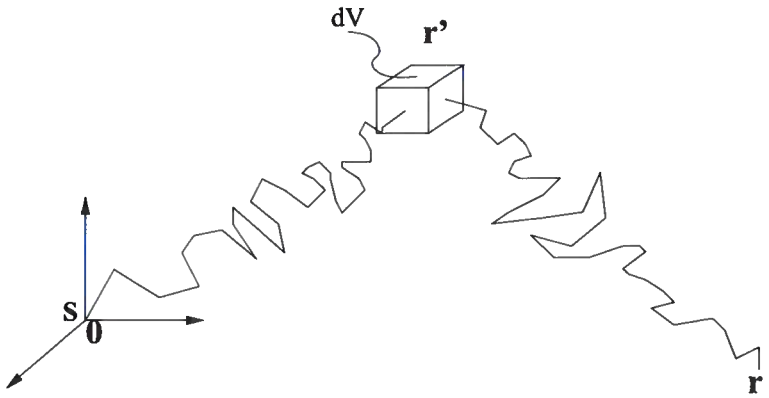

Figure 3.2. A random walk particle going from source **S** at the origin to volume element dV at $\mathbf{r}'$, and then to receiver at $\mathbf{r}$.

3.5.1 Random Walk Probability and Time of Flight Distribution

In this section we summarize the derivation of the traveltime change of diffuse waves caused by a spatially localized slowness perturbations. Let's assume that the seismic energy transport can be described as a random walk. This is a good approximation for a strongly heterogeneous media where multiply scattered waves are produced. Under this assumption, the averaged intensities in a multiple-scattering medium can be modeled as a diffusion process. Thus, the space and time evolution of diffusive intensity in the media due to an intensity impulse at the origin at time $t = 0$ is given by $P(\mathbf{r}, t)$, as defined in Eq. (3.1). In multiple scattering of waves this diffusive energy corresponds to the ensemble averaged or mean intensity $\langle I \rangle$.

We can interpret $P(\mathbf{r}, t)$ in different way, viewing the diffusion as a random walk process. In random walk theory,the product $P \times dV$ also represents the joint probability of time and position of a particle on a random walk of visiting a volume element dV at location $\mathbf{r}$ at a given time t Roepstorff (1994). If, at time $t = 0$, a normalized intensity impulse is generated at the source, the total energy within some region V at some later time is given by the integral

$$W(V,t) = \int_V P(r,t)dV(r). \tag{3.7}$$

Integration over all space gives the total energy of the system, which by the normalization is $W(t) = 1$. The quantity $W(V,t)$ is equal to the probability of a particle on a random walk of visiting the volume region V at a time t.

We now consider the probability that a random walk particle leaves a source at $\mathbf{s}$ at time $t = 0$, visits a volume element dV at $\mathbf{r}'$ at time t' and arrives at $\mathbf{r}$ at time t as is depicted in Figure 3.2. This probability is equal to the product of two probabilities: the probability of the particle of going from $\mathbf{s}$ to $\mathbf{r}'$ in a time t', and the probability of going

from $\mathbf{r}'$ to $\mathbf{r}$ in a time $t - t'$, i.e.,

$$P_P(\mathbf{r}', \mathbf{r}, \mathbf{s}, t', t) = P([\mathbf{r}', \mathbf{s}, t'] \cap [\mathbf{r}, \mathbf{r}', t - t']) = P(\mathbf{r}', \mathbf{s}, t')P(\mathbf{r}, \mathbf{r}', t - t'), \tag{3.8}$$

where the symbol $\cap$ means intersection and P_P stands for the probability of the paths P visiting the volume element at location $\mathbf{r}'$. Thus, the probability of going from $\mathbf{s}$ to $\mathbf{r}'$ and from $\mathbf{r}'$ to $\mathbf{r}$ is equal of the product of the two probabilities. This is another way of saying that the two events (going from $\mathbf{s}$ to $\mathbf{r}'$ and from $\mathbf{r}'$ to $\mathbf{r}$) are independent. This probability represents the probability of paths going through a volume element located at $\mathbf{r}'$.

The probability of a particle to travel from the source to the receiver is given by the solution to the diffusion equation given on Eq. 3.1. This solution also gives the time-dependent intensity $P(\mathbf{r}, \mathbf{s}, \mathbf{t})$ at the receiver location. Now, if we sum the contribution to the probabilities of waves traveling with all possible diffuse paths going from source at location $\mathbf{s}$ to receiver at location $\mathbf{r}$ we obtain

$$P(\mathbf{r}, \mathbf{s}, t) = \sum_P P_P(\mathbf{r}', \mathbf{r}, \mathbf{s}, t). \tag{3.9}$$

If we now replace the sum over paths in Eq. 3.9 with integration over volume we have:

$$\int_V P_P(\mathbf{r}', \mathbf{r}, \mathbf{s}, t)dV(\mathbf{r}') = \int_V P(\mathbf{r}', \mathbf{s}, t')P(\mathbf{r}, \mathbf{r}', t - t')dV(\mathbf{r}') = \int_V P(\mathbf{r}', \mathbf{r}, \mathbf{s}, t, t')dV(\mathbf{r}'), \tag{3.10}$$

where $P(\mathbf{r}', \mathbf{r}, \mathbf{s}, t, t') = P(\mathbf{r}', \mathbf{s}, t')P(\mathbf{r}, \mathbf{r}', t - t')$ is the probability of a particle going from source to the receiver while visiting a volume element dV at $\mathbf{r}'$ at time t'. Note that we have replaced a summation over all possible paths P with the integral over volume. The integrand $P(\mathbf{r}', \mathbf{r}, \mathbf{s}, t, t')$ contains the contributions to the intensity of all paths which are initiated at the source location $\mathbf{s}$ go through $\mathbf{r}'$ and end at the receiver located at $\mathbf{r}$. By integrating over all the volume where scattering occurs we are summing the contributions over all possible paths from the source to the receiver. Eq. 3.10 is a restatement of the Chapman-Kolmogorov equation (Roepstorff, 1994)

$$\int_V P(\mathbf{r}, \mathbf{r}', t)P(\mathbf{r}', \mathbf{s}, t')dV = P(\mathbf{r}, \mathbf{s}, t + t'), \tag{3.11}$$

which states that a process starting at $t = 0$ at location $\mathbf{s}$ reaches $\mathbf{r}$ at t via one of the possible values $\mathbf{r}'$ at a intermediate time t'.

From the left side of Eq. 3.11 the probability of going from $\mathbf{s}$ to $\mathbf{r}$ in a time t depends only in the distance between $\mathbf{s}$ and $\mathbf{r}$ and the time t. If we integrate the right side of Eq. (3.8) over all space, and apply the Chapman-Kolmogorov property, the intensity at the receiver $\mathbf{r}$ at time t due to an impulse source at $\mathbf{s}$ at time $t = 0$ is equal to

$$P(\mathbf{r}, \mathbf{s}, t) = \int_V P(\mathbf{r}', \mathbf{s}, t')P(\mathbf{r}, \mathbf{r}', t - t')dV(\mathbf{r}'), \tag{3.12}$$

which is exactly the same as Eq. 3.10, where we considered the sum over paths. Now, we realize that $P(\mathbf{r},\mathbf{s},t)$ is also the diffuse intensity at receiver $\mathbf{r}$ due to a unit intensity impulse at the source $\mathbf{s}$ at time t. This intensity $P(\mathbf{r}',\mathbf{s},t')$ is the diffuse intensity at a time t' at $\mathbf{r}'$ due to a source at $\mathbf{s}$ activated at time t=0, and $P(\mathbf{r},\mathbf{r}',t-t')$ is the intensity at $\mathbf{r}$ at time t due to an impulse source at $\mathbf{r}'$ on a time $t-t'$. Thus, we can identify $P(\mathbf{r},\mathbf{r}',t-t')$ with the Green's function $G(\mathbf{r},\mathbf{r}',t-t')$ which describes the intensity at the receiver $\mathbf{r}$ at a time $t-t'$ due to a normalized impulse source located at $\mathbf{r}'$ at time t'. We can write Eq. (3.12) therefore as follows :

$$P(\mathbf{r},\mathbf{s},t) = \int_V P(\mathbf{r}',\mathbf{s},t')G(\mathbf{r},\mathbf{r}',t-t')dV(\mathbf{r}'). \tag{3.13}$$

This equation holds for all times $0 < t' < t$ Roepstorff (1994). If we integrate both sides of Eq. (3.13) over time t' over the values $0 < t' < t$ we obtain :

$$tP(\mathbf{r},\mathbf{s},t) = \int_V \int_0^t P(\mathbf{r}',\mathbf{s},t')G(\mathbf{r},\mathbf{r}',t-t')dt'dV(\mathbf{r}'), \tag{3.14}$$

where we can identify $P * G = \int_0^t P(\mathbf{r}',\mathbf{s},t')G(\mathbf{r},\mathbf{r}',t-t')dt'$ as the time convolution of the intensities at $\mathbf{r}'$ with the Green's function $G(\mathbf{r},\mathbf{r}')$. If we divide both sides of Eq. (3.14) by $P(\mathbf{r},\mathbf{s},t)$ we arrive at the following integral representation for the traveltime of the diffuse wavefield,

$$t = \frac{1}{P(\mathbf{r},\mathbf{s},t)} \int_V \int_0^t P(\mathbf{r}',\mathbf{s},t')G(\mathbf{r},\mathbf{r}',t-t')dt'dV(\mathbf{r}'). \tag{3.15}$$

We have obtained in Eq. (3.15) an integral representation for the time t at $\mathbf{r}$ of the diffuse intensity due to an impulse source at $\mathbf{s}$. In the multiple scattering model $P(\mathbf{r},t)$ represents the mean or average intensity $< I(\mathbf{r},t) >$ of the wavefield. Thus the time t corresponds to the traveltime of the diffuse intensity. The traveltime t is the traveltime of waves coming from many different diffuse paths (as predicted by the diffusion approximation) and arriving at the receiver at a time t. The sum of the contributions from the diffuse paths of traveltime t generates in the average the diffuse intensity $P(\mathbf{r},t)$ as we saw in Eq. 3.10.

If we define the kernel $K(\mathbf{r}',\mathbf{r},\mathbf{s},t)$ as

$$K(\mathbf{r}',\mathbf{r},\mathbf{s},t) = \frac{1}{P(\mathbf{r},\mathbf{s},t)} \int_0^t P(\mathbf{r}',\mathbf{s},t')G(\mathbf{r},\mathbf{r}',t-t')dt', \tag{3.16}$$

we can express the traveltime t as the following volume integral:

$$t = \int_V K(\mathbf{r}',t)dV(\mathbf{r}'), \tag{3.17}$$

where $K(\mathbf{r}',\mathbf{r},\mathbf{s},t)$ represents the time of flight distribution or path length dependence of multiply scattered waves with a source at location $\mathbf{s}$ and receiver at location $\mathbf{s}$. The

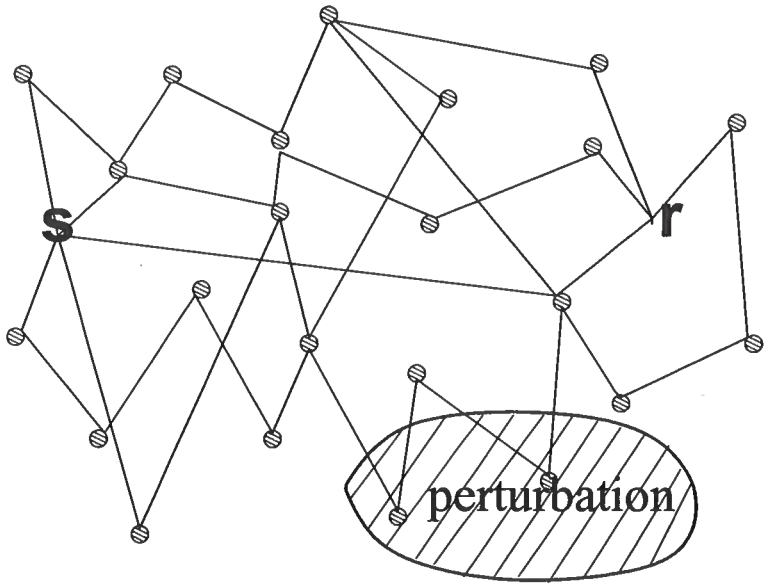

Figure 3.3. Model with multiple scatterers after a small time-lapse perturbation has been introduced. The paths remain the same after the perturbation.

integration kernel $K(\mathbf{r}', \mathbf{r}, \mathbf{s}, t)$ represents the normalized probability distribution function of wave intensity visiting a volume element dV located at position $\mathbf{r}'$ for a given source and receiver configuration.

3.5.2 Integral Representation for the Mean Traveltime Change of the Diffuse Wavefield

When the scatterers in a multiple scattering material move, or when the background velocity of the medium changes, the diffuse wavefield changes, reflecting the changes that occur in the waves traveling different scattering paths through the medium. In Diffusing Acoustic Wave Spectroscopy (Cowan *et al.*, 2002), these fluctuations of the multiply scattered wavefield are measured and analyzed to provide a sensitive technique for probing the dynamics of the scatterers. Here, we use a similar approach, considering only changes in the diffuse wavefield which arise due to a spatially localized change change in background velocity or slowness.

Let us assume that a spatially localized change in the velocity as shown in Figure 3.3, has been introduced on a time scale T which is much larger than the time scale t at which wave propagation occurs. With the time of flight distribution we can now calculate the mean traveltime change of diffuse waves. We introduce a localized perturbation on a time T after we propagated waves through the medium as in Figure 3.3. Notice that some of the multiple scattering paths traverse the perturbation while others do not. Therefore the mean traveltime change of waves with diffuse paths of traveltime t at the receiver will be

an average over the traveltime change over all diffuse paths of traveltime t.

We perturb the slowness in the medium to obtain an expression for the previously defined mean traveltime change. We work under the assumption that the perturbation is weak so that the scattering coefficient doesn't change, and the waveform for each scattering path stays approximately the same. Also, the scattering paths remain unchanged so that the only difference between the unperturbed and the perturbed field is the traveltime. If the mean slowness of the medium is denoted by s we can calculate the mean length $\langle L(t) \rangle$ of the multiple scattering paths at time t by dividing Eq. 3.17 by s,

$$\langle L(t) \rangle = \int_V \frac{1}{s} K(\mathbf{r}', t) dV(\mathbf{r}'), \tag{3.18}$$

where we have put s inside the integral since it is independent of location. If we now multiply the length of the multiple scattering paths by the slowness perturbation $\delta s(\mathbf{r}')$ we obtain the mean traveltime change of the diffuse waves with traveltime t. If we introduce the factor $\delta s(\mathbf{r}')$ into the integral on the right side of Eq. 3.18 the result of the new integral is the average or mean traveltime change for the multiple scattering paths with path length L.

$$\langle \tau(t) \rangle = \int_V K(r', t) \frac{\delta s}{s}(\mathbf{r}') dV(\mathbf{r}'), \tag{3.19}$$

where $\langle \tau(t) \rangle$ is the mean traveltime change of the multiply scattering waves with path length $\langle L(t) \rangle$ due to the relative slowness perturbation $\delta s/s$. Note that this average is weighted by the intensity, since the integration kernel K represents the normalized intensity of diffuse paths of traveltime t, and this is what it is needed in Eq. 3.6.

In summary, to calculate the traveltime change for a particular source and receiver configuration we need to integrate the kernel K weighted by the slowness perturbation $\delta s/s$ over all the integration volume. The kernel K is obtained by convolving the intensities at the receiver P with the Green's function G and dividing the result by the intensities at the receiver $\mathbf{r}$ at time t due to a source at $\mathbf{s}$. For a source and receiver at different locations, the time convolution $P * G$ does not have an analytical solution so it must be evaluated numerically. For the special case of coincident source and receiver, an analytical solution for this convolution can be obtained. In Appendix A we calculate the kernel K for coincident source and receiver for two- and three-dimensional media. In 3D the kernel K is given by

$$K_{3D}(\mathbf{r}, t) = \frac{1}{2\pi D r} \exp\left[\frac{-r^2}{Dt}\right]. \tag{3.20}$$

From Eq. 3.20 we see that the main contributions to the traveltime change comes from paths located close to the coincident source and receiver location. Also, we can see that for a fixed distance r the integration kernel K increases with time t. In multiple scattering, the effective distance traveled by diffuse waves is proportional to the square root of distance ($r \sim \sqrt{Dt}$). For smaller value of the diffusion coefficient, the stronger the scattering is and the smaller the effective distance traveled by diffuse waves (wave paths become more

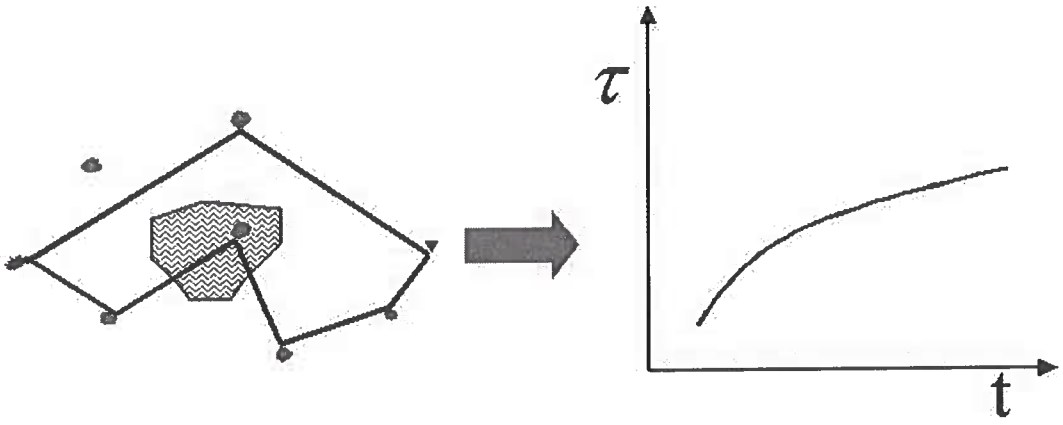

Figure 3.4. Left: A 2D model with random scatterer distribution with a localized slowness perturbation (shaded area). A particular diffuse path from source to receiver is shown. Right: mean traveltime change as a function of time due to the localized slowness perturbation.

localized around the source and receiver location). Thus with increased time, diffuse waves sample the same region multiple times and consequently the traveltime change will increase with time.

For the special case of 2D wave propagation the integration kernel K is (see Appendix A for derivation)

$$K_{2D}(\mathbf{r},t) = \frac{1}{2\pi D}\exp\left[\frac{-r^2}{2Dt}\right]K_0\left[\frac{r^2}{2Dt}\right], \tag{3.21}$$

where K_0 is the modified Bessel function of the second kind and D is the diffusion constant. We see that the behavior of K as a function of distance r and time t is similar to that of 3D wave propagation. If we insert Eq. (3.21) into Eq. (3.19) and integrate over area instead of volume we obtain:

$$\langle\tau(t)\rangle = \frac{1}{2\pi D}\int_A e^{\frac{-r^2}{2Dt}}K_0\left[\frac{r^2}{2Dt}\right]\frac{\delta s}{s}(\mathbf{r})dA(\mathbf{r}), \tag{3.22}$$

where r is the distance of the scatterer (or slowness perturbation $\delta s/s(\mathbf{r})$) to the coincident source and receiver. In Eq. (3.22), we have obtained an expression relating the traveltime change (τ) of the diffuse wavefield to the slowness perturbations ($\delta s/s$) in a multiple scattering medium for coincident source and receiver. In general, for a given perturbation in slowness, we can predict the mean traveltime change τ for any source and receiver configuration by calculating the integral in Eq. (3.19). To calculate this integral we need to know the slowness perturbation as a function of position an a good estimate of the diffusion coefficient D. We can estimate the diffusion coefficient using an independent method as shown in the next section.

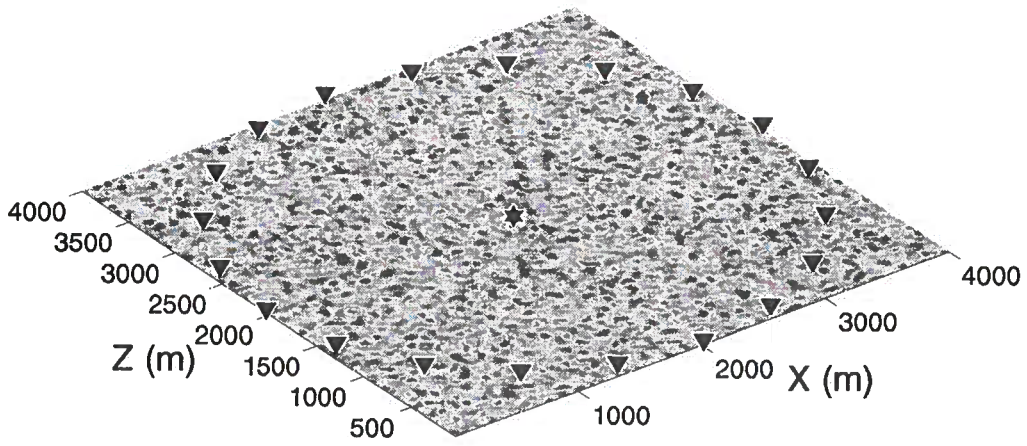

Figure 3.5. Representation of a 2D random velocity model with a Gaussian autocorrelation function. A source (star) is placed in the center. 20 receivers (asterisk) are located around the source.

Figure 3.4 shows an example of the traveltime change for a localized slowness perturbation. Given a velocity model with a random distribution of scatterers (right panel of Figure 3.4) we calculate the mean traveltime change τ of the diffuse paths propagating through the medium due to a localized slowness perturbation as a function of time t and plot the result on the right panel of Figure 3.4. In the last section, we test this theory with synthetic seismograms calculated with finite-differences.

3.6 Finite-Difference Simulations of Multiple Scattering

Having derived the relation between the mean traveltime change of diffuse waves and the slowness perturbations in a 2D medium, we validate the theory with finite-difference simulations of multiply scattered waves in a multiple scattering medium. In this section we summarize the parameters we used to generate the synthetic seismograms useful for our study of multiple scattering.

To generate synthetic seismograms for our study of multiple scattering we use a fourth-order 2D acoustic finite-difference code that propagates a finite-duration pulse through a specified velocity field. Following Frankel and Clayton (1986) we model the 2D velocity field as a constant-background model with added random velocity fluctuations that constitute the scatterers. The total velocity field can be decomposed as

$$v(\mathbf{r}) = v_0 + v_r(\mathbf{r}), \tag{3.23}$$

where v_0 is the background velocity and v_r are the random velocity fluctuations with a

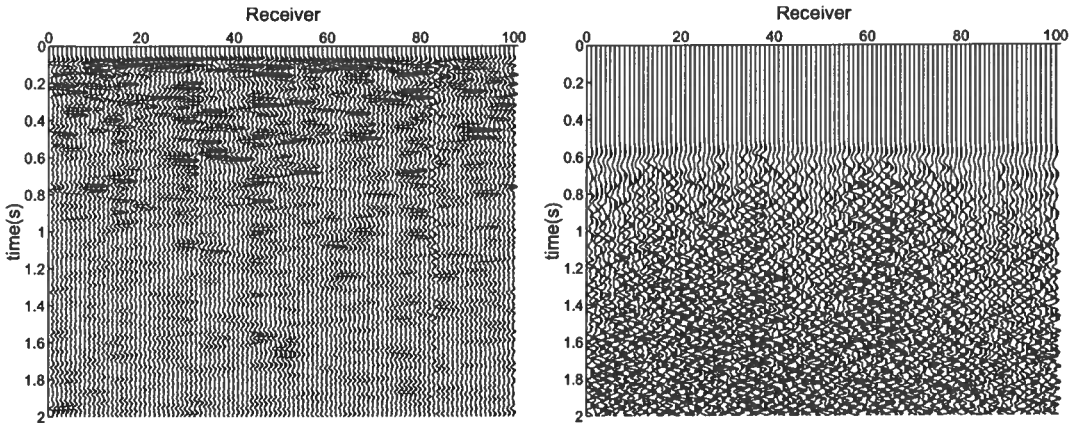

Figure 3.6. Seismograms recorded at 250 m(left) and 3000 m(right) from the source.

Gaussian autocorrelation function.

The velocity fluctuations are characterized by a Gaussian autocorrelation function with correlation distance a, with zero mean and standard deviation σ (see Figure 3.5 for a representation of the velocity model). The autocorrelation function of the velocity fluctuations v_r has the form :

$$\langle v_r(\mathbf{r}), v_r(\mathbf{r}+\mathbf{r}')\rangle = \sigma^2 \exp\left[\frac{-r^2}{a^2}\right]. \tag{3.24}$$

The synthetic seismograms were created by transmitting a band-limited pulse with a dominant wavelength of 240 m. The autocorrelation a length was set to 40 m, which is much smaller than the wavelength. The mean or background velocity v_0 is equal to 6000 m/s. To ensure strong scattering, we created a velocity field with a standard deviation of 25 percent about the mean velocity value. To test the validity of the diffusion approximation for our numerical model we setup a numerical experiment where we placed a source in the middle of the model and recorded the seismograms on an array of receivers around the source as depicted on Figure 3.5. Since the medium is statistically homogeneous we expect that the average intensity for receivers located at equal distance from the source should obey the diffusion equation. Figure 3.6 shows 100 synthetic seismograms computed at a distance of 250 m (left) and 3000 m (right) from the source. Note the strength of the multiple scattered arrivals after the highly attenuated ballistic arrival, especially for a distance of 3000 m from the source.

The average intensity of the synthetic seismograms is obtained by averaging the square of all calculated waveforms at a given distance to the source. We assume that because our 2D medium has homogeneous statistical properties, averaging over different receiver locations is equivalent to averaging over different realizations of the random velocity model. This gives us the time evolution of the intensities for each source-receiver offset. After fitting the calculated intensities with the solution of the diffusion equation, we obtain the estimated

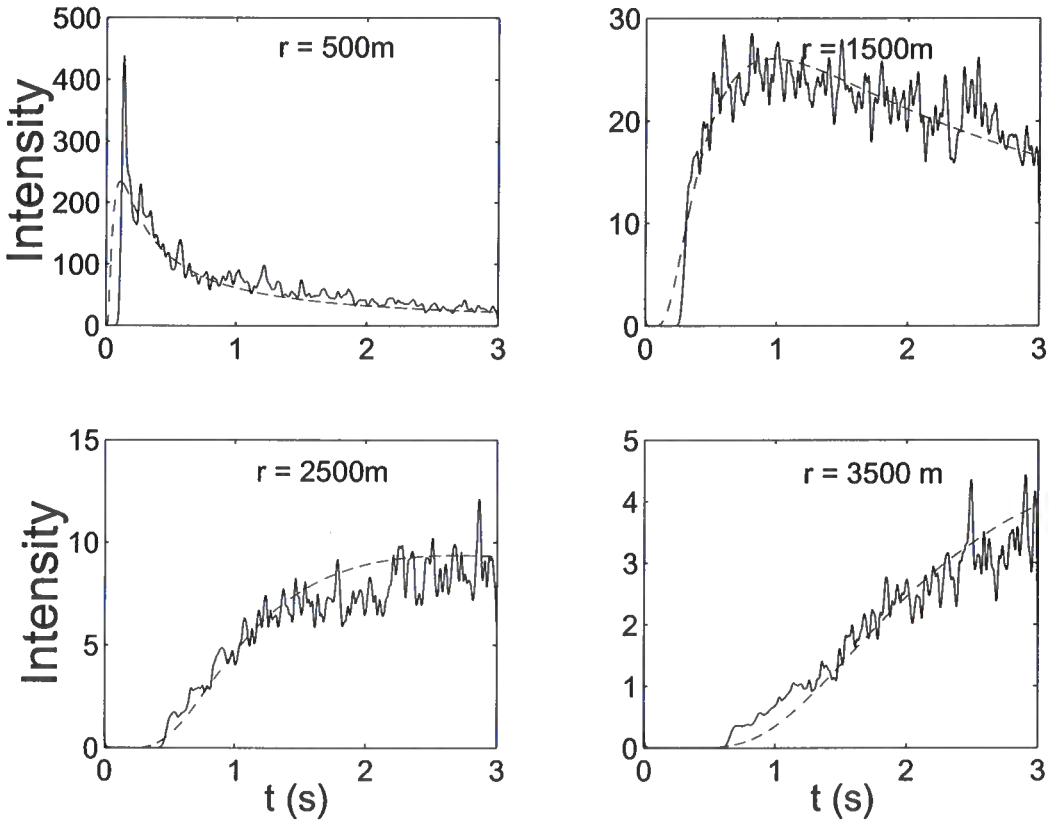

Figure 3.7. Actual averaged intensities (solid line) versus the diffusion curve (dashed line) for 500, 1500, 2500 and 3500 m. The diffusion value used for all the diffusion curves is the estimated mean value of 5.78×10^5 m^2/s.

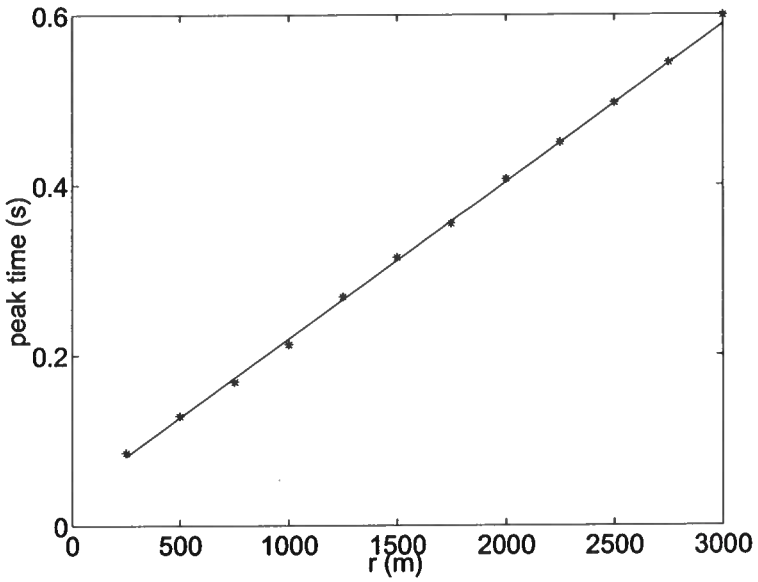

Figure 3.8. Regression of the move-out of the peak of the coherent pulse as a function of source-receiver distance. The slope of the regression fit gives us the energy velocity $v_e = 5280 \pm 25m/s$. The asterisks show the traveltime measurements and the solid line represents the best linear fit.

value for the diffusion coefficient of $D = (5.78 \pm 0.41) \times 10^5 m^2/s$.

3.7 Perturbations of the Energy Velocity from Perturbations of the Mean Velocity

When scattering is strong energy propagates with the energy velocity v_e which can be related to the diffusion coefficient D and transport mean free path l^* using Eq. 3.2. This velocity is different to the mean velocity v_0 of our 2D random velocity model on Eq. 3.23. When scattering is not too strong, this velocity is approximately the same as the velocity of coherent pulse or ballistic wave which propagates coherently through the medium. The energy velocity can be substantially smaller than the mean velocity because of the slowing down of the ballistic pulse caused by multiple scattering.

The energy or transport velocity characterizes the dynamics of the diffusion process. Despite the rather straightforward argument that leads to this conclusion, the exact expression for the transport velocity of classical waves in random media is difficult to calculate. In general, for a source wavelet of a given frequency, the energy velocity becomes a complicated function of the mean velocity and of the distribution of the random velocity fluctuations. Explicit formulas for the energy velocity for media with discrete scatterer distribution with constant n (average number density of scatterers) have been obtained (Tatarski, 1963; Frisch, 1968; van Tiggelen & Lagendijk, 1998). However, for a medium with continuous

random fluctuations there are no explicit formulas for the energy velocity of the medium.

We can estimate the energy or group velocity from our finite-difference synthetic measurements by measuring the velocity of the coherent or ballistic wave as it propagates through the medium. The coherent wave is computed by averaging the wavefield from different receivers. If we calculate the coherent wavefield for several source-receiver distances we can measure the traveltime of the peak of the coherent pulse for each distance and perform a linear regression of the traveltimes to obtain the transport or energy velocity. Figure 3.8 shows the traveltime picks for different several source-receiver separations and the best linear fit. The estimated energy velocity from the linear regression is $v_e = 5280 \pm 25m/s$. Notice that the energy velocity is much smaller than the mean velocity v_0 of our velocity model with random velocity fluctuations.

We are interested in the relation between a perturbation in energy slowness s with a perturbation in the mean slowness s_0. More specifically we are concerned in estimating the relative energy slowness perturbation $\delta s/s$ with which we can model the mean traveltime change of multiply scattered waves. Let the slowness field obtained by taking the inverse of the random velocity field be our unperturbed slowness field s_{unp}. Let us introduce after a given age T (the temporal scale on which changes in the scattering medium occur) a perturbation in the background slowness δs_0 so that the perturbed slowness field s_{pert} can be written as

$$s_{pert} = s_{unp} + \delta s_0. \tag{3.25}$$

A constant change in the mean slowness s_0 gives rise to a constant change in the energy slowness s. Thus,

$$\frac{\delta s}{s} = C\frac{\delta s_0}{s_0}, \tag{3.26}$$

where C is a constant of proportionality which relates the relative change in the energy slowness with the relative change in the mean slowness. For small changes in the slowness, like the ones we use to perturb the medium, we have also

$$\frac{\delta s}{s} = -\frac{\delta v_e}{v_e}, \tag{3.27}$$

where δv_e is the perturbation on the effective velocity v_e. This δv_e has nothing to do with the random velocity fluctuations that characterize our random velocity. It represents the change of the energy velocity of the random velocity model.

Eq. 3.27 tells us that we can obtain the relative change in the energy slowness from the relative change in the energy velocity. In theory, we could estimate this change by measuring the energy velocity from the velocity of the coherent pulse before and after a constant perturbation in the mean slowness has been introduced. Since multiple scattering amplifies small changes in the medium, we use instead the scattered wavefield to estimate the relative effective slowness perturbation $\delta s/s$. By measuring the changes in the mean traveltime of the diffuse waves before and after the perturbation we obtain $\delta v_e/v_e$ using Eq. 3.5:

$$\frac{\delta v_e}{v_e} = -\frac{\delta t}{t} = -\frac{\langle \tau(t) \rangle}{t}, \tag{3.28}$$

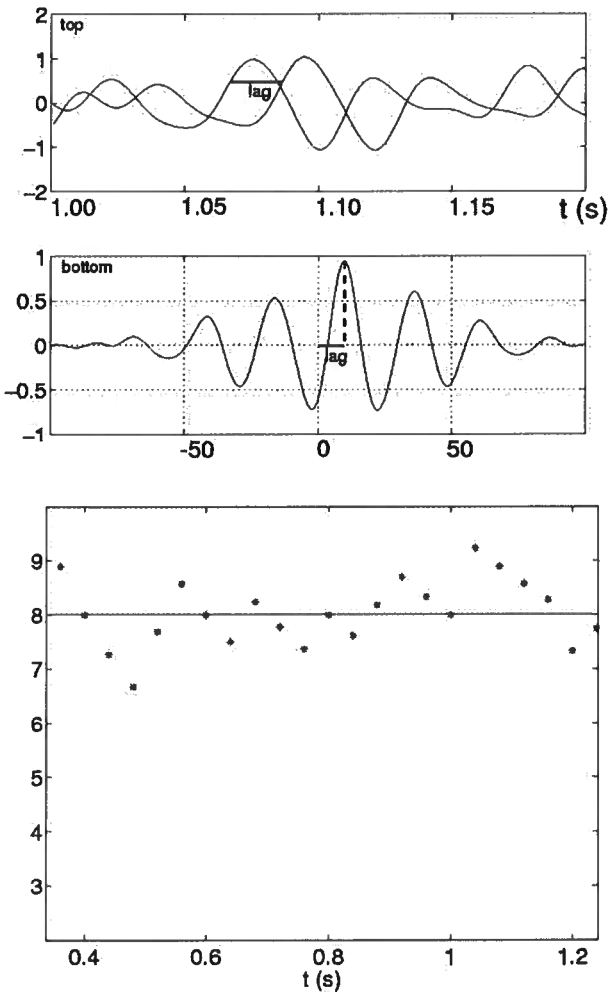

Figure 3.9. Estimation of the time lag by cross-correlation of unperturbed and perturbed wavefield (top). Energy slowness perturbation ($\delta s/s \times 10^3$) estimates from coda wave interferometry using Eq. (3.5) for a constant relative perturbation in the mean slowness $\delta s_0/s_0 = 0.01$ (bottom). The time axis t refers to the center of the time window on which the cross-correlation of the unperturbed and perturbed fields was calculated.

where $\langle \tau(t) \rangle$ is the traveltime change of multiply scattered waves arriving at different times t caused by a energy velocity perturbation. We calculated the multiply scattered seismograms before and after introducing a homogeneous change on the mean slowness $\delta s_0/s = .01$. Next, we use a time-windowed cross-correlation to compute the time lag between the perturbed and the unperturbed seismograms for different time windows. Using Eq. 3.28 we estimate the change of the energy or transport velocity in the multiple scattering medium for each time window. This process is exemplified in Figure 3.9. The left panels show both the perturbed and unperturbed waveforms (top) and their calculated cross-correlation (bottom) for a specific time window.

The location of the maximum of the cross-correlation corresponds to the time lag between the unperturbed and perturbed seismograms. By repeating this analysis over different time windows we obtain an estimation of the mean traveltime change $\langle \tau(t) \rangle$ of the multiply scattered waves as a function of time. Once we have $\langle \tau(t) \rangle$ we can calculate $\delta s/s$ using Eq. 3.28 for each time window and the result is shown on the right panel of Figure 3.9 as a function of the center of the time window t. As a result we obtain that for a 0.01 (one percent) constant perturbation in the mean slowness $\delta s_0/s$ the resultant perturbation in the energy slowness $\delta s/s$ is $0.0080 \pm .0005$, therefore, $C \approx 0.8$.

3.8 Traveltime Change for a Localized Time-Lapse Perturbation in the Slowness: Synthetic Examples

We test our theory with finite-difference simulations of acoustic waves in the multiple scattering regime before and after a time-lapse localized slowness perturbation has been introduced in the model. We perturb the random velocity model which represents the unperturbed medium by adding a localized slowness perturbation to it. We show two examples of localized slowness perturbations where we calculate the mean traveltime change of multiply scattered waves with Eq. 3.19 for several source-receiver configurations, and compare this predicted traveltime changes with the estimated traveltime changes obtained from the time-windowed cross-correlation of the unperturbed and perturbed synthetic seismograms.

3.8.1 Example 1

When the perturbation of the slowness is homogeneous in space the mean traveltime change can be calculated using Eq. 3.28. In the case of a localized slowness perturbation we obtain the mean traveltime change $\langle \tau(t) \rangle$ by calculating the integral specified in Eq. 3.19. We use as a first example a localized perturbation of the mean slowness in the shape of a square with sides of length equal to 3000 m as shown in Figure 3.10. The magnitude of the slowness perturbation is $\delta s_0/s_0 = 0.0050$.

We first analyze the unperturbed and perturbed synthetic seismograms for the receiver **R1** located inside the perturbed region of our model 2000 m away from the source. Figure 3.11 shows both the unperturbed and perturbed seismograms for receiver **R1**. The seismograph consists of diffuse or multiply scattered waves that have followed a multitude of paths from the source to the receiver. Notice the strength of the coda waves for late times.

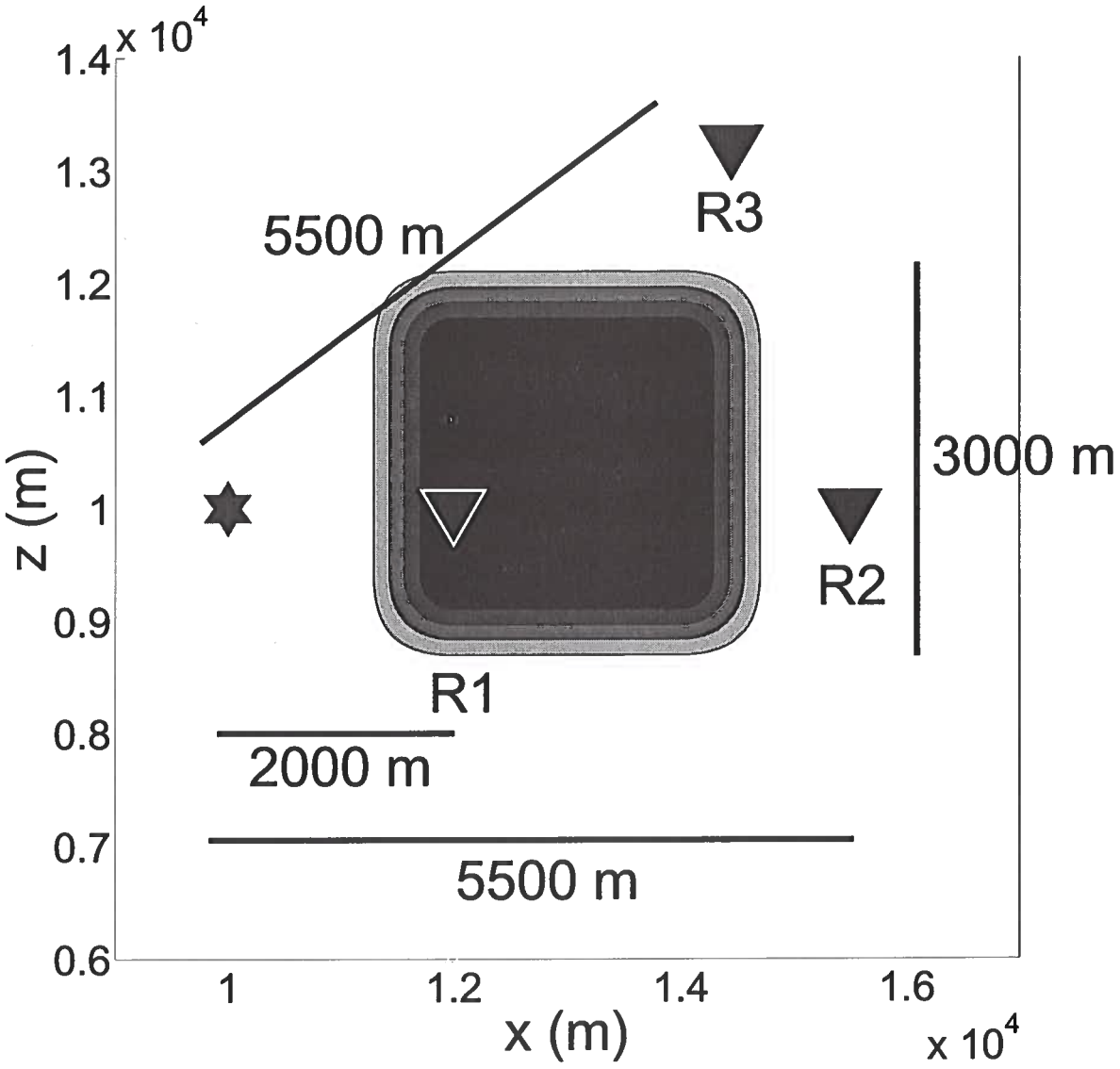

Figure 3.10. Perturbation of the slowness added to the medium. The side length of the square is 3000 m and the relative magnitude of the perturbation is $\delta s_0/s_0 = 0.0050$. Source is shown as a star and three receivers are shown as triangles.

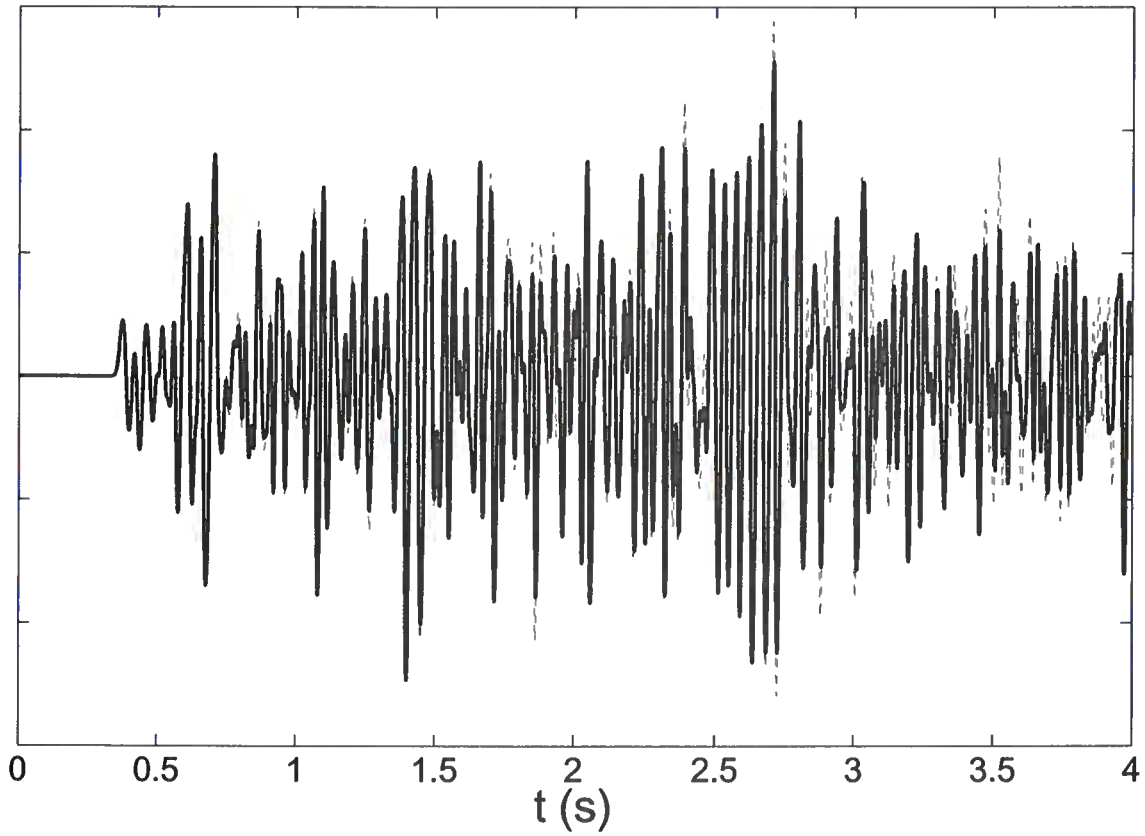

Figure 3.11. Unperturbed (solid) and perturbed (dashed) synthetic seismograms recorded at the receiver R1 located 2000 m away from the source.

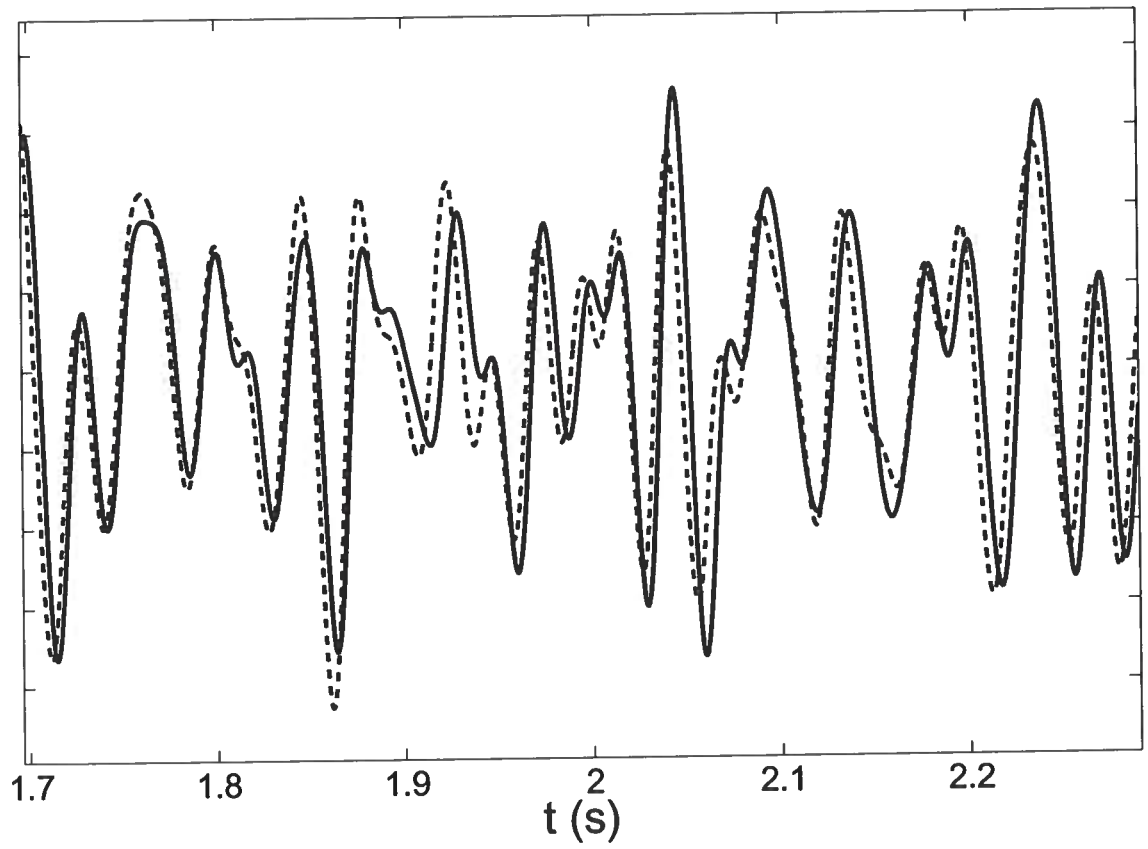

Figure 3.12. Zoom of the unperturbed (solid) and perturbed (dashed) synthetic seismograms recorded at the receiver R1 located 2000 m away from the source. Note the time lags between the unperturbed and perturbed seismograms at different times.

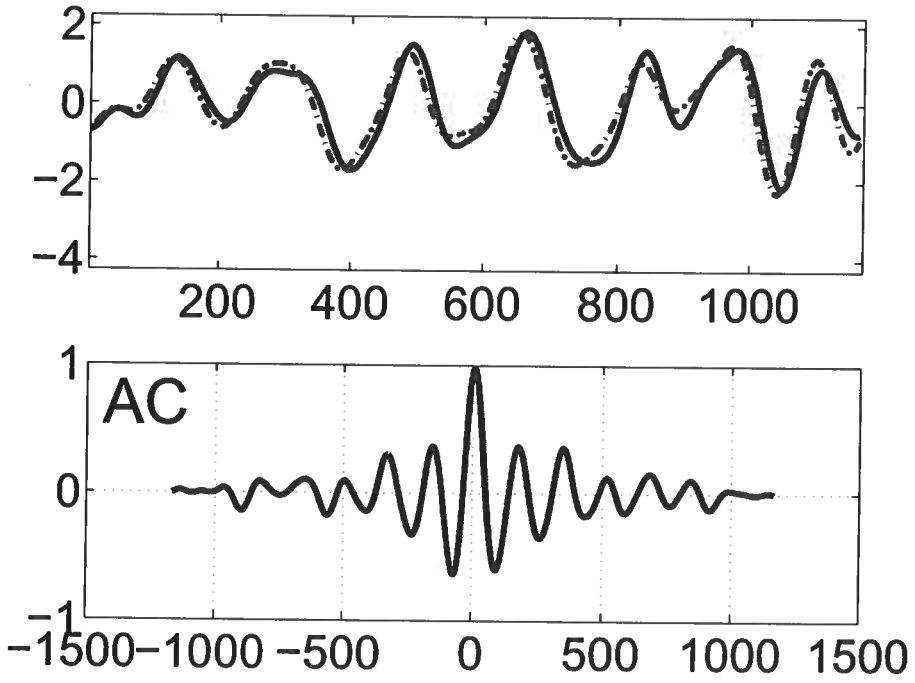

Figure 3.13. Time windowed cross-correlation of the unperturbed and perturbed seismograms for receiver R1 for a time window around $t = 2.4s$. The horizontal axis indicates the time sample number.

At first sight there seems to be no substantial difference between the wavefield before and after the perturbation. However, zooming at around 2.10 s (see Figure 3.12) we see that the unperturbed seismogram lags in time with respect to the perturbed seismogram. More careful inspection indicates that the behavior of the time lags with traveltime is systematic, i.e., the lag is increasing with traveltime t. Also, even though there are small changes in the traveltimes, the unperturbed and perturbed seismograms are well correlated. Figure 3.13 shows the unperturbed and perturbed wavefields (top) on a time window around 2.5 s and the calculated time-windowed cross-correlation (bottom). The unperturbed and perturbed seismograms are well correlated, judging by the correlation coefficient.

We calculate the theoretical mean traveltime change for multiply scattered waves that would be recorded at the receiver **R1** and compare the result with the mean traveltime change estimated from the synthetic seismograms using the time-windowed cross-correlation. Figure 3.14 shows good agreement between the theoretical and the measured mean traveltime change $\langle \tau(t) \rangle$.

We also calculated the mean traveltime changes for the receivers **R2** and **R3** located 5500 m away from the source. Even though the distance to the source is the same for both receivers, their locations with respect to the perturbation is different and therefore the mean traveltime change is different for the two receivers. The theoretical traveltime change

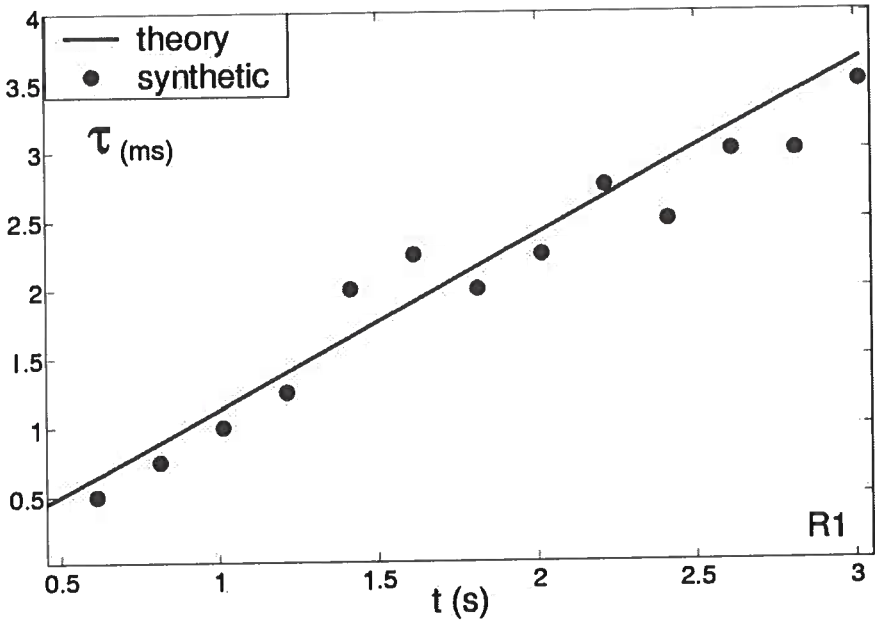

Figure 3.14. Theoretical versus measured mean traveltime change for receiver R1 located 2000 m away from the source.

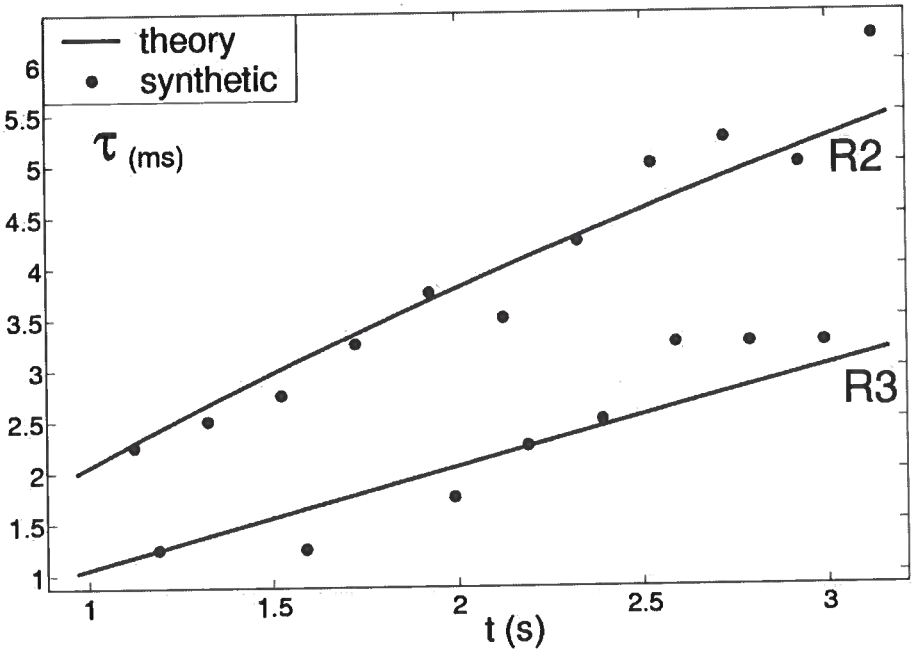

Figure 3.15. Theoretical versus measured mean traveltime change for receivers R2 and R3 located 5500 m away from the source.

for receiver **R2** is almost twice the traveltime change for receiver **R3**. This sensitivity of the mean traveltime change with the relative source and receiver locations with respect to the perturbations can be exploited in an inversion scheme to estimate the slowness change from measurements of the mean traveltime change at different receiver locations. Notice also that for all receiver there are fluctuations on the measured traveltime change about the theoretical value. We explore the origin of these fluctuations and how to minimize them in the next section.

3.8.2 Example 2

In this example we consider a localized slowness perturbation in the shape of a square with half the side length used in Example 1 (see Figure 3.16). I consider three receivers positioned at different locations with respect to the slowness perturbation, and then calculate the theoretical mean traveltime change for the three receiver locations.

Figures 3.17 and 3.18 show the mean traveltime change for receiver **R1** and **R2** respectively. We can see that in both cases the traveltime change increases with traveltime and both show a similar behavior (i.e., the slope of the traveltime change decreases with traveltime). The receiver **R2** is located farther from the source and from the slowness perturbation. Consequently, the number of paths which scan the perturbation with respect to the number off all possible paths is smaller in comparison with receiver **R1** which is located closer to the source and to the perturbation. As a result the mean traveltime change for receiver **R2** is smaller than the mean traveltime change for receiver **R1**. This conclusion follows from the random walk probabilities and from the time of fight distribution $K(\mathbf{r}, t)$.

Figure 3.19 shows the mean traveltime change for receiver **R3**. This receiver is located even farther away from the localized slowness perturbation and as a result the predicted mean traveltime change is the smallest amongst the three receivers. The measured mean traveltime change is close in magnitude to the time sampling interval ($dt = 0.250ms$), as evidenced by the "jumps" in the measured mean traveltime change. The moveout of the mean traveltime change curve is different, with the slope increasing with traveltime. Again, this is good example of the sensitivity of the mean traveltime change to the relative source and receiver locations.

3.9 Fluctuations of the Mean Traveltime Change

In the synthetic examples of the previous section I observed fluctuations of the measured mean traveltime change of the diffuse waves around the theoretical value calculated using Eq. 3.19. These fluctuations are due to the random nature of the diffuse or scattered wavefield. The main assumption behind our theory is that the spatial and temporal evolution of the average intensities can be described as a diffusion process. Based on this assumption, we approximated the diffuse wavefield at time t as the superposition of random walks from source to receiver with traveltime t. Finally, we assumed that (based on the diffusion approximation) the scattered wavefield produced as a result of wave propagation through the random medium approximates a diffuse field in the average.

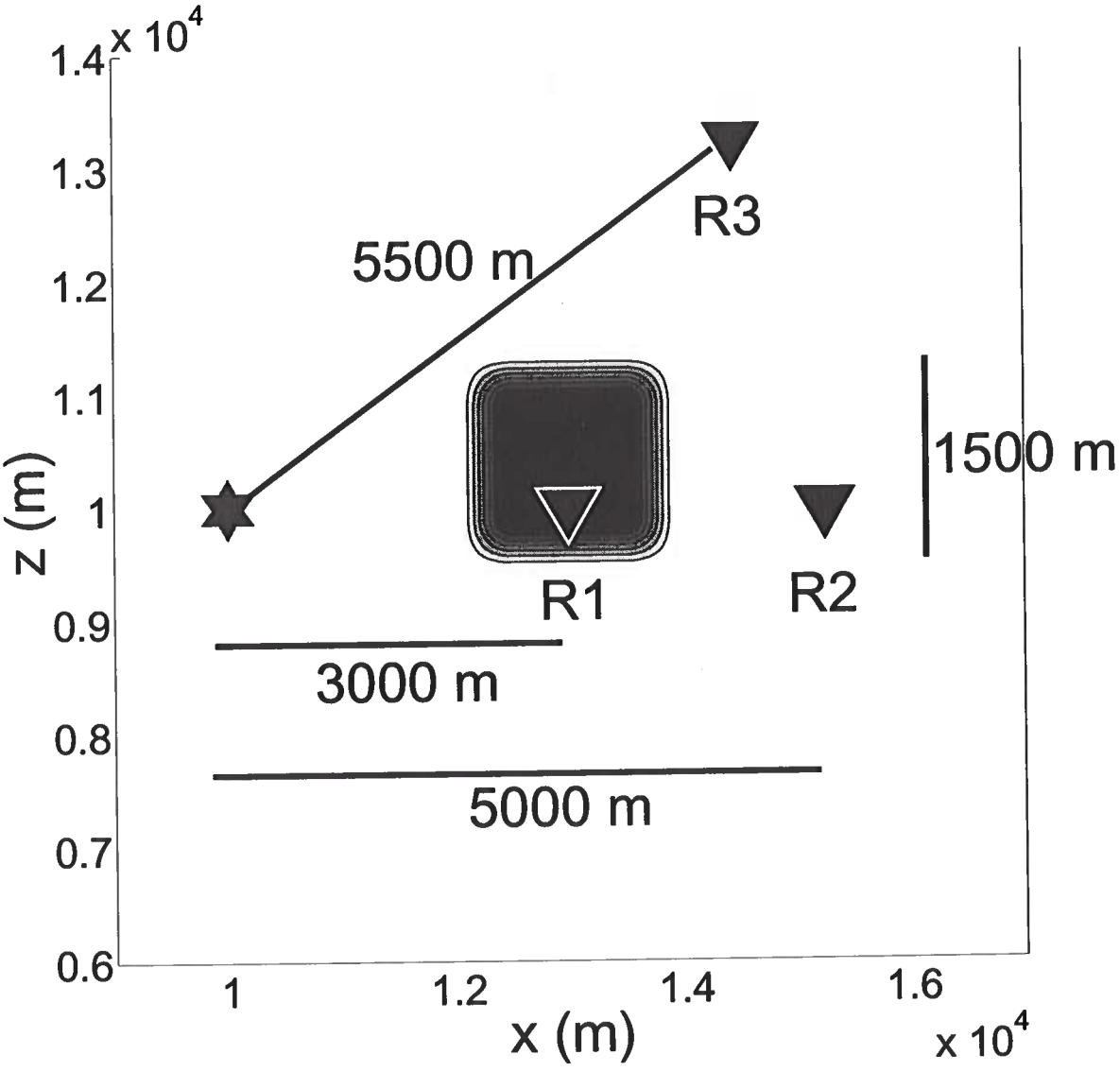

Figure 3.16. Perturbation of the slowness added to the medium. The side length of the square is 1500 m and the relative magnitude of the perturbation is $\delta s_0/s_0 = 0.0075$. Source is shown as a star and three receivers are shown as triangles.

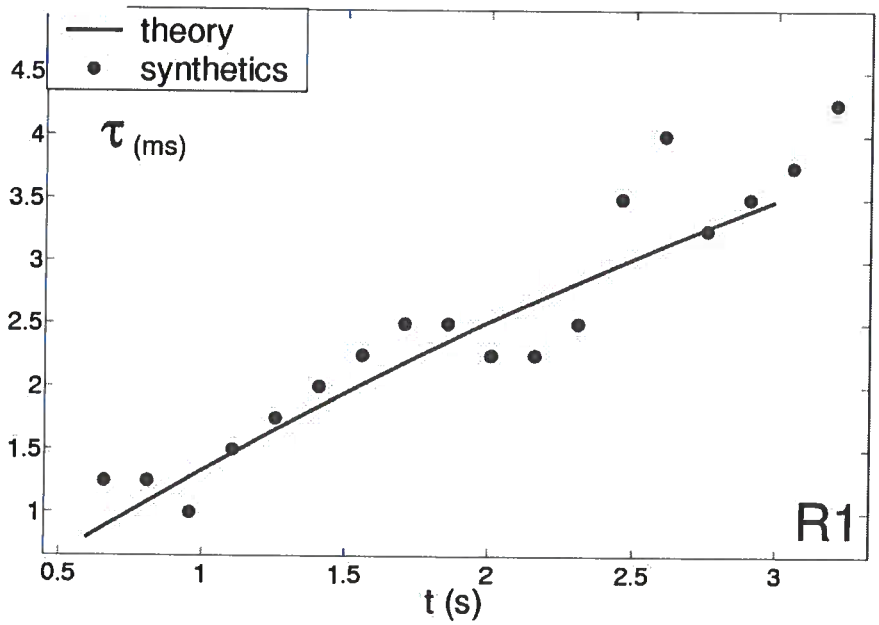

Figure 3.17. Theoretical versus measured mean traveltime change for receiver R1 located 3000 m away from the source.

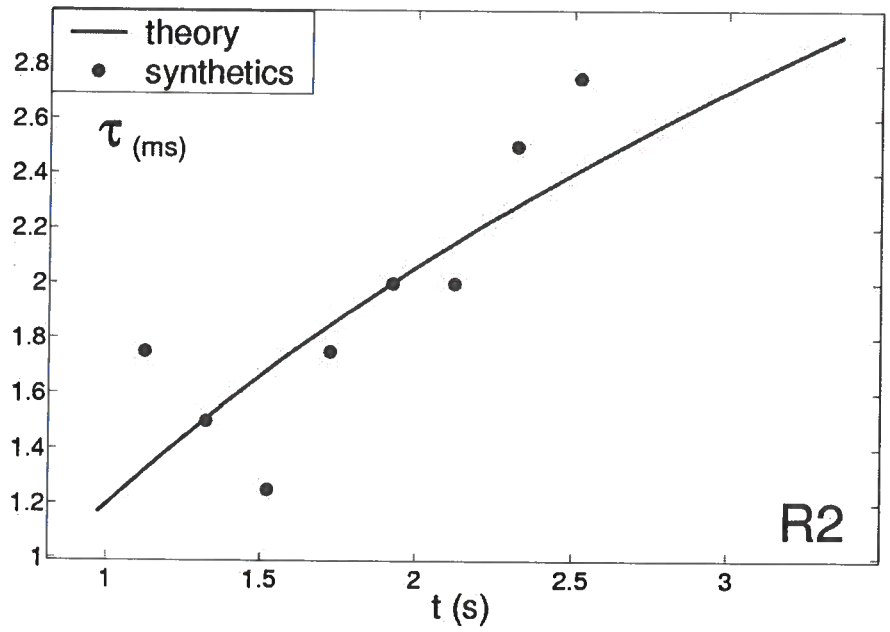

Figure 3.18. Theoretical versus measured mean traveltime change for receiver R2 located 5000 m away from the source.

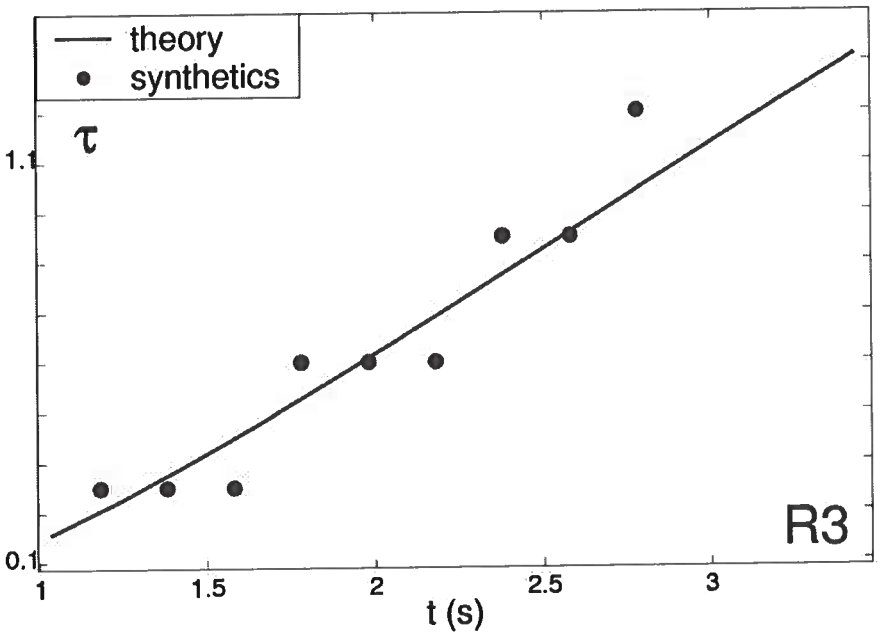

Figure 3.19. Theoretical versus measured mean traveltime change for receiver R3 located 5500 m away from the source. The mean traveltime change is in ms.

The wavefield recorded at a receiver **R** due to a source impulse at **S** can be thought of as the superposition of a multitude of waves on random walks. Each of those waves samples a different region of the random medium. The total wavefield is built upon the interference of all those waves following different trajectories. In other words, the diffuse wavefield is the superposition of a multitude of waves with diffuse paths from the source to the receiver.

The diffusion approximation states that in the average the wavefield can be regarded as a diffuse wavefield. In that sense we can see the wavefield for a given source and receiver pair as the single realization of a random experiment. The fluctuations of the measured mean traveltime change are due to the fact the we only have a single realization of the experiment. In other words, the fluctuations are due to departures from the diffusive behavior of the scattered wavefield.

In the examples shown in Section 3.8 we measured the mean traveltime change from the synthetic seismograms using a time-windowed cross-correlation technique. The measured mean traveltime change measured in this way is approximately an average of the time lags for the many scattering events on that time window. The window length that we use in the time-windowed cross-correlation can help us to minimize the fluctuations of the measured mean traveltime change. Consider an event that arrives at the receiver at time t. This wave at time t has a certain length which is approximately equal to the dominant period T_{dom} of the wavefield. On a window of length Δ we will have at most n different events, where $n = \Delta/T_{dom}$.

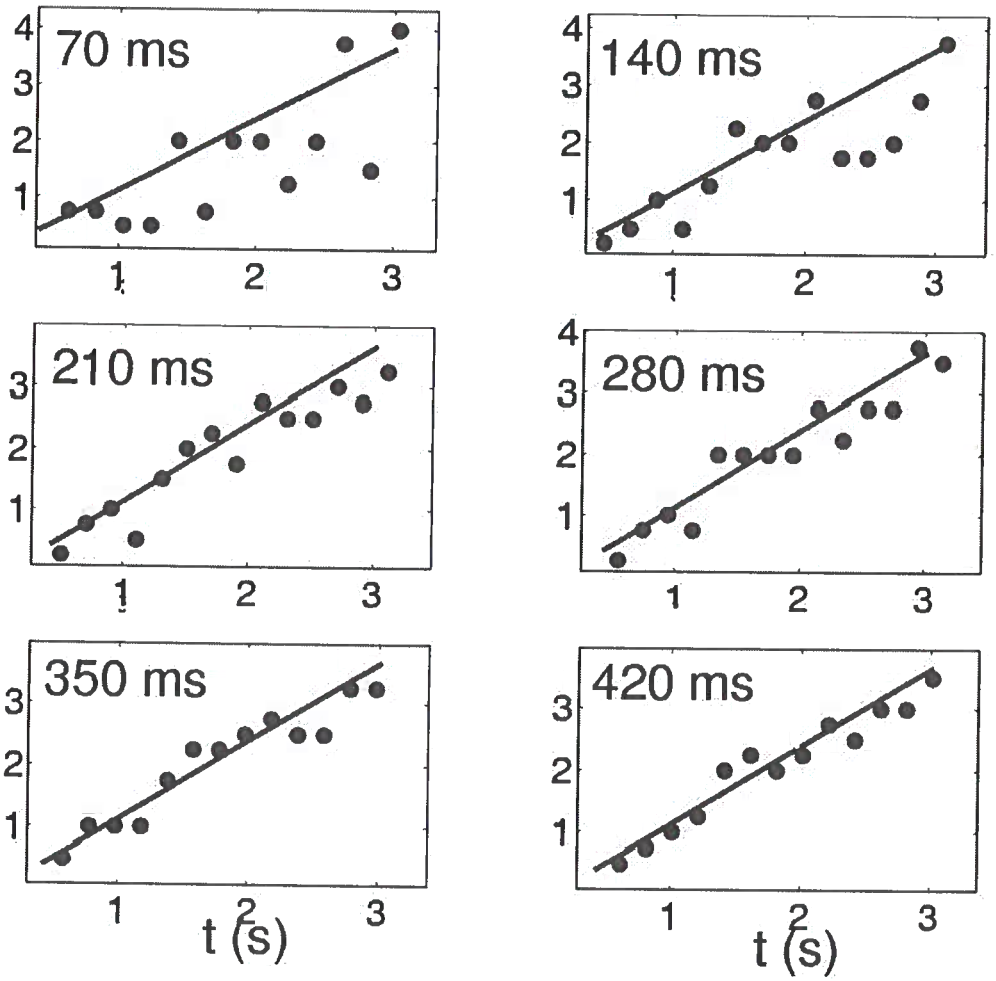

Figure 3.20. Mean traveltime change $\langle \tau(t) \rangle$ estimated from the synthetic seismograms for receiver R1 using different window lengths on the cross-correlation. The mean traveltime change is in ms. Note the reduction in the fluctuations of the measured mean traveltime change (circles) around the theoretical value (solid line) for larger window lengths. The dominant period is 40 ms.

Each scattering event at time t within the specified time window $[t-\Delta/2, t+\Delta/2]$ is considered to be a distinct realization of the diffuse wavefield (since for each arrival time t the waves sample different regions in the random medium). We can identify the traveltime change of this scattering event as a random variable with a distribution that can be characterized with a mean $\langle\tau(t)\rangle$ and a standard deviation $\sigma_\tau(t)$. The fluctuations on the measured traveltime change are related to $\sigma_\tau(t)$.

Assuming that the mean traveltime change $\langle\tau(t)\rangle$ has approximately the same distribution for the n scattering events on the time window, then the traveltime change on the time window can be defined as a sample mean (Tenorio, 2003):

$$\langle\tau(t)\rangle = \frac{\tau_1 + ... + \tau_n}{n}, \tag{3.29}$$

where n is the number of scattering events in the time window. Then, by averaging the traveltime change of the many scattering events the standard deviation of the sample mean $\sigma_{\langle\tau\rangle}(t)$ (after averaging over different traveltime changes on the time window) is related to the standard deviation of the mean traveltime change $\sigma_\tau(t)$ for a given scattering event in the following way

$$\sigma_{\langle\tau\rangle}(t) = constant \times \frac{\sigma_\tau}{\sqrt{\frac{\Delta}{T_{dom}}}} = constant \times \frac{\sigma_\tau}{\sqrt{n}}, \tag{3.30}$$

where n is the number of scattering events on the time window $[t-\Delta/2, t+\Delta/2]$. Eq. 3.30 implies that we can reduce the fluctuations of the estimated mean traveltime change $\langle\tau(t)\rangle$ by choosing a larger time window length Δ on the time-windowed cross-correlation. Snieder (2003) obtained a similar result for the decrease of the magnitude of the cross terms on the average intensity $\langle I\rangle$. Larger contributions from the cross terms to the average intensity implies larger departures from the diffusive behavior.

The decrease of the fluctuations with the increase of the time window length Δ can be appreciated on Figure 3.20 where we plot the measured mean traveltime change (circles) versus the theoretical mean traveltime change (solid line) using different window lenghts on the time-windowed cross-correlation for the receiver **R1** on the Example 1 of the previous section. We see that the fluctuations of the measured traveltime change decrease with a incresing window length Δ. For this synthetic example the dominant period T_{dom} is 40 ms. The length of the time window L on Figure 3.20 varies from 70 ms to 420 ms.

3.10 Tomography with Diffuse Waves

Eq. (3.17) relates the mean traveltime change at time t $< \tau(t) >$ with a localized slowness perturbation $\delta s/s(\mathbf{r})$. Note that Eq. (3.17) is in the form of a standard linear inverse problem as there is a linearized relation between the data (mean traveltime change for different times t) and the unknown parameters of the medium (localized slowness perturbation) which we want to retrieve by mean of an inversion procedure. In Section 3.8 we showed that the mean traveltime change as function of time changes for different receiver

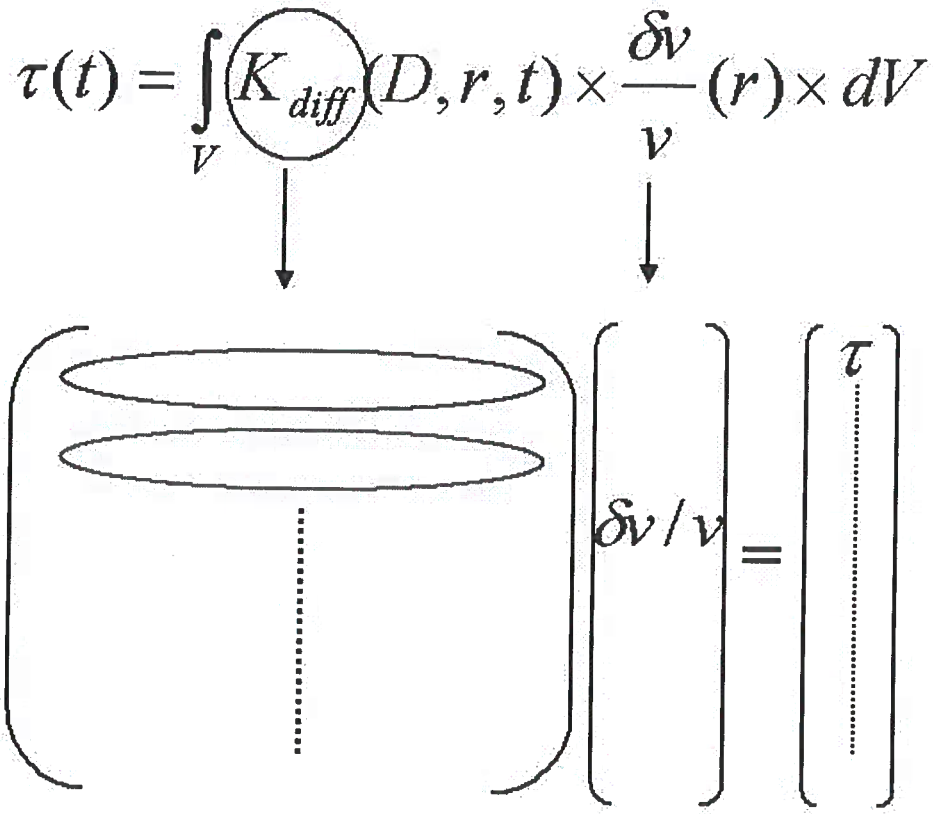

Figure 3.21. Schematic view of the tomographic problem in matrix form. The sensitivity kernel K relates linearly the unknown parameter $\delta s/s$ with the measured traveltime change $< \tau(t) >$. Each row in the matrix operator corresponds to a different receiver location.

locations. This sensitivity of the mean traveltime change to the relative source and receiver location with respect to the localized slowness perturbation can be exploited in the inversion scheme.

The goal of the inversion is to obtain the shape and magnitude of the slowness perturbation from the measured traveltime changes at different receiver locations. This is similar to the transmission tomography problem with the added complication that we are not only taking singly scattered waves but all multiply scattered waves. For a given time t and for a fixed source location we can setup the inverse problem in matrix form using different receivers as is shown in Figure 3.21. The matrix operator (calculated using the time of flight distribution K) which multiplies the unknown parameter vector (slowness perturbation $\delta s/s(\mathbf{r})$ as a function of position) generates the data (mean traveltime change for different receiver locations). Each row in the matrix corresponds to an observation of mean traveltime change for a specific receiver.

3.11 Discussion and Conclusions

For a homogeneous change in the mean slowness s_0, the size of the effective slowness perturbation is proportional to the size the mean slowness perturbation. We estimated the constant of proportionality C between the relative change of the mean slowness $\delta s_0/s$ and the relative change of the energy or transport slowness $\delta s/s$.

We have developed a theory that relates the mean traveltime changes of the diffuse wavefield to localized perturbations of the effective velocity for 2D acoustic waves. This theory was developed by means of the representation theory for the diffuse wavefield in a multiple-scattering medium. One of the main results from our theory is that the mean traveltime changes can be obtained by integrating the slowness perturbations weighted by the kernel $K(\mathbf{r}', \mathbf{r}, \mathbf{s}, t)$ over the whole area where multiple scattering occurs. The kernel $K(\mathbf{r}, t)$ describes the relation of the mean traveltime changes of the diffuse wavefield with the diffusion constant, time, and the distance to the perturbation. The estimated mean traveltime changes from the finite-difference simulations indicate that the theory accurately predicts the time evolution of the mean traveltime perturbations.

The mean traveltime change is sensitive to the source and receiver locations relative to the localized perturbation. This sensitivity can be exploited in a future inversion scheme to infer the energy velocity or slowness from the measurements of mean traveltime change for an ensemble of source receiver pairs. There is a linearized relation between the mean traveltime change of multiply scattered waves and the localized slowness perturbation.

The key assumption made in our approach is that the transport of acoustic waves can be described within the diffusion approximation. This assumption greatly simplifies the calculation of the time of flight distribution $K(\mathbf{r}', \mathbf{r}, \mathbf{s}, t)$. However, this is only an approximation for describing waves in strongly scattering media, and in some instances it may break down.

REFERENCES

A., Turner, & Weaver, R. 1995. Time dependence of multiply scattered diffuse ultrasound in polycrystalline media. *J Acoust. Soc. Am.*, **97**, 2638–2644.

Aki, K. 1969. Analysis of the seismic coda of local earthquakes as scattered waves. *J.G.R*, **74**, 615–631.

Aki, K., & Chouet, B. 1975. Origin of coda waves: source, attenuation and scattering effects. *J. Geoph. R.*, **80**(23), 3322–3341.

Alford, R., & Kelly, K. 1974. Accuracy of finite-difference modeling of the acoustic wave equation. *Geophysics*, **39**(6), 834–842.

Bleistein, N., Cohen, J., & Stockwell, J. 2001. *Mathematics of Multidimensional Seismic Imaging, Migration and Inversion.* Interdisciplinary Applied Mathematics, vol. 13. Springer.

Boas, D., Campbell, L., & Yodh, A. 1995. Scattering and imaging with diffusing temporal field correlations. *Phys. Rev. Letters*, **75**(9), 1855–1857.

Braile, L., Keller, G., Mueller, S., & Prodehl, C. 1995. *Seismic techniques, in Continental Rifts:Evolution, Structure, Tectonics.* Elsevier, New York.

Chernov, L.A. 1960. *Wave Propagation in a Random Medium.* McGraw-Hill, New York.

Claerbout, J. 1985. *Imaging the Earth's Interior.* Blackwell.

Cowan, M., Beaty, K., Liu, Z., & Sheng, P. 1998. Group velocity of acoustic waves in strongly scattering media: Dependance on the volume fraction of scattterers. *Phys. Rev. E*, **58**, 6626–6636.

Cowan, M., Jones, I., Page, J., & Weitz, D. 2002. Diffusing acoustic wave spectroscopy. *Phys. Rev. E*, **65**(066605), 1–11.

Dainty, A., & Toksoz, M. 1990. Array analysis of seismic scattering. *Bull. Seism. Soc. Am.*, **80**(6), 2242–2258.

Davis, T., Terrel, M., Cardona, R., Benson, R.D., Kendall, R., & Winarsky, R. 2003. Multicomponent seismic characterization and monitoring of the CO2 flood at Weyburn Field, Saskatchewan. *The Leading Edge*, **22**(7), 696.

Elmore, W.C., & Heald, M.A. 1969. *Physics of Waves.* Dover Pubilcations.

Foldy, L. 1945. The multiple scattering of waves. *Physical Review*, **67**(1), 107–119.

Frankel, A., & Clayton, R. 1984. A finite-difference simulation of wave propagation in two dimensional random media. *Bull. Seism. Soc. Am.*, **74**(6), 2167–2186.

Frankel, A., & Clayton, R. 1986. Finite difference simulations of seismic scattering: Implications for the propagation of short-period seismic waves in the crust and models of crustal heterogeneity. *J. Geoph. R.*, **91**(b6), 6465–6489.

Frisch, U. 1968. Wave Propagation in Random Media. *Pages 75–198 of:* Bharucha-Reid, A.T. (ed), *Probabilistic methods in applied mathematics.* Academic Press.

Gao, L. 1983. Effects of multiple scattering on coda waves in three-dimensional medium. *Pageoph.*, **121**(1), 3–15.

Gao, L. 1985. Coda wave amalysis for distinguishing attenuation due to isotropic scattering from attenuation due to absorption. *Pageoph.*, **122**, 1–9.

Gradshteyn, J.S., & Ryzhik, I.M. 1973. *Table of Integrals, Series, and Products.* 7 edn. New York: Academic Press.

Herraiz, M. 1987. Coda waves: a review. *Pageoph.*, **125**(4), 499–577.

Ishimaru, A. 1978. *Wave propagation and scattering in random media.* IEEE PRESS.

Jensen, J. 2002. *Imaging of complex media with acoustic and seismic waves.* Springer.

Jian, Z., Pearce, J., & Mittleman, D.M. 2003. Characterizing Individual Scattering Events by Measuring the Amplitude and Phase of the Electric Field Diffusing through a Random Medium. *Phys. Rev. Lett.*, **93**(3), 339031–339034.

Karal, F.C., & Keller, J.B. 1964. Elastic, electromagnetic and other waves in a random medium. *J. Math. Phys.*, **5**, 537–547.

Kelly, K.R., Treitel, S., & Alford, R.M. 1976. Synthetic seismograms: a finite-difference approach. *Geophysics*, **41**, 2–7.

Kopnichev, Y. 1977. The role of multiple scattering in the formation of a seismogram's tail. *Inveztiya Academy of Science USSR, Physics of the Solid Earth*, **13**, 394–398.

Kuga, Y. 1993. Velocity of coherent and incoherent electromagnetic waves in a dense strongly scattering medium. *Phys. Rev. B*, **48**(17), 155–158.

Langenberg, K.J., Marklein, R., & Mayer, K. 2002. Applications to nondestructive testing with ultrasound. *In:* Sabatier, P.C., & Pike, E.R. (eds), *Scattering and inverse scattering in pure and applied science.* Academic Press, San Diego.

Lemieux, P., Vera, M., & Durian, D. 1998. Diffusing-light spectroscopies beyond the diffusion limit: The role of ballistic transport and anisotropic scattering. *Phys. Rev. E*, **57**(4), 4998–4515.

Li, G. 2003. 4D seismic monitoring of CO2 flood in a thin fractured carbonate reservoir. *The Leading Edge*, **22**(7), 690.

Lin, J., & Ishimaru, A. 1974. Multiple-scattering of waves by a uniform random distribution of discrete isotropic scatterers. *J. Seis. Soc. Am.*, **56**(6), 1695–1700.

Maret, G., & Wolf, P.E. 1987. Multiple light scattering from disordered media. The effects of brownian motion of scatterers. *Z. Phys. B.-Condensed Matter*, **65**, 409–413.

Margerin, L., & Campillo, M. 2000. Monte Carlo simulation of multiple scattering of elastic waves. *J. Geoph. R.*, **105**(b4), 7873–7892.

Margerin, L., Campillo, M., & van Tiggelen, B. 1998. Radiative transfer and diffusion of waves in a layered medium:new insight into coda Q. *Geophys. J. Int.*, **134**, 596–612.

Morse, P., & Feshbach, H. 1953. *Methods of Theoretical Physics.* McGraw-Hill Book company, Inc.

Muller, G., Roth, M., & Korn, M. 1992. Seismic-wave traveltimes in random media. *Geophys. J. Int*, **110**, 29–41.

Paasschens, J. 1997. Solution of the time dependent Boltzman equation. *Phys. Rev. E*, **53**, 1135–1141.

Page, H., & Schriemer, H. 1997. Classical wave propagation in strongly scattering media. *Physica A*, **241**, 64–71.

Page, J., & Sheng, P. Group velocity in Strongly Scattering media. *Science*, **271**.

Page, J., Schriemer, H., Bailey, A., & Weitz, D. 1995a. Experimental test of the diffusion approximation for multiply scattered waves. *Phys. Rev. E*, **52**(3), 3106–3114.

Page, J.H., Schriemer, H.P., Bailey, A.E., & Weitz, D.A. 1995b. Experimental test of the diffusion approximation for multiply scattered waves. *Phys. Rev. E*, **52**(3), 3106–3114.

Roepstorff, G. 1994. Path Integral Approach to Quantum Physics: An Introduction. *Springer.*

Sato, H. 1993. Energy transportation in one- and two-dimensional scattering media: analytic solutions of the multiple isotropic scattering model. *Geophys. J. Int.*, **112**, 141–146.

Sato, H., & Fehler, M. 1998. *Seismic wave propagation and scattering in the heterogeneous Earth.* Academic Press.

Scales, J., & Van Wijk, K. 1999. Multiple scattering attenuation and anisotropy of ultrasonic surface waves. *Applied Physics Letters*, **74**(25), 3899–3901.

Schriemer, H., Cowan, M., Page, J., Liu, Zhengyou, & Weitz, D. 1997. Energy Velocity of Diffusing waves in strongly scattering media. *Phys. Rev. Lett.*, **79**(17), 3166–3191.

Shapiro, S. A., & Kneib, G. 1993. Seismic attenuation by scattering: theory and numerical results. *Geophys. J. Int.*, **114**, 373–391.

Shapiro, S.A., & Hubral, P. 1999. *Elastic waves in Random Media: Fundamentals of seismic stratigraphic filtering.* Springer.

Sheng, P. 1995. *Introduction to wave scattering, localization , and mesoscopic phenomena.* Academic Press.

Skipetrov, S.E., & Maynard, R. 2003. Diffuse Waves in Nonlinear Disordered Media. *Pages 75–97 of:* van Tiggelen, Bart, & Skipetrov, Sergey (eds), *Wave Scattering in Complex Media: From Theory to Applications.* Nato Science Series, vol. 107. Kluwer Academic Publishers.

Snieder, R. 1999. Imaging and averaging in complex media. *Pages 405–454 of:* Fouque, J.P. (ed), *Diffuse Waves in Complex Media.* Kluwer Academic Publishers.

Snieder, R. 2002. Coda wave interferometry and the equilibration of energy in elastic media. *Phys. Rev. E*, **66**, 046615–1,8.

Snieder, R. 2003. *Extracting the Green's function from the correlation of coda waves, an alternative derivation based on stationary phase.* Submitted to Phys. Rev. E., manuscript EE9122.

Snieder, R., Gret, A., Douma, H., & Scales, J. 2002. Coda wave interferometry for estimating nonlinear behavoir in seismic velocity. *Science*, **295**(22), 2253–2255.

Spagnolo, G., Ambrosini, D., Ponticiello, A., & Paoletti, D. 1996. Evaluation of diffusion in liquids by digital speckle pattern interferometry: computer simulation and experiments. *Eur. J. Phys.*, **17**, 51–59.

Stein, S., & Wysession, M. 2003. *An introduction to seismology, earthquakes and earth structure.* Blackwell Publishing.

Tatarski, V. 1963. Propagation of waves in a medium with strong fluctuation of the refractive index. *Soviet Physics Jetp*, **17**, 458–463.

Tenorio, L. 2003 (october). *Lectures for Applied Statistics.*

Tourin, A., Fink, M., & Derode, A. 2000. Multiple Scattering of Sound. *Waves Random Media*, **10**, R31–R60.

Turner, J. 1998. Scattering and Diffusion of seismic waves. *Bull. Seism. Soc. Am.*, **88**(1), 276–283.

van Albada, M., & van Tiggelen, B. 1991. Speed of propagation of classical waves in strongly scattering media. *Phys. Rev. Letters*, **66**(24), 3132–3135.

van Tiggelen, B., & Lagendijk, A. 1998. Coherent Beam, Diffuse Bean and Speckles: the Old View. *Pages 6–10 of:* Group, POAN Research (ed), *New Aspects of Electromagnetic and Acoustic Wave Diffusion.* Springer Tracts in Modern Physics, no. 144. Springer.

Weaver, R. 1982. On diffuse waves in solid media. *J. Acoust. soc. am.*, **71**(6), 1608–1609.

Weitz, D.A., & Pine, D.J. 1993. Diffusing Wave Spectroscopy. *Pages 652–720 of:* Brown, W. (ed), *Dynamic light scattering, The method and some applications.* Oxford: Clarendon Press.

Wesley, J. P. 1965. Diffusion of seismic energy in the near range. *J. Geophys. Res.*, **70**, 5099–5106.

Wu, R. 1982. Attenuation of short period seismic waves due to scattering. *Geoph. Res. Letters*, **9**(1), 9–12.

Yodh, A., & Chance, B. 1995. Spectroscopy and Imaging with Diffusing Light. *Physics Today*, **48**, 34–40.

Yodh, A., Tromberg, B., & Pine, D. 1997. Diffusing photons in turbid media. *J. Opt. Soc. Am.*, **14**, 851–858.

Zeng, Y., & Aki, K. 1991. Scattering wave energy propagation in a random isotropic scattering miedium. *J. Geoph. Res.*, **96**(b1), 607–619.

Zhang, Z., & Sheng, P. 1999. Wave transport in random media: the ballistic to diffusive transition. *Phys. Rev. E*, **60**(4), 4843–4850.

APPENDIX A

SENSITIVITY KERNEL K

We start from the expression:

$$K(\mathbf{r}',t) = \int_0^t \frac{P(\mathbf{r}'-\mathbf{s},t')(\mathbf{r}-\mathbf{r}',t-t')}{P(\mathbf{r},t)}dt', \tag{A.1}$$

$P(\mathbf{r},t)$ is the intensity at the receiver located at $\mathbf{r}$ due to a normalized impulse source at the origin at time t=0, and is given by Paasschens (1997). It is equal to the Green's function $G(\mathbf{r},t)$ in 2D

$$P(\mathbf{r},t) = \frac{1}{4\pi Dt}\exp\left[\frac{-r^2}{4Dt}\right]. \tag{A.2}$$

The time convolution $P * G$ is given by

$$P(\mathbf{r}',\mathbf{s}) * G(\mathbf{r},\mathbf{r}') = \int_0^t P(\mathbf{r}',t')P(\mathbf{r}-\mathbf{r}',t-t')dt'. \tag{A.3}$$

Substituting Eq. (A.2) into Eq. (A.3) gives for coincident source and receiver($\mathbf{r}=\mathbf{s}=\mathbf{0}$)

$$P_r(\mathbf{r}',\mathbf{r},\mathbf{s},t) = (P(\mathbf{r}',\mathbf{s}) * G(\mathbf{r},\mathbf{r}'))(t) = \int_0^t \frac{e^{\left[\frac{-r'^2}{4Dt'}\right]}}{4\pi Dt'}\frac{e^{\left[\frac{-r'^2}{4D(t-t')}\right]}}{4\pi D(t-t')}dt'. \tag{A.4}$$

As there is symmetry around $t/2$ we can write after renaming $\mathbf{r}'$ as $\mathbf{r}$:

$$P_r(\mathbf{r}',\mathbf{r},\mathbf{s},t) = \frac{2}{(4\pi D)^2}\int_0^{t/2}\frac{e^{\left[\frac{-r^2}{4D}\frac{t}{t'(t-t')}\right]}dt'}{t'(t-t')}. \tag{A.5}$$

Next, we set $\epsilon = \frac{1}{t'(t-t')}$ we obtain

$$P_r(\mathbf{r}',\mathbf{r},\mathbf{s},t) = \frac{2}{(4\pi D)^2}\int_{\frac{4}{t^2}}^{\infty}\frac{e^{\left[\frac{-r^2t\epsilon}{4D}\right]}d\epsilon}{\sqrt{\epsilon^2t^2-4\epsilon}}. \tag{A.6}$$

Now setting $\nu = r^2t(\epsilon - \frac{4}{t^2})$

$$P_r(\mathbf{r}',\mathbf{r},\mathbf{s},t) = \frac{2}{(4\pi D)^2}e^{\left[\frac{-r^2}{t}\right]}\int_0^{\infty}\frac{e^{-\nu}d\nu}{\sqrt{\nu^2+\frac{\nu r^2}{Dt}}}. \tag{A.7}$$

This integral can be calculated identifying it as a integral of the type

$$\int_0^\infty \frac{e^{-px}dx}{\sqrt{x(x+a)}} = e^{ap/2}K_0(\frac{ap}{2}), \tag{A.8}$$

for $a > 0$ and $p > 0$. The solution to the integral in Eq. A.8 can be found in Gradshteyn & Ryzhik (1973). Making $p = 1$ and $a = \frac{r^2}{Dt}$ Eq. A.8 becomes

$$(P * G)(\mathbf{r}, t) = \frac{2}{(4\pi D)^2 t} \exp\left[\frac{-r^2}{2Dt}\right] K_0\left[\frac{r^2}{2Dt}\right], \tag{A.9}$$

where K_0 is the modified Bessel function of the second kind. Substituting Eqs. (A.4) and (A.2) into Eq. (A.1), we arrive at the expression for the kernel $K(\mathbf{r}, t)$ in two dimensions for coincident source and receiver :

$$K_{2D}(\mathbf{r}, t) = \frac{1}{2\pi D} \exp\left[\frac{-r^2}{2Dt}\right] K_0\left[\frac{r^2}{2Dt}\right]. \tag{A.10}$$

To obtain the sensitivity kernel K in three-dimensional media we substitute Eq. A.2 with the Green's function for the diffusion equation in 3D

$$P(\mathbf{r}, t) = \frac{1}{(4\pi Dt)^{3/2}} \exp\left[\frac{-r^2}{4Dt}\right]. \tag{A.11}$$

After solving the integral defined in Eq. A.1 we obtain the expression for the kernel $K(\mathbf{r}, t)$ in three dimensions for coincident source and receiver

$$K_{3D}(\mathbf{r}, t) = \frac{1}{2\pi Dr} \exp\left[\frac{-r^2}{Dt}\right] \tag{A.12}$$